SLURRY PREPARATION OF ZEOLITE AND METAL - ORGANIC FRAMEWORK FOR EXTRUSION BASED 3D - PRINTING

A Thesis

Submitted to the Faculty

of

Purdue University

by

Nishant Hemant Hawaldar

In Partial Fulfillment of the

Requirements for the Degree

of

Master of Science in Mechanical Engineering

May 2018

Purdue University

Indianapolis, Indiana

THE PURDUE UNIVERSITY GRADUATE SCHOOL
STATEMENT OF COMMITTEE APPROVAL

Dr. Jing Zhang, Chair

Department of Mechanical and Energy Engineering

Dr. Hazim El–Mounayri

Department of Mechanical and Energy Engineering

Dr. Andres Tovar

Department of Mechanical and Energy Engineering

Approved by:

Dr. Sohel Anwar

Chair of the Graduate Program

I dedicate this thesis to my parents Hemant Hawaldar and Usha Hawaldar who have supported me through all the ups and downs of my life with their generosity, love, and care. Without them, I would not be where I am today.

ACKNOWLEDGMENTS

Immensely grateful thanks to Dr. Jing Zhang for his guidance as a teacher, mentor, advisor, and friend throughout this study. The encouragement and motivation given by Dr. Zhang are the driving gears for this study. As a mentor, he continuously played as a captain in our team which led us to achieve our goals. He has certainly contributed to my growth as an individual and as a researcher providing me with an outstanding example of professionalism and intelligence. I would also like to thank Dr. Andres Tovar and Dr. Hazim El –Mounayri, both for being on my thesis committee. Both of them have always assisted me with their expertise in the field of Additive Manufacturing, which has helped me to under numerous concepts and advancement in this field. I would also like to appreciate the assistance provided directly or indirectly by various faculty and staff at Indiana University - Purdue University Indianapolis, especially in the Department of Mechanical and Energy Engineering. I would like to thank Dr. Jian Xie, Dr. Yadong Liu and Dr. Jong Eun Ryu for allowing us to perform experiments at their laboratory. I would also like to thank Dr. Yeon-Gil Jung, Changwon National University, South Korea for helping us in evaluating SEM/XRD/EDS analysis results for Zeolite samples Additionally, I would like to thank my laboratory partners, and friends Piyush Pai Raikar and Xuehui Yang for supporting me and enriching my life. I might want to particularly express gratitude toward Dr. Jing Zhang, for giving me a chance to work in his research group and for giving such a decent research project. Finally, I would also like to dedicate this work to my father, Hemant Hanmant Hawaldar.

TABLE OF CONTENTS

Page

LIST OF TABLES

LIST OF FIGURES

Figure Page

Figure Page

SYMBOLS

$\mathring{A}$	Angstrom
ml	Milliliter
V	Volt
A	Ampere
rpm	revolution per min
N	Newton
$^{\circ}C$	Degree Celsius
$TORR$	Unit of pressure

ABBREVIATIONS

3D	Three Dimensional
AM	Additive Manufacturing
BET Test	Brunauer - Emmett - Teller Test
CCS	Carbon Capture and Separation
DOE	U. S. Department of Energy
DHTA	2,5- Dihydroxyterephthalic Acid
DMF	N,N-Dimethylformamide
EDS	Energy - Dispersive X-ray Sprectroscopy
HV	Vicker Hardness
IUPAC	International Union of Pure and Applied Chemistry
IZA	International Zeolite Association
MOF	Metal Organic Framework
PSA	Pressure-Swing Adsorption
PSD	Pore size Distribution
SEM	Scanning Electron Microscope
TGA	Thermogravimetric analysis
THT	Tetrahydrothiophene
XRD	X-ray diffraction

ABSTRACT

Hawaldar, Nishant Hemant. M.S.M.E., Purdue University, May 2018. Slurry Preparation of Zeolite and Metal - Organic Framework for Extrusion Based 3D - Printing. Major Professor: Jing Zhang.

Extrusion based 3D printing is one of the emerging additive manufacturing technologies used for printing a range of materials from metal to ceramics. In this process, the required material is extruded from the extruder in the form of a slurry. Zeolite and MOFs are mainly used for CO_2 adsorption in the form of pellets and beads due to their good adsorptive property. Researchers are developing monoliths of Zeolite and MOFs and fabricate them using traditional extrusion and implement them in the gas adsorption applications as an option for beads and pellets by developing a monolithic structure. Previous research on Zeolite 13X and 5A have shown good structural and physical properties in monolith form. In this study, we developed slurry of two molecular sieve Zeolite 3A and 4A monoliths powders, mixing it with bentonite clay, methyl cellulose, and PVA as a binder. The slurry preparation was carried out at room temperature. Once the 3D printed samples are dried at room temperature, a sintering process was performed to increase mechanical strength. To be used in real-time applications, the 3D printed Zeolite sample need to have sufficient mechanical strength. The BET surface area test showed good results for Zeolite 13X compared to available literature. The surface area calculated for 3D printed Zeolite 13X was 767m^2/g and available literature showed 498 m^2/g for 3D printed Zeolite 13X. The microhardness values of 3D printed Zeolite samples were measured using a Vicker hardness tester. The hardness value of the 3D - printed Zeolite samples increased from 8.3 $\pm$ 2 to 12.5 $\pm$ 3 $HV_{0.05}$ for Zeolite 13X, 3.3 $\pm$ 1 to 7.3 $\pm$ 1 $HV_{0.05}$ for Zeolite 3A, 4.3 $\pm$ 2 to 7.5 $\pm$ 2 $HV_{0.05}$ for Zeolite 4A, 7.4 $\pm$ 1 to 14.0 $\pm$ 0.5 $HV_{0.05}$ for Zeolite

5A respectively. The SEM, EDS and XRD analysis was performed for 3D printed samples before and after sintering to evaluate their structural properties. The SEM analysis reveals that all 3D printed Zeolite samples retained their microstructure after slurry preparation and also after the sintering process. The porous nature of 3D printed Zeolite walls was retained after the sintering process. The EDS analysis showed that the composition of 3D printed Zeolite samples remained somewhat similar with minor variation for before and after sintering. The framework structure of Zeolite Type X for Zeolite 13X and Zeolite Type A for Zeolite 3A, 4A, 5A were in good shape after sintering as standard peak intensity points were retained. Zn-MOF-74 was synthesized using solvothermal synthesis which is a well established synthesis process used for the synthesis of MOFs. We also developed slurry for Zn-MOF-74 using bentonite clay and PVA as binders and printed small parts using hand printing.

1. INTRODUCTION

1.1 Background

Additive manufacturing (AM) or 3D printing techniques is on the urge of todays manufacturing world due to their capability to produce components with complex geometry in relatively short time. The AM technology got introduce to this manufacturing world in 1980s for the first time for plastics and polymers. But considering decades of research and advancement in AM techniques, different 3D - Printed technologies were invented for metals, plastics, polymers, ceramics, glass and sand [1]. Compared to different types of materials that we can print, ceramics have a broad range of favorable properties, including high melting temperature, high mechanical strength, and good thermal stability [2]. The crude oil, coal and gas are the main energy resources available in world. When we burn fossil fuels to obtain energy, carbon dioxide is produced instantaneously [3]. The concentration of carbon dioxide in the atmosphere has been increasing, due to burning of fossil fuels to obtain energy, which is generally believed to increase the temperature of the Earth [4]. This will suffer the future generation unless todays scientists manage to construct a means of reducing the release of carbon dioxide into the atmosphere. Currently the only large point source of carbon dioxide emission into atmosphere is power plants. So capturing this large point source of carbon dioxide is one the possible way to decrease carbon dioxide emissions [5]. Currently researchers are working on developing 3D printers for some inorganic material like Zeolite and organic material like metal organic frameworks (MOFs) [6] [7]. Basically these materials are used in separation, adsorption, reaction and storage of various industrial gases like carbon dioxide, [8] nitrogen, [9], neon, argon, krypton, [10]and hydrogen [11]. **Chapter 2** of the thesis will focus on the slurry preparation of different Zeolite powders and print them using

the customized 3D printer. Referring to the previous work done in developing on 3D - printed molecular sieve type 13X and 5A Zeolite powders which have a pore diameter of 8Å and 5Å. The pore diameter of any molecular sieve allows it to use in a different application such as gas separation and adsorption. So in **Chapter 2**, we will also develop a slurry of molecular sieve Zeolite 3A and 4A which has a pore diameter of 3Å and 4Å respectively and will study their surface morphology of 3D Printed samples Furthermore, micro-structure analysis, material properties will be examined and compared with literature. Referring to the work done in **Chapter 2** on preparing slurry for molecular sieve Zeolites, **Chapter 3** presents a study on the synthesis of Metal-Organic Frameworks (MOFs) material Zn-MOF-74 using well-established synthesis process. Then **Chapter 4** will focus on the synthesized Zn-MOF-74 slurry preparation for 3D printing using the same customized 3D printer. At the end **Chapter 5** will conclude the work done in **Chapter 2**, **Chapter 3,** and **Chapter 4** and will discuss on future work.

1.2 Literature Review

1.2.1 Zeolite

Porous solids are basically classified into three categories based on their pore size diameters. First category is Microporous solids that have pore size of 2 μm or bellow, second category comes under Mesoporous solids with pore size from 2μm to 50 μm and third category of porous solids is known as Macroporous solids with pore size above 50 μm. [12–14]

Zeolites are naturally found inorganic crystalline structures with multidimensional channel systems. It was discovered by mineralogist A.F. Cronstedt in 1976 which when heated, appeared to boil due to very fast water loss [15]. Zeolite is made up of tetrahedrally organized molecules, for example, aluminum or silicon, which are bound to oxygen atoms. Positively charged cations such as Na+, K+ or Ca2+, are required to make the framework as aluminum atom contributes with a negative charge. The

negatively charged Zeolite framework yields a strong electrical field gradient and charge balancing cations [15]. International Zeolite Association (IZA) was organized in 1973 at the 3rd International Molecular Sieve Conference to promote and encourage the development of all aspects of zeolite science and technology. IZA has a database of all naturally available and artificially synthesized Zeolites. Under International Union of Pure and Applied Chemistry (IUPAC) IZA has authorization to develop framework codes for different Zeolites. According to IZA, Zeolite 3A, 4A, and 5A falls under LTA (Linde Type A) framework type and Zeolite 13X falls under FAU (Faujasite) framework type.**Fig 1.1** shows the 3D framework image of Zeolite Type A and Zeolite Type X [16]. The electrostatic interactions between this electrical field gradient of the Zeolite and the gas molecules are the driving force for CO2 uptake. The quadrupole moment of CO2 molecule leads to uneven charge distribution for short period of time, compared to van der Waals forces. There will be an attraction between the positive charge on the gas molecule and electrical field gradient of the Zeolite when one side is slightly positive. Due to high porosity, Zeolites have a large surface area that can accommodate high capacity of CO2 intake. The presence of aluminum and exchangeable metal cations makes Zeolite more hydrophilic, and disadvantage causes Zeolite molecule to bound water and has lower CO2 uptake. [17] Adsorption is a surface phenomenon in which the atoms, molecules and ions of gas, liquid or sometimes dissolved solids adhere to the surface creating a film of the adsorbate on the surface of the adsorbent. According to IUPAC adsorption is defined as an increase in the concentration of a dissolved substance at the interface of a condensed and a liquid phase due to the operation of surface forces. Adsorption can also occur at the interface of a condensed and a gaseous phase [18]. Generally adsorption process is classified into two types, physisorption and chemisorptions. Physisorption is a characteristic of weak van der Waals forces and chemisorption is a characteristic of covalent bonding. The amount or capacity of any material to adsorb is generally calculated by surface area of a material. BET theory is used to calculate the surface area of the material. The BET theory was developed by Stephen Brunauer, Paul

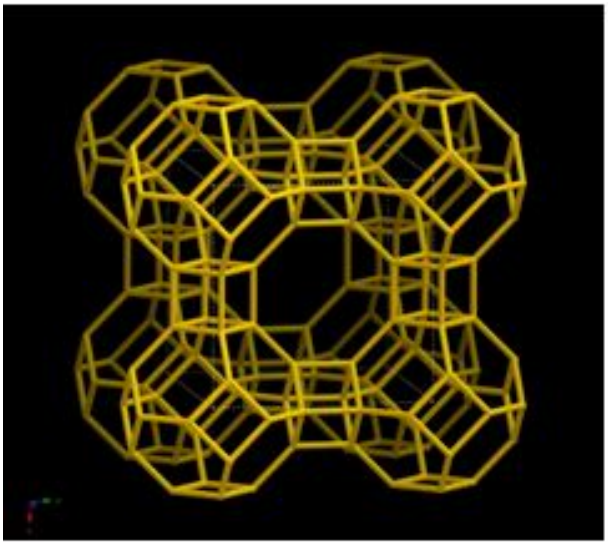

(a)

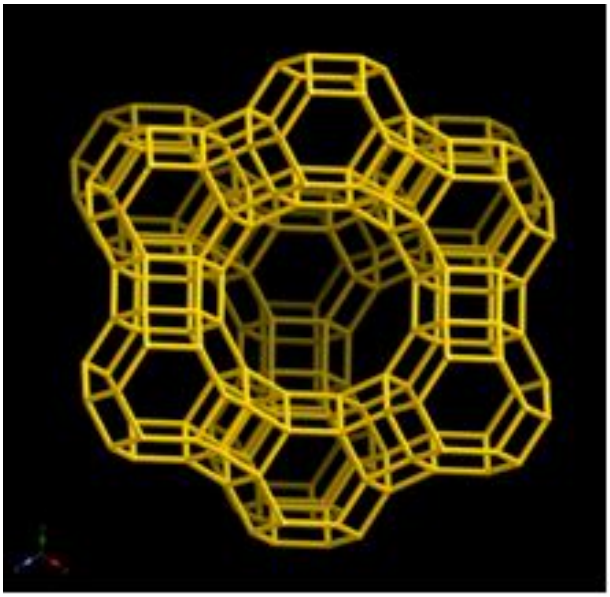

(b)

Fig. 1.1.: Framework of Zeolite : (a) Zeolite Type A (b) Zeolite Type X [16]

Hugh Emmett, and Edward Teller in 1938. They published this theory in the Journal of the American Chemical Society which explains the process of physical adsorption of gas molecules on a solid surface and serves as the basis for an important analysis

technique for the measurement of the specific surface area of materials [19]. Nitrogen at boiling temperature of 77K is commonly used as an adsorbate in calculating the surface area using BET theory.

1.2.2 Metal - Organic Framework (MOFs)

Over a decade, many research groups are doing research on developing new Metal-Organic Framework materials because of their exceptional properties like high adsorption capacity, custom tuned pore size diameter, surface area and larger volume [20]. These exceptional properties allow MOFs materials with a potential applications in the field of gas purification, gas separation, gas storage, catalysis and biomedical applications [21]. The commonly used techniques for carbon dioxide storage and separation like carbon capture and separation (CCS) [22], pressure-swing adsorption (PSA) and chemical adsorption by amine solutions are highly expensive processes and consume more amount of energy compared to the metal-organic frameworks (MOFs). PSA process is an adsorption based separation process which requires low energy but need to have a high CO_2 selectivity [23]. On the other hand the chemical adsorption process requires high energy for regeneration of adsorbents, and possesses low thermal stability which leads to loss of effectiveness over time and loss due to evaporation. But on the other hand, MOFs possess higher surface area with higher pore density and can be easily synthesized without any expensive setup. These synthesized MOFs possess higher purity and have good crystalline form [24]. Current research shows commercial application of MOF in the field of gas purification where the traces of chemical components from various gases are being removed. The parts per million (ppm) level of sulfur components from various gases van be removed using MOFs. Other application of MOFs is in the removal of molecules like anime, phosphines, alcohols which are generally odor generating molecules which is possible because of the MOFs structure with an accessible open metal sites [25]. The tetrahydrothiophene (THT, odorant) removal from natural gas at room temperature was

achieved using an electrochemically prepared Cu-EMOF in a fixed bed reactor [26]. This resulted in a reduction in sulfur content from 10-15 ppm to 1 ppm [26] MOFs structures have long been used in the SOx/NOx removal from automotive exhaust as three-way catalytic convertors and also used in removal of volatile organic compounds from various gases [27]. Gases are mainly required in power plants for energy production and hence we need them to store and use as we require them. But most of the gases require a high - pressure tanks equipped with a multistage compressor unit for storage. This storage facility requires high end maintenance which is more expensive so we need a cheaper option for storage. Researchers have studied several porous materials like Zeolite or activated porous carbons for storing gases. However, the unique structure of MOFs tends to have a high storage capacity of a number of gases. The amount of gas that can be stored in a specific storage mainly depends on what type of gas being stored along with temperature and pressure of the gas. MOF materials also play a vital role in specific gas storage as different MOFs can be used to store different gases. As we all know hydrogen is considered as one of the essential and abundantly available gases as fuel for the future because of its high energy density, clean burning, and its potential to be produced renewably [28]. In coming years hydrogen will be used as an alternative for gasoline and coal but for this we need to store hydrogen. Recent study uses solar energy to convert water into H_2 and combusting this H_2 for energy will convert it back to water. Doing so will require an advance hydrogen storage facility along with the transportation facility from the storage facility to required destination. Currently, U.S. Department of Energy (DOE) is developing a hydrogen vehicle as an alternative to current CO2 emission and fuel crises. This hydrogen vehicle will be suitable for ambient conditions and will have quick and safe refueling method [29]. Storage capacity of any MOF depends on pore size diameter; in case of hydrogen storage the MOFs with larger pore size diameter will not show good storage capacity due to poor attraction of hydrogen molecules to the surface of MOFs pore walls. So while selecting the MOFs for hydrogen storage the pores need to be larger in size than the hydrogens pore size diameter. One of

the best MOF with better hydrogen storing capacity is MOF-5 which has cubic Zn-terephthalate network [30].But MOF-5 can only shows high storage capacity at 77 K but going with higher temperature of 298 K it shows poor performance in storage [11]. Along with hydrogen MOFs are also used in CO2 storage as rising level of atmospheric CO2 is a global issue [31]. Recently many different MOFs are been developed with higher uptake capacity of CO2 like MOF-210, MOF-200, MOF-177, MOF-5, HKUST-1, NU-100. MOF-210 has surface area of 10450 m2 g-1 which is one of the only know highest surface area of any MOF till date. MOF-210 is constructed from 4,4 ',4" -[benzene-1,3,5-triyl-tris(ethyne-2,1-diyl)]tribenzoate (H3BTE), biphenyl-4,4'-dicarboxylate (H2BPDC), and zinc(II)nitrate hexahydrate. [32] **Fig 1.2** illustrates different MOFs used in the field of gas storage till date.

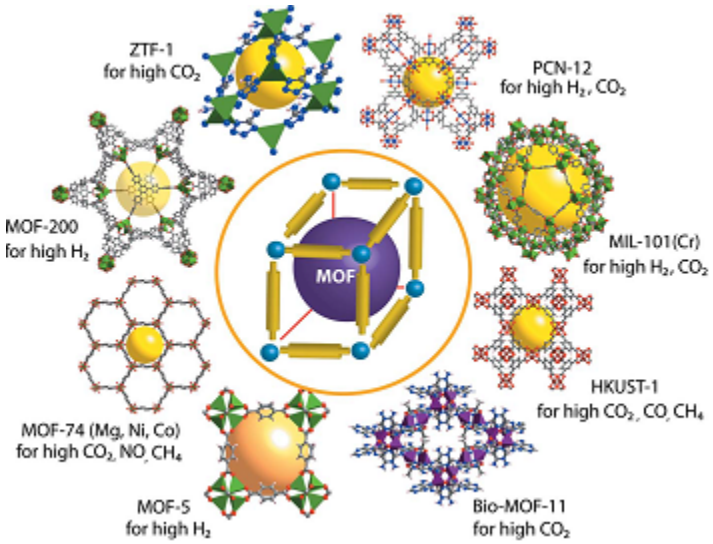

Fig. 1.2.: Schematic representation of some important MOFs used for gas storage. [21]

Gas separation is a method which separates the combinations of gases into particular gas components [33]. MOFs are one of the achievable materials used for gas separation due to the fact they have the higher surface area, adjustable pore sizes, and controllable surface properties [34, 35]. MOFs pore sizes can be refashioned by using

different chemicals however in case of Zeolites pores are challenging to control due to its inflexible tetrahedral oxide skeletons [36–39].The separating a gas from a combination of multiple gases is vital due to the fact if one gas is unsafe to the atmosphere, it is necessary to get rid of that particular gas instead of getting rid of all the gases. The removal of carbon dioxide (CO_2) [40] and methane (CH_4) [41] from natural gas is essential since these two are dangerous gases to the surroundings which lead to global warming [42]. The gas separation is achieved using the adsorptive property of MOFs, because of the shape and size of the MOF molecule which allows only certain components having shape and size smaller than itself from the gas mixture preventing remaining components of gas mixtures. The allowed component from gas mixture gets adsorbed into pores which are known as molecular sieving effect. Along with this, the thermodynamics equilibrium effect caused due to the different adsorbent surface and packing interactions causes adsorption of some components over the surfaces. The kinetic effect caused due to different diffusing rates leads certain components from the gas mixture to get adsorbed into the pores of MOFs and obstructing other components.

Numbers of techniques are developed for separation of gas components from the mixture such as distillation, pressure or thermal swing adsorption-desorption and membrane based separation [43]. Zeolite adsorbents are used in the separation of nitrogenoxygen (air), nitrogenmethane, and noble gas (e.g. KrXe). MOF adsorbents are recently used for purification of methane in natural gas. Currently, researchers are studying on the removal of tetrahydrothiophene (THT) [44] from natural gas using Cu-EMOF which was electrochemically prepared fixed bed reactor [25, 26]. Recently some of the MOFs have also been investigated in the field of biomedical applications. The toxicity of the materials which are used to synthesize MOFs is the main issue that should be considered before using MOFs in the biomedical applications. The study shows that we can use MOFs to carry drugs [45] but we need to consider some important factors like nontoxicity and biocompatibility; the drug loading capacity should be high with efficient delivery rate and should achieve control over release

and matrix degradation of the biomedical materials. The recent study done on MIL-100 and MIL-101 for carrying biomedical materials showed good results, where they were used to load anti-inflammatory drug called Ibuprofen into MIL-100 and MIL-101 pores [45]. 0.35 g and 1.4 g of Ibuprofen was loaded per gram of MIL-100 and MIL-101 respectively.After loading stability of both the MOFs were maintained and approximately after 3 days for MIL-100 and 6 days for MIL-101 the complete guest loading was achieved into a simulated body fluid solution [45].

1.3 Motivation and Objective

As the increase of CO_2 percentage is becoming a global issue many researchers are developing new techniques for removal of CO_2 from the air. Zeolite and MOFs are available in powder form but when it comes to using it for CO_2 removal application they are used in the form of beads and pellets. As we cannot use the direct powdered Zeolite and MOFs, the easiest way is to use conventional extrusion process. We decided to introduce the additive manufacturing technique combining with the extrusion process. The materials that are extruded using extrusion process are basically in the slurry form. So the main objective of this research was to develop slurries of Zeolite and MOFs powders and 3D print them using a customized 3D printer. The structural and physical properties of 3D printed samples will be then evaluated and compared with the available literature data.

2. EXTRUSION BASED 3D PRINTING OF ZEOLITE

2.1 Introduction

Extrusion is a manufacturing process in which an object is created of the fixed cross- sectional profile. A material is pushed through a die or an extruder of desired cross-section [46]. We can extrude materials ranging from metals, alloy metals, plastics, ceramics, and some advance materials like metal ceramic composites, metal organic frameworks. Extrusion is mostly used for making plastic and metal parts, as it can be molded into different shapes easily by applying heat. But on the other hand considering physical and micro - structural properties of ceramics and composite materials it is hard to extrude by just applying heat. So the easiest option for extruding such materials is making slurry (paste) by adding binders and then as per application we can do post processes like sintering. In this study we used the customized 3D printer developed for our previous work on extrusion based 3D printing of ceramic with some modifications [47].

2.2 Experimental Section

2.2.1 Materials

In this study different molecular sieve Zeolite like 13X, 3A, 4A and 5A is used. The chemical formulas for molecular sieve Zeolites are listed in **Table 2.1.** The chemical properties of Zeolite 13X 3A, 4a, and 5A are listed from **Table 2.2-2.5.**

Table 2.1.: Chemical formulas

Molecular Sieve Zeolite	**Chemical formula**
Zeolite 13X	$Na_{86}[(AlO_2)_{86}(SiO_2)_{106}] \cdot H_2O$
Zeolite 5A	$Na_{12}[(AlO_2)_{12}(SiO_2)_{12}] \cdot 27H_2O$
Zeolite 4A	$Na_{12}[(AlO_2)_{12}(SiO_2)_{12}] \cdot XH_2O$
Zeolite 3A	$Na_{12}[(AlO_2)_{12}(SiO_2)_{12}] \cdot 27H_2O$

Table 2.2.: Physical properties of Zeolite 13X

Physical property	**Value**
Pore diameter	8 Å
Loss on ignition @ 575°C	1.38 Wt %
H2O Capacity @ 17.5 TORR	33.20 #100#
Wet Screen (+100)	0.02
Apparent Density	30.30 lb/ft3

Table 2.3.: Physical properties of Zeolite 5A

Physical property	**Value**
Pore diameter	5 Å
Loss on ignition @ 575°C	2.10 Wt %
H2O Capacity @ 17.5 TORR	27.10 #100#
Wet Screen (+100)	0.00
Apparent Density	27.00 lb/ft3

Table 2.4.: Physical properties of Zeolite 4A

Physical property	**Value**
Pore diameter	4 Å
Loss on ignition @ 575°C	1.41 Wt %
H2O Capacity @ 17.5 TORR	26.50 #100#
Wet Screen (+100)	0.00
Apparent Density	32.00 lb/ft3

Table 2.5.: Physical properties of Zeolite 3A

Physical property	**Value**
Pore diameter	3 Å
Loss on ignition @ 575°C	1.54 Wt %
H2O Capacity @ 17.5 TORR	23.70 #100#
Wet Screen (+100)	0.00
Apparent Density	32.00 lb/ft3

Molecular sieve are the category of materials which has pores that allows the passage of molecules of certain size through it. So pores size will be responsible for allowing particular gas or liquid molecule to get adsorb into a molecular sieve Zeolite. Molecules with greater size than the pore size will not get adsorb into the pores. So for Zeolite 3A molecule larger than 3Å will not be get adsorbed, same for Zeolite 4A, 5A, and 13X molecules greater than 4 Å, 5 Å and 8 Å respectively will not get adsorb. As we know Zeolite is an alkali metal alumino-silicate compound, and with different metals we get different Zeolites. Zeolite 13X has sodium form of type X crystal structure which can adsorb molecules than can be

adsorbed by Zeolite 3A, 4A and 5A. Mostly Zeolite 13X is used for H_2O and CO_2 adsorption. Along with this Zeolite 13X can absorb molecules greater than pore diameter such as aromatics and branched-chain hydrocarbons. The sequence rate of adsorption is $SF_6, CHCL_3, CHBr_3, CHI_3, N-C_3F_8$, $CCL_4, N-C_4F_{10}, N-C_7H_{16}, CBr_4$, $C_6H_6, B_5H_{10}, (CH_3)_3N, C(CH_4)_4$, $(C_2H_5)_3N, C(CH_3)C_3CL, C(CH_3)_3Br$,and$C(CH_3)_3CH$. Zeolite 3A has a pore size of 3 Å. Zeolite 3A has potassium form of the type A crystal structure. The 3 Å pore size is created when part of the sodium ions of the 4 Å are replaced by potassium ions. The sequence rate of adsorption rate is helium, neon, nitrogen and water. Zeolite 4A has a pore size of 4Å. Zeolite 4A has sodium forms of the Type A crystal structure. The sequence rate of adsorption is argon, krypton, xenon, ammonia, carbon monoxide, $C_2H_4, C_2H_2, CH_3OH, C_2H_5OH$, $CH_3CN_2, CS_2, CH_3CL, CH_3Br$, and carbon dioxide. Zeolite 5A has a pore size that is 5Å. Zeolite 5A has calcium form of Type A crystal structure. The sequence rate of adsorption is C_3-C_{14}, C_2H_5CL, C_2H_5Br, CH_3L, $C_2H_5NH_2, CH_2CL_2CH_2Br_2, CHF_2CL$, $CHF_3, CF_4, (CH_3)NH_2$,$B_2H_6CF_2CL_2$, $CHFCL_2$, and CF_3CL. Zeolite 5A is basically used for separation of normal and isomerous alkane and sometimes in pressure swing adsorption (PSA) for gases. There are some advantages of Zeolite Type A like high adsorption speed, and higher contamination resistance, stronger crushing strength, increasing cyclic times which provide an extended product life. Zeolite 3A is mostly used in the moisture removing applications.

2.2.2 Slurry Preparation of Zeolite 13X and 5A

The slurry preparation starts with mixing the ingredients with correct proportion as shown in **Table 2.6** which then will be loaded into an extruder for 3D printing. The mixing of chemical binders will be carried out at room temperature. Two separate slurries were prepared for Zeolite 13X and 5A referring previous work done by Harshal et al. for the slurry preparation of Zeolite 13X and 5A [6]. The Zeolite 13X (Advanced Specialty Gas Equipments) and 5A (D.B.Becker) mixed with bentonite

clay (Sigma Aldrich) as a binder, methyl cellulose (DOW Chemicals) as a plasticizing organic binder, and poly(vinyl) alcohol (PVA) (ACROS Organics) as a co-binder. The hydroxyl groups from methyl cellulose contribute to additional particle cohesion which helps for Zeolite monolith strength. The magnetic stirrer (Fisher Scientific) was used at 1200 rpm to mix the powders **(Fig 2.1)**. This helped to form a homogeneous mixture of powders, which results in bubble free slurry formation. After obtaining a homogeneous powder mixture, the homogeneous powder mixture was divided into small batches of 5 g. Sufficient amount of deionized water (DI water) was added and mixed at 1200 rpm till homogeneous aqueous slurry with suitable viscosity was achieved. Every 30 min we added 5 g of powder mixture along with deionized water (DI water) to maintain viscosity of slurry.

Table 2.6.: Composition of 3D - Printed Zeolite 13X, 5A monoliths

Monoliths	**Zeolite (Wt%)**	**Bentonite clay(Wt%)**	**Methyl cellulose(Wt%)**	**PVA (Wt%)**
1	80	15	3.5	1.5
2	85	10	3.5	1.5

Fig. 2.1.: Magnetic stirrer

2.2.3 Slurry Preparation of Zeolite 3A and 4A

Now the slurry preparation for molecular sieve Zeolite 3A and 4A powders will be performed taking reference to the slurry preparation of Zeolite 13X and 5A. The molecular sieve Zeolite 13X and 5A has pore diameter of 8Å and 5Å respectively but Zeolite 3A and 4A has pore diameter of 3Å and 4Å respectively. As pore diameter of any molecular sieve Zeolite plays an important role in gas adsorption and separation property, we need to consider it while preparing the slurry and further implementation for gas adsorption applications. The chemicals used for preparing the slurry of Zeolite 3A and 4A will be same except the weight fraction. The compositions of all the chemicals that will be used are shown in **Table. 2.7**. Compared to the Zeolite 13X and 5A we increased the weight percent loading in case of Zeolite 3A and 4A slurry preparation. Apart from this all the procedure remains same.

Table 2.7.: Composition of 3D - Printed Zeolite 3A, 4A monoliths

Monoliths	**Zeolite (Wt%)**	**Bentonite clay(Wt%)**	**Methyl cellulose(Wt%)**	**PVA (Wt%)**
1	90	7	2	1
2	95	3	1.5	0.5

2.2.4 3D Printing of Zeolite

A circular grated disc and a square grated design was chosen to be the geometric shape for our prints as the samples will be further used for gas adsorption tests. The circular grated disc with 15mm diameter and 5mm thickness was designed in PTC Creo Parametric **(Fig. 2.2)** and then converted into .stl file for input to 3D printer.

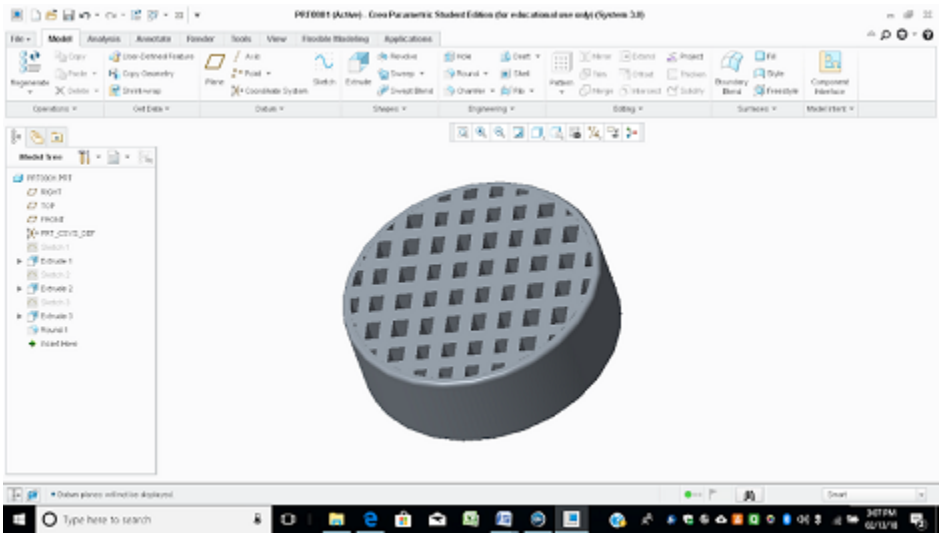

Fig. 2.2.: CAD design

The 3D printing of Zeolite slurry was initially done by hand extrusion though a 30ml syringe with 0.50 mm diameter needle to check the viscosity of slurry. As per

the literature available we performed multiple trails to get the desired viscosity, by changing amount of deionized water (DI water) added to make the slurry. **Fig 2.3** shows that during our first trial for Zeolite 5A we were not able to get desired viscosity of the slurry. Comparing **Fig 2.3 (a)** with **Fig 2.3 (b)** we can see some amount of shrinkage of 3D - Printed samples after drying at room temperature. For second trail we reduced the amount of deionized water (DI water) and loaded 2g powder mixture per 30 mins. The slurry was stirred 1 hour extra for second trail. **Fig 2.4** shows the 3D - Printed Zeolite samples for second trails. During second trail we printed square grate sample along with the circular grate. Some amount of shrinkage in size for both the samples i.e. square and circular was observed after the drying at room temperature. **Fig 2.5 (a) and (b)** shows the Zeolite 5A samples after drying at room temperature.

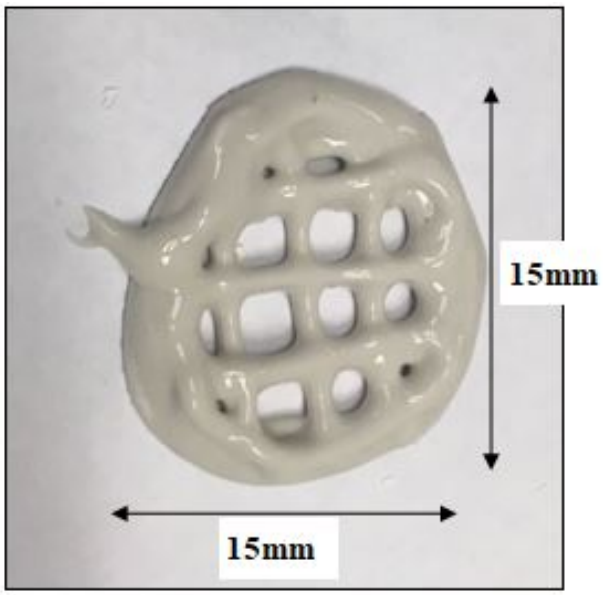

(a)

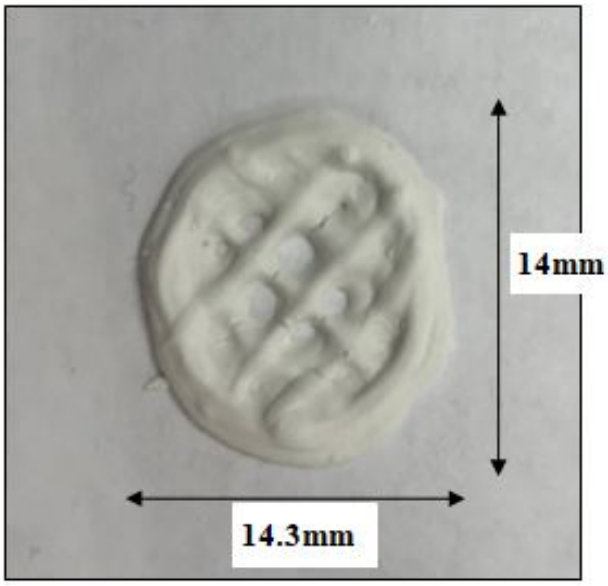

(b)

Fig. 2.3.: 3D - Printed Zeolite 5A First trail : (a) Before drying (b) After drying

After achieving the desired viscosity we decided to print using the customized 3D printer. Before loading the Zeolite slurry into the extruder, we performed dry run tests to prevent flaws and to avoid the wastage of slurry. Dry run test helped us to

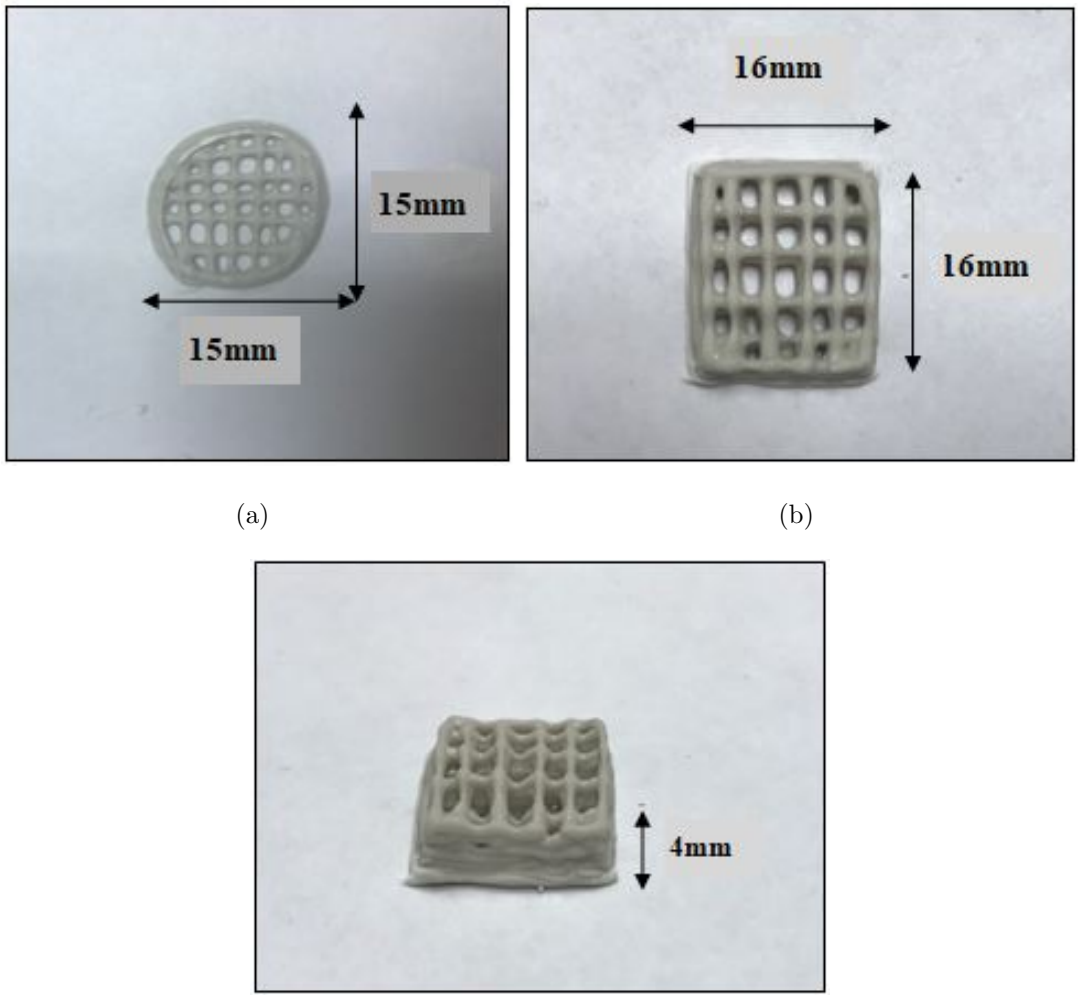

(a) (b)

(c)

Fig. 2.4.: 3D - printed Zeolite 5A Second trail : (a) Circular grate (b) Square grate (c) Side view of square grate

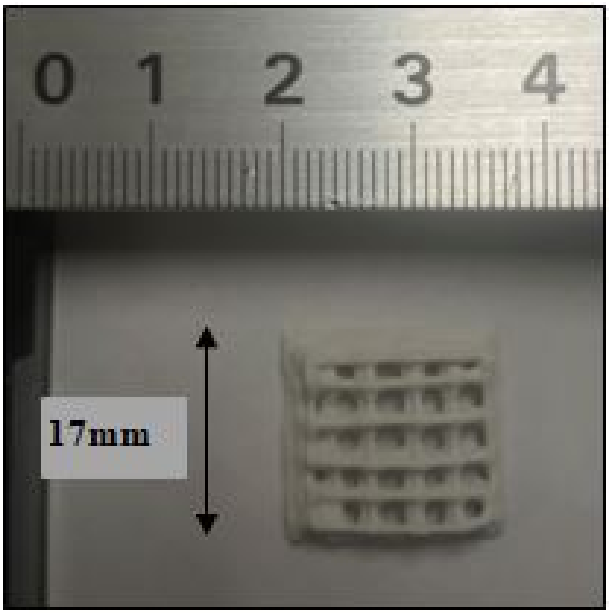

(a)

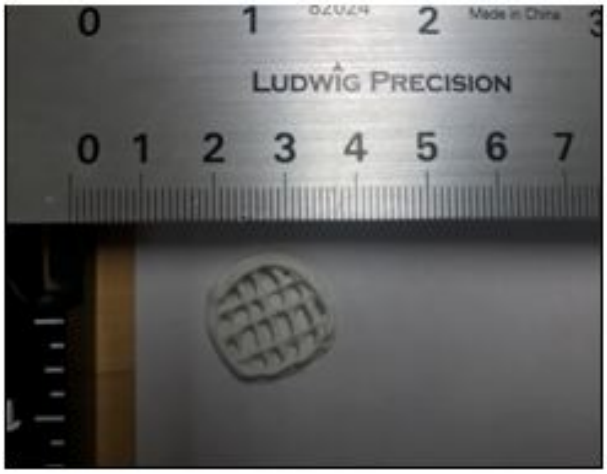

(b)

Fig. 2.5.: 3D - Printed Zeolite 5A samples : (a) After drying (square grate) (b) After drying(circular grate)

adjust the distance between extruder and bed. We successfully printed samples of Zeolite 13X, 3A and 4A using the customized 3D printer which are shown in **Fig. 2.6**

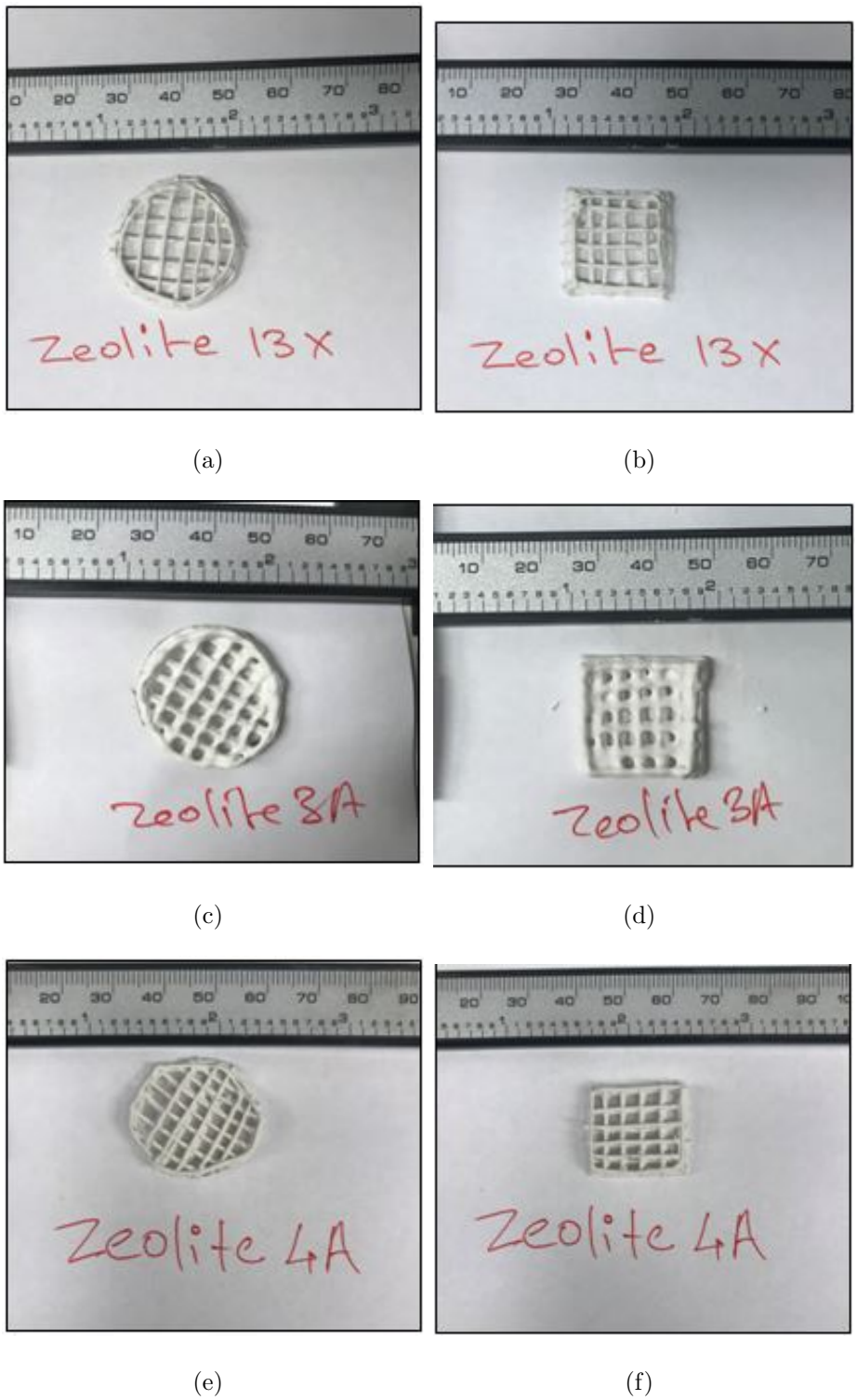

(a) (b)

(c) (d)

(e) (f)

Fig. 2.6.: 3D - Printed Zeolite samples : (a) After drying(circular grate) (b) After drying(Square grate) (c) After drying(circular grate)(d) After drying(Square grate)(e) After drying(circular grate)(f) After drying(Square grate)

2.2.5 Sintering of 3D - Printed Zeolite

The 3D - Printed Zeolite samples will be initially dried at room temperature to partially remove the present water content. To allow the polymer linker (PVA) and methyl cellulose to accumulating high strength and to avoid skin cracking the 3D - Printed samples were placed into oven (MTI corporation) and heated at 100°C which will remove the remaining water content **(Fig 2.7)**. After heating into an oven at 100°C the 3D - printed samples were sintered in a temperature controlled furnace at 700°C at the rate of 20°C /min for 2-4 hr. This will help in decomposing and removing the co-binder, methyl cellulose, and PVA. Sintering removes the organic content which results in increased mesoporosity of the 3D - Printed Zeolite sample, in addition also enhances the mechanical strength of the 3D - Printed Zeolite.

Fig. 2.7.: Oven for sintering

The sintering temperature was kept same for all the Zeolite samples. After sintering was done at at 700°C the Zeolite samples were cooled at room temperature. **Fig 2.8 (a)** shows the Zeolite 4A square grate sample after being sintered. Some amount of

shrinkage was seen after sintering along with some cracks which is shown in **Fig 2.8 (b)**. The cracks were seen for all the 3D -printed Zeolite samples after sintering.

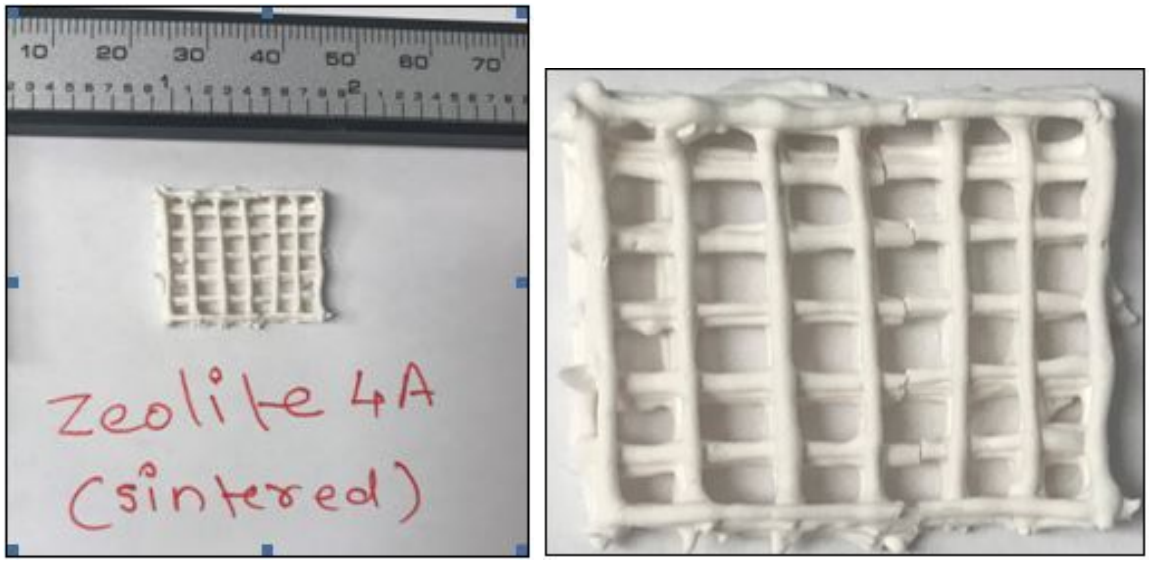

(a) (b)

Fig. 2.8.: Zeolite 4A samples(sintered) : (a) Square grate (b) Magnified image

2.2.6 Characterization of Zeolite Monolith

We calculated the surface area of 3D Printed Zeolite 13X monolith samples using the gas analyzer (Quantachrome Instruments). Physisorption isotherms of N_2 were collected at 77K for determining the textural properties of 3D printed Zeolite 13x monoliths. Degassing of all the 3D printed sample was carried out before all the measurements using degassing equipment (Autosorb iQ Station 2, Quantachrome Instruments) at 300°C for 3 h. After degassing the isotherms will be used for evaluating the surface area. X-ray Diffractometer (Rigaku Miniflex ,Tokyo, Japan) was used for X-ray diffraction (XRD) with 0.02o/step at the rate of 147.4 s/step. Structural morphology of 3D - printed Zeolite samples was studied using scanning electron mi-

croscope (SEM), along with Energy - Dispersive X-ray Spectroscopy (EDS) analysis for composition percentage. (JEOL Model JSM-5610, Tokyo, Japan)

2.2.7 Mechanical Testing

The micro-hardness of 3D - Printed Zeolite samples before and after sintering are calculated using Vickers hardness test. We selected microhardness test due to the size and geometry of the 3D - Printed Zeolite samples. The Vicker hardness tester (Model 900-391, Phase II, Upper Saddle River, NJ, USA) shown in **Fig. 2.9** was used for measuring the micro-hardness. The specimens for hardness test were prepared using hot mounting press (EQ-MP-300 Mounting Press, MTI Corporation) shown in **Fig. 2.10** The indentation tests for Vicker hardness test were performed on the top surface of the mounting specimen at room temperature. The indentation was done at load for 15 sec. The indent mark for Zeolite 3A before sintering is shown in **Fig 2.11**

Fig. 2.9.: Vicker Hardness Tester

Fig. 2.10.: Hot mounting press

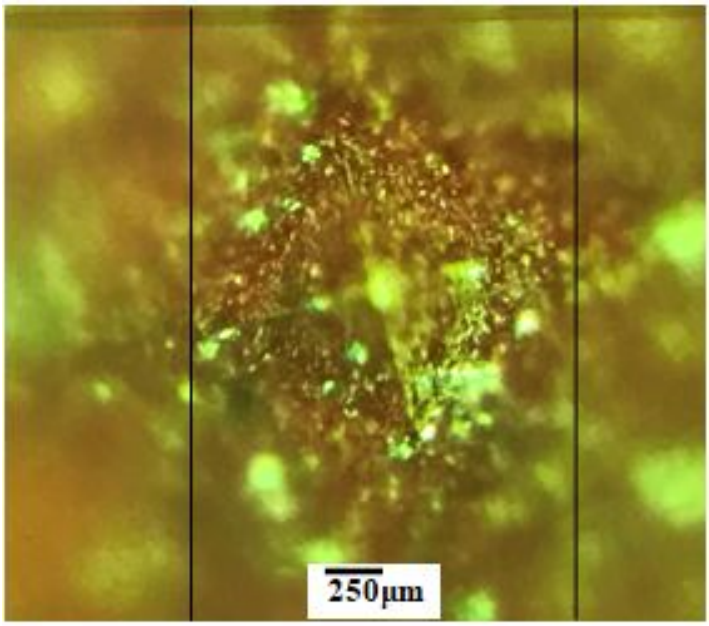

Fig. 2.11.: Indent mark on unsintered Zeolite 3A sample

2.3 Results and Discussion

2.3.1 Physical Properties of 3D Printed Zeolite

Physisorption isotherms of N_2 collected at 77K of 3D printed Zeolite 13x monoliths showed uptake at low partial pressure (P/P∘) as per **Fig. 2.12** which clearly indicated the adsorption in the micropores of Zeolite 13X.The gradual increase of uptake at high P/Po with the hysteresis was seen, indicates the capillary condensation in mesopores. [48] The BET surface area for 3D printed Zeolite 13X was found out to be 767m^2/g, using a Multi-Point BET plot shown in **Fig. 2.13**

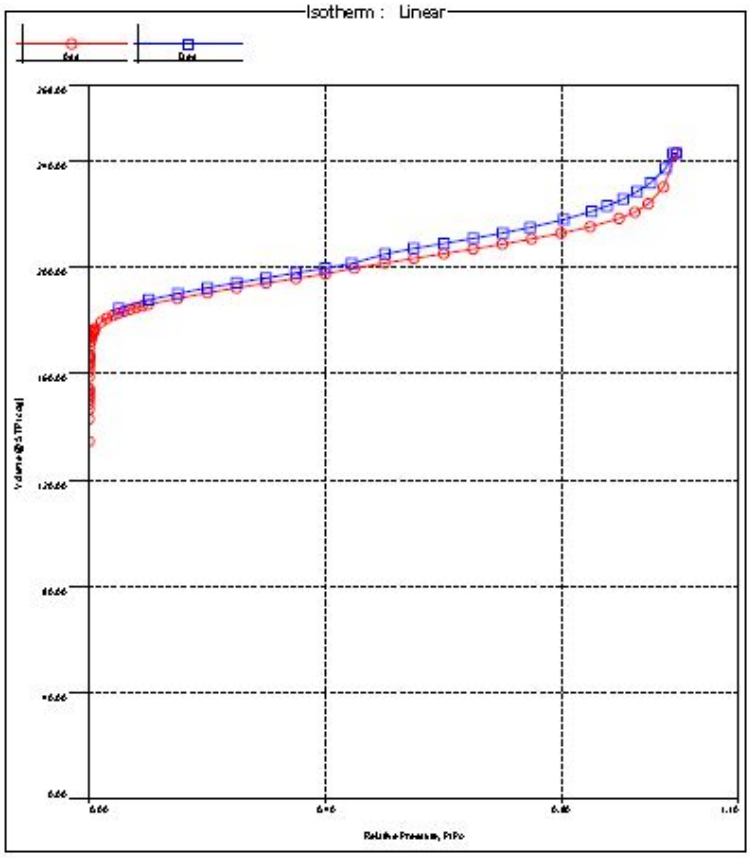

Fig. 2.12.: N_2 physisorption isotherm for 3D printed Zeolite 13X

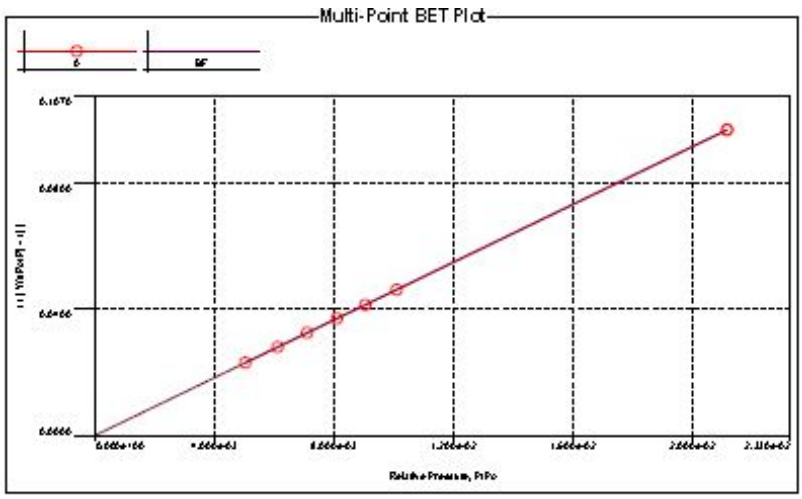

Fig. 2.13.: Multi-point BET plot of Zeolite 13X

2.3.2 Structural Properties of 3D - Printed Zeolite

Micro-structure and composition of the 3D-printed zeolite samples before and after sintering were analyzed using SEM and EDS, respectively. SEM images with low- magnification and high-magnification for 3D - Printed Zeolite 13X, 3A, 4A, and 5A samples before sintering and after sintering (a-l) are shown in **Fig.2.14 - Fig. 2.37** respectively.The magnified view of the channel structure is shown in **Fig.2.21** (c) and (d) for Zeolite 3A clearly illustrates the macroporous nature of the walls, with pores in the range of 5-50μm. The SEM image shown in **Fig.2.24** (i) and (j) of Zeolite 3A particles at 5 μm shows more cohesiveness of particles after sintering which resulted in increased strength. Visual comparison of the SEM image at 2.5μm shows that the particle shape for all the Zeolite at green state was nearly cubical except for Zeolite 13X which was rather more irregular.Moreover, the SEM images of all the 3D - printed Zeolite samples indicate that the particle distribution was even and not disturbed after vigorous stirring during slurry preparation and some particle agglomeration was observed after sintering. The sintered bodies were easily broken compared to the green bodies, indicating the post-heat treatment should be controlled to give some mechanical properties to the sintered body. The phase did

not change after sintering in all samples. It was hard to find the difference in the microstructure, composition, and phase before and after heat treatment. The EDS analysis of all the Zeolite samples was done and compared with the standard EDS analysis provided by the company. As we can see from **Fig. 2.38 Fig. 2.41** there is not that much change

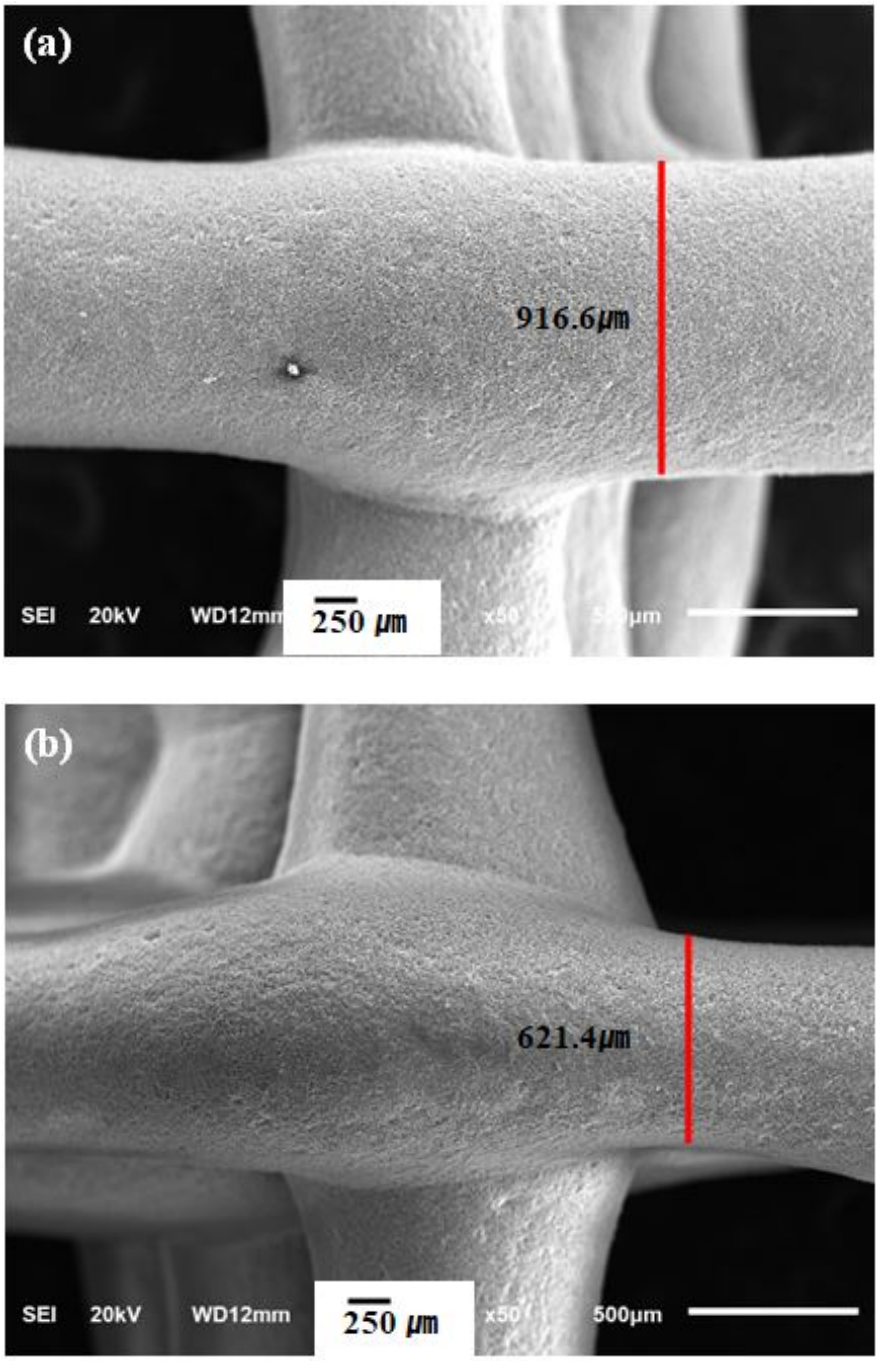

Fig. 2.14.: SEM Images of (a) green state Zeolite 13X and (b) sintered Zeolite 13X 3D - printed monoliths at 250μm magnification

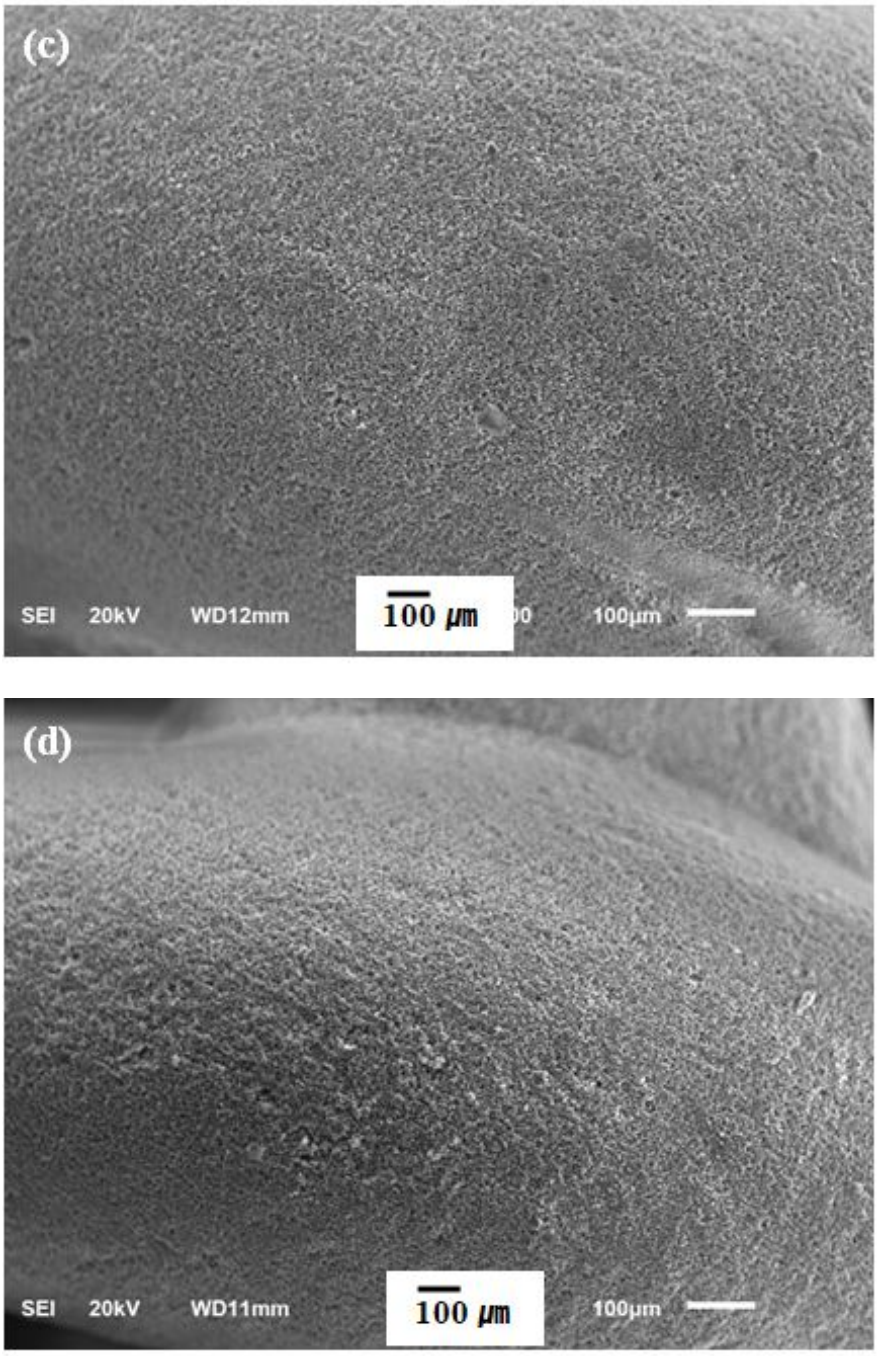

Fig. 2.15.: SEM Images of (c) green state Zeolite 13X and (d) sintered Zeolite 13X 3D - printed monoliths at 100μm magnification

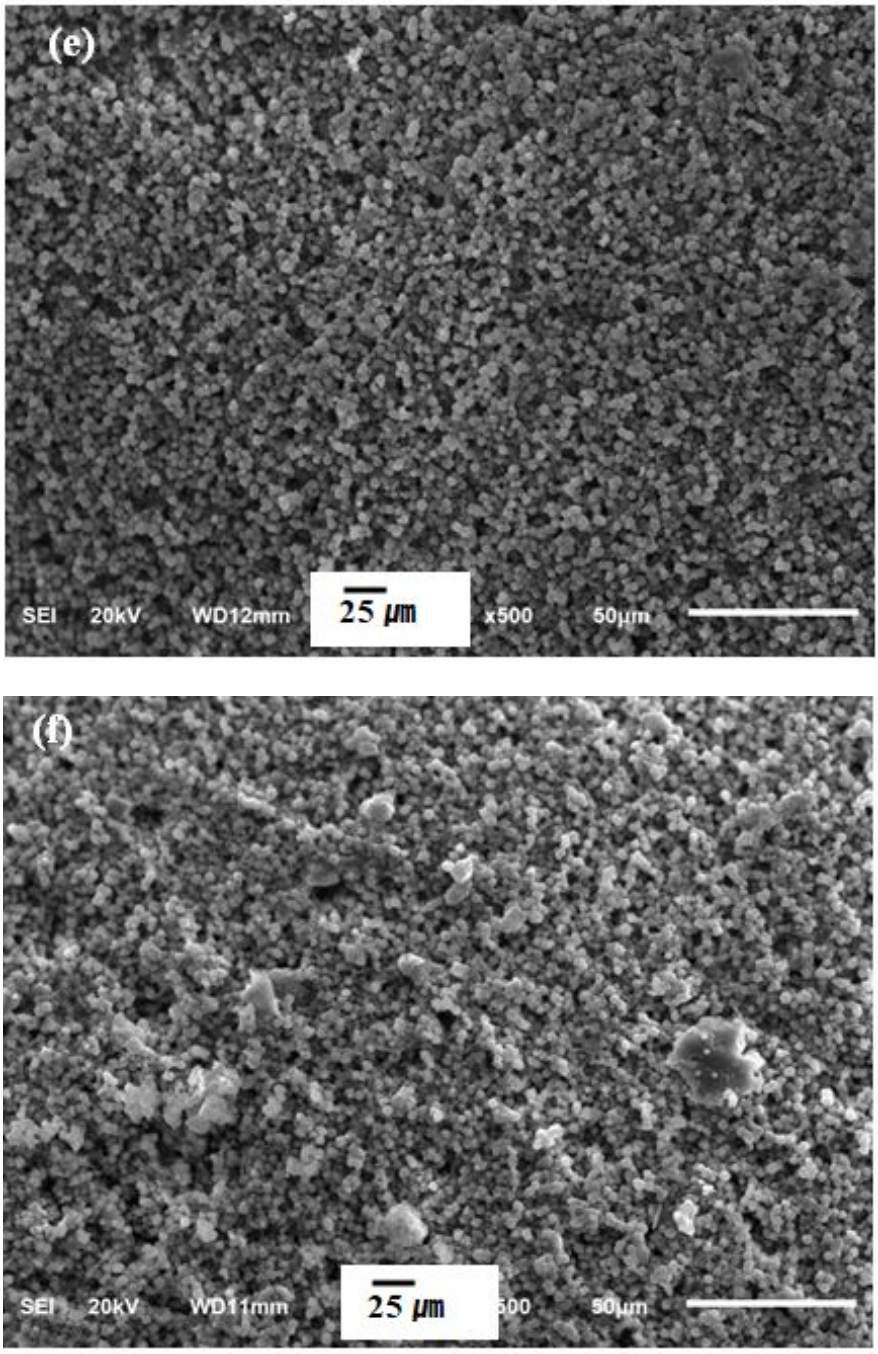

Fig. 2.16.: SEM Images of (e) green state Zeolite 13X and (f) sintered Zeolite 13X 3D - printed monoliths at 25μm magnification

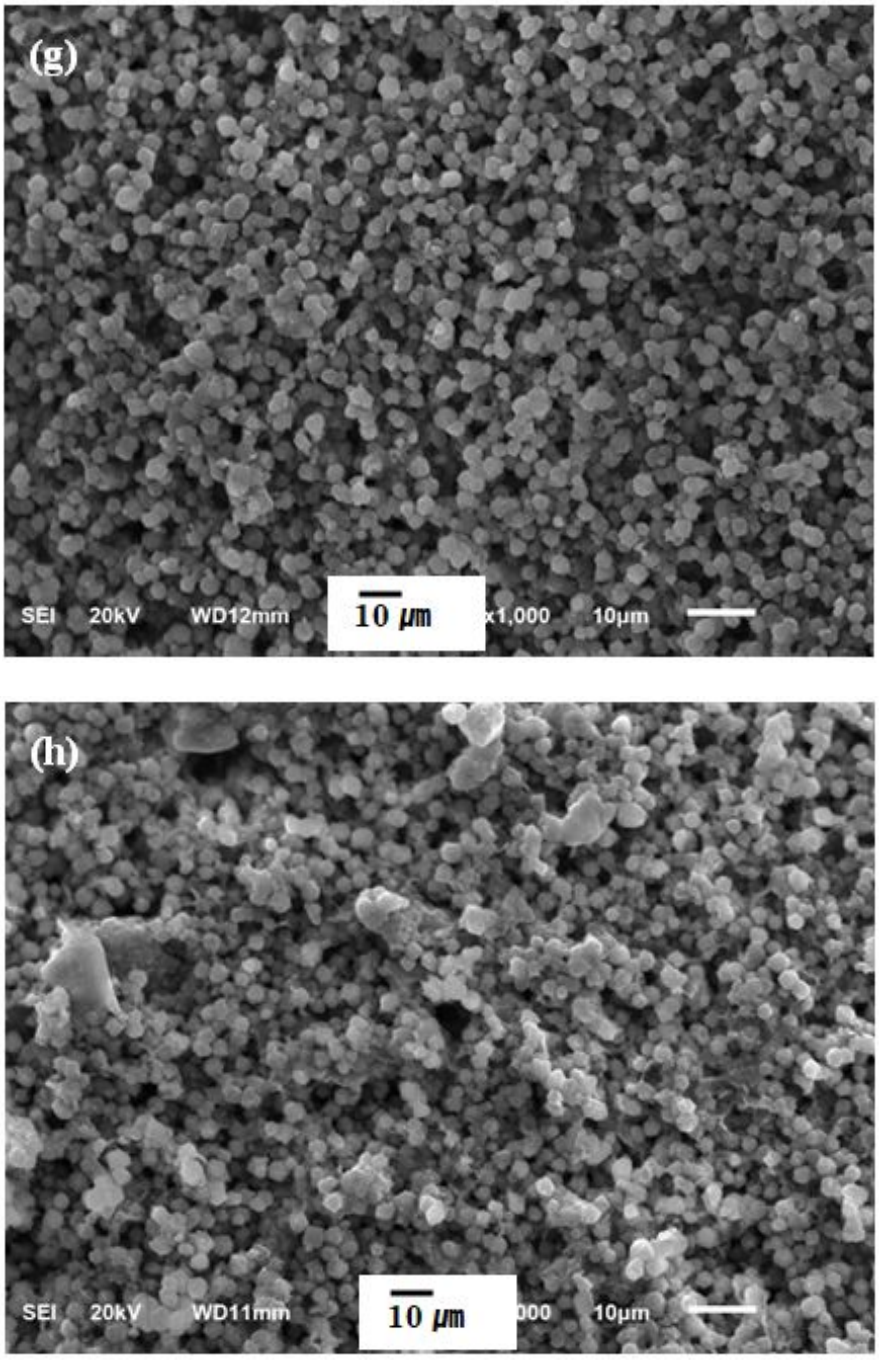

Fig. 2.17.: SEM Images of (g) green state Zeolite 13X and (h) sintered Zeolite 13X 3D - printed monoliths at 10μm magnification

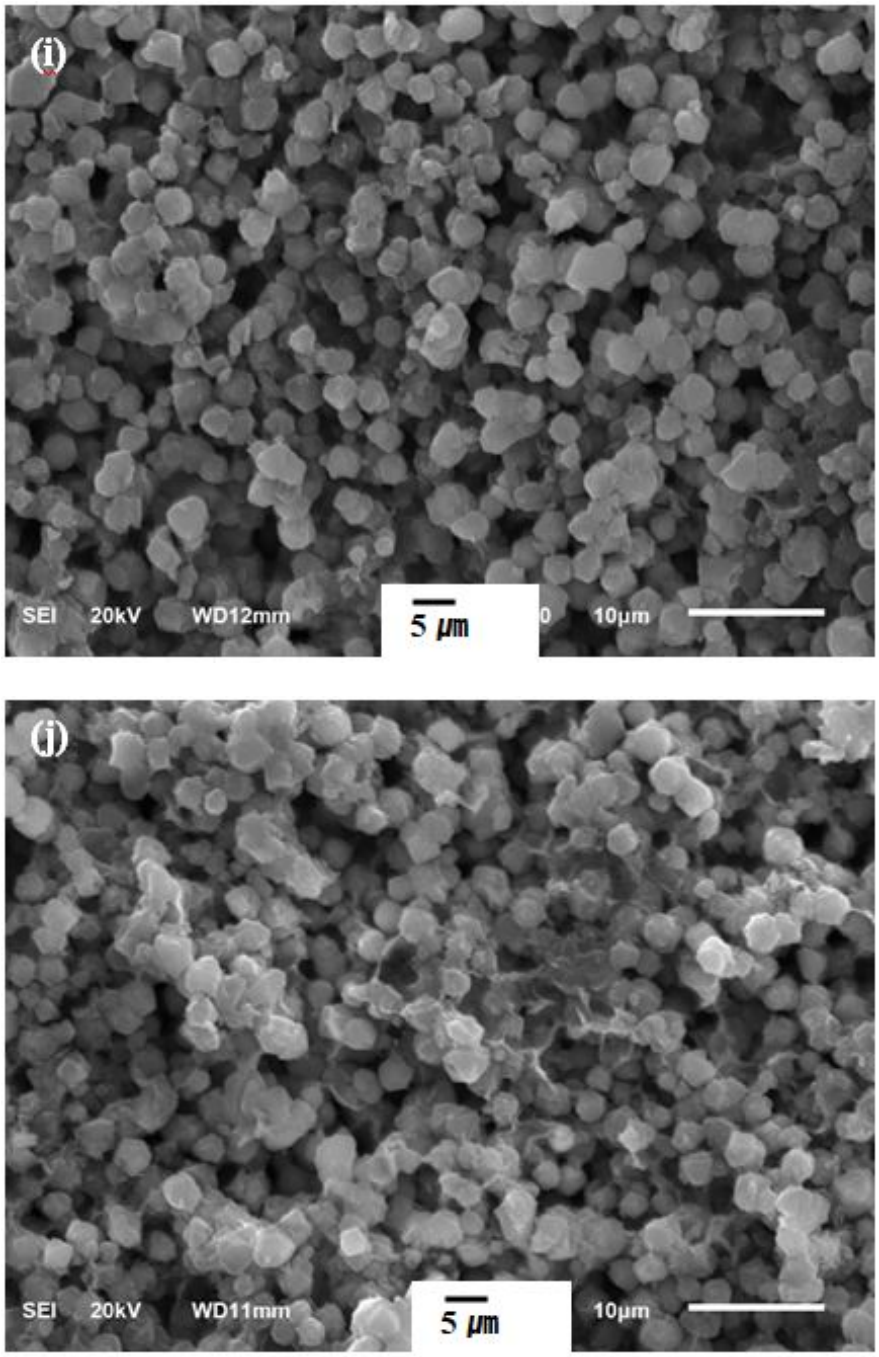

Fig. 2.18.: SEM Images of (i) green state Zeolite 13X and (j) sintered Zeolite 13X 3D - printed monoliths at 5μm magnification

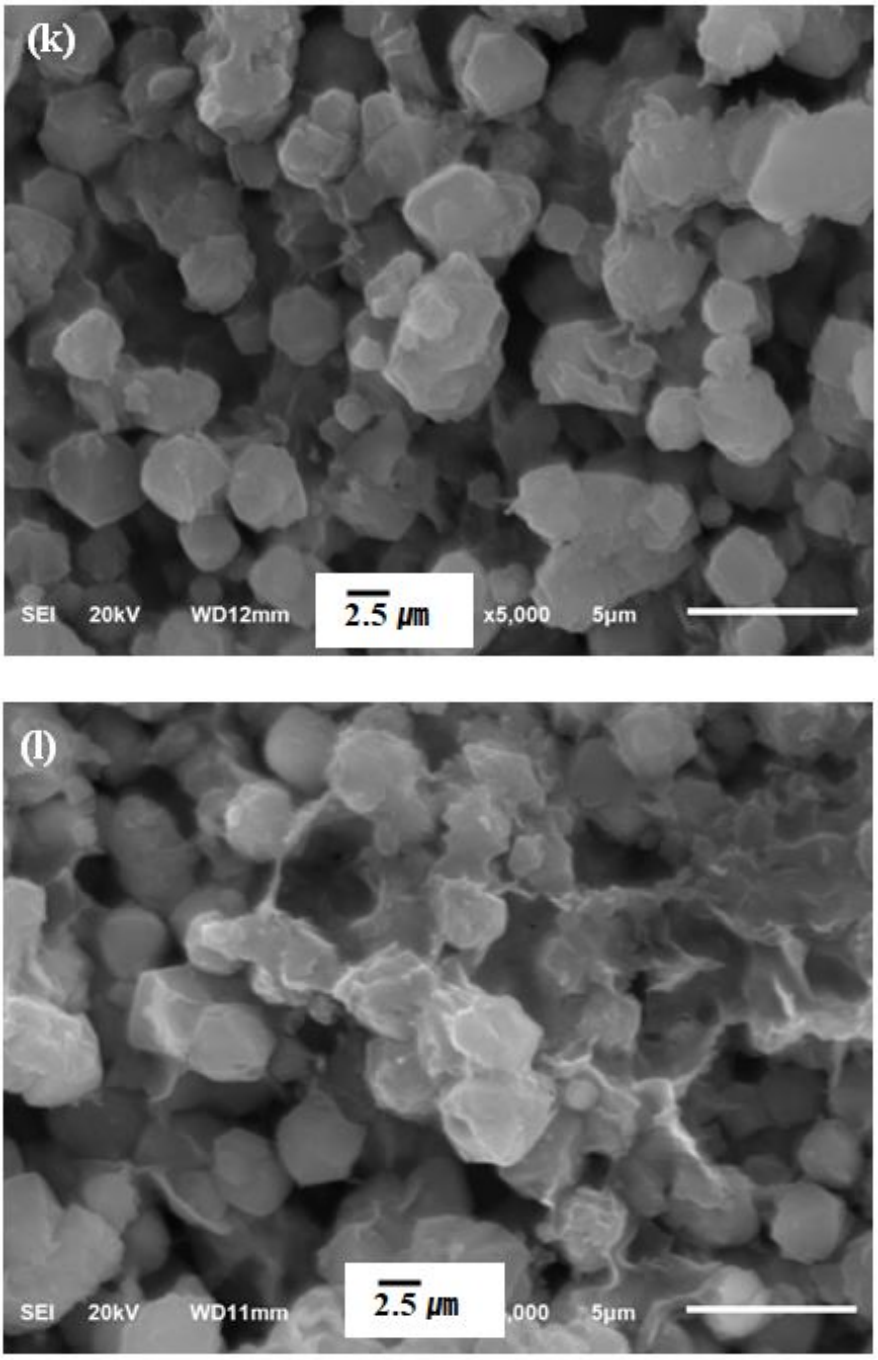

Fig. 2.19.: SEM Images of (k) green state Zeolite 13X and (l)sintered Zeolite 13X 3D - printed monoliths at 2.5μm magnifications

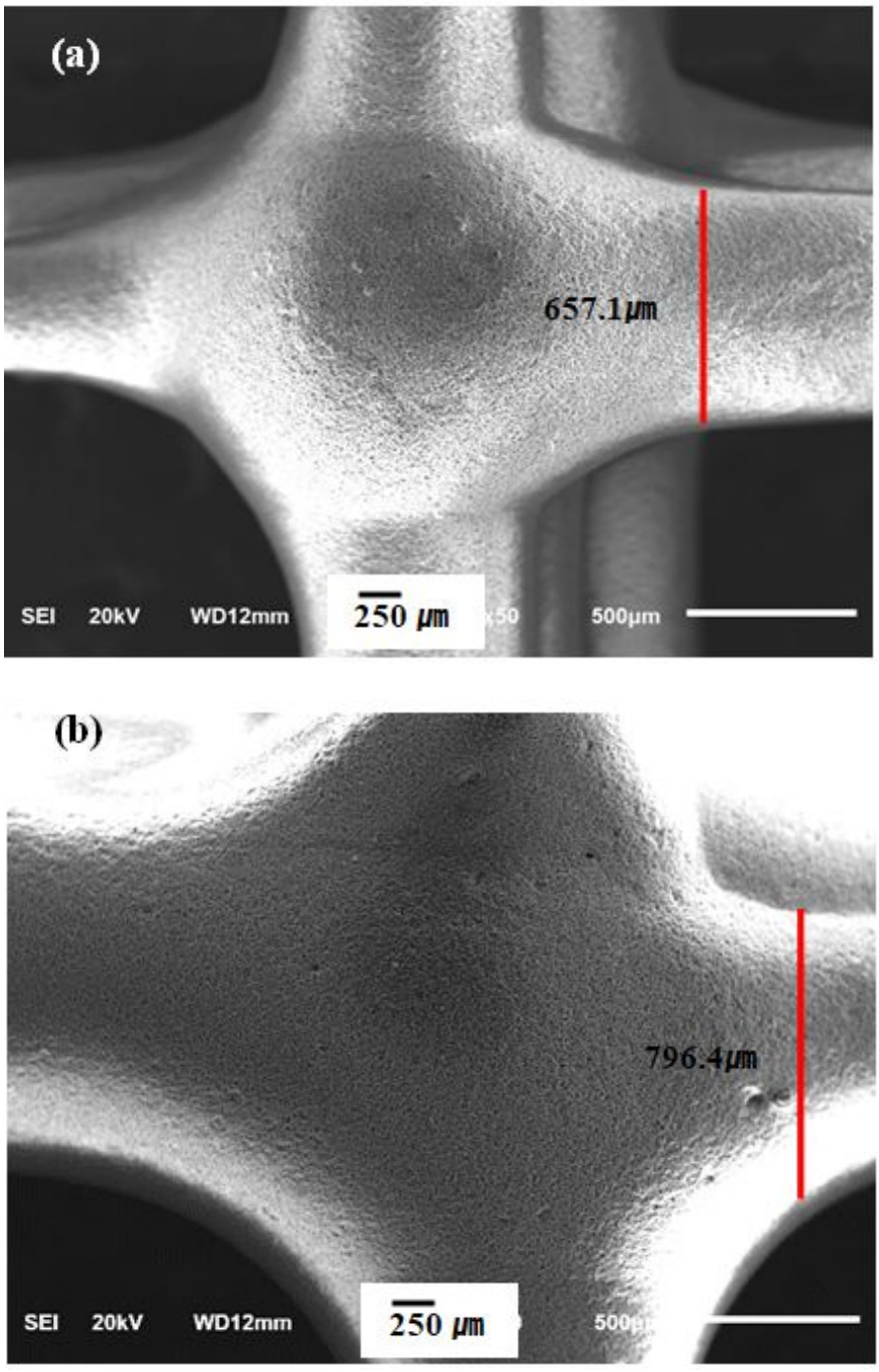

Fig. 2.20.: SEM Images of (a) green state Zeolite 3A and (b) sintered Zeolite 3A 3D - printed monoliths at 250μm magnification

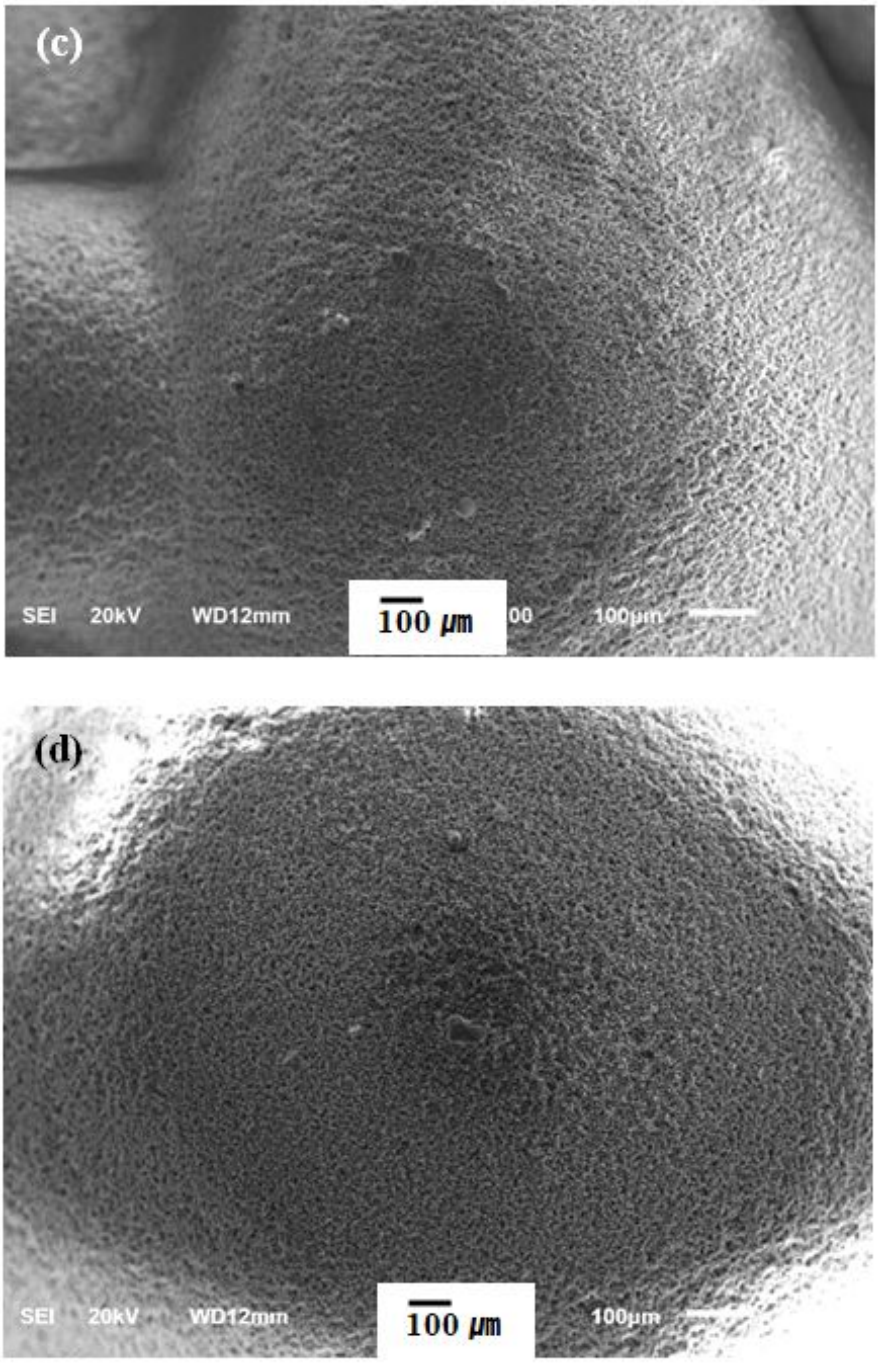

Fig. 2.21.: SEM Images of (c) green state Zeolite 3A and (d) sintered Zeolite 3A 3D - printed monoliths at 100μm magnification

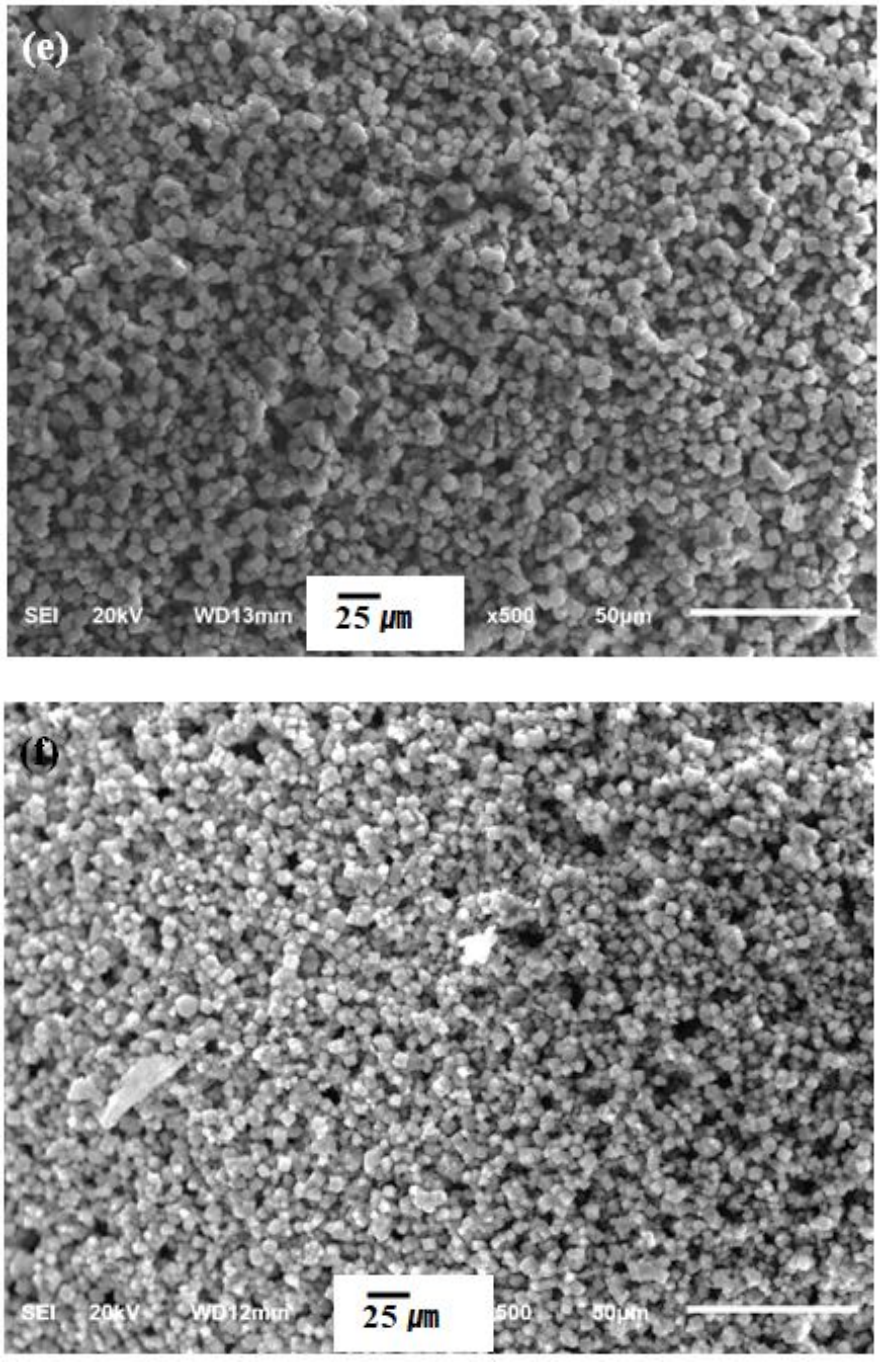

Fig. 2.22.: SEM Images of (e) green state Zeolite 3A and (f) sintered Zeolite 3A 3D - printed monoliths at 25μm magnification

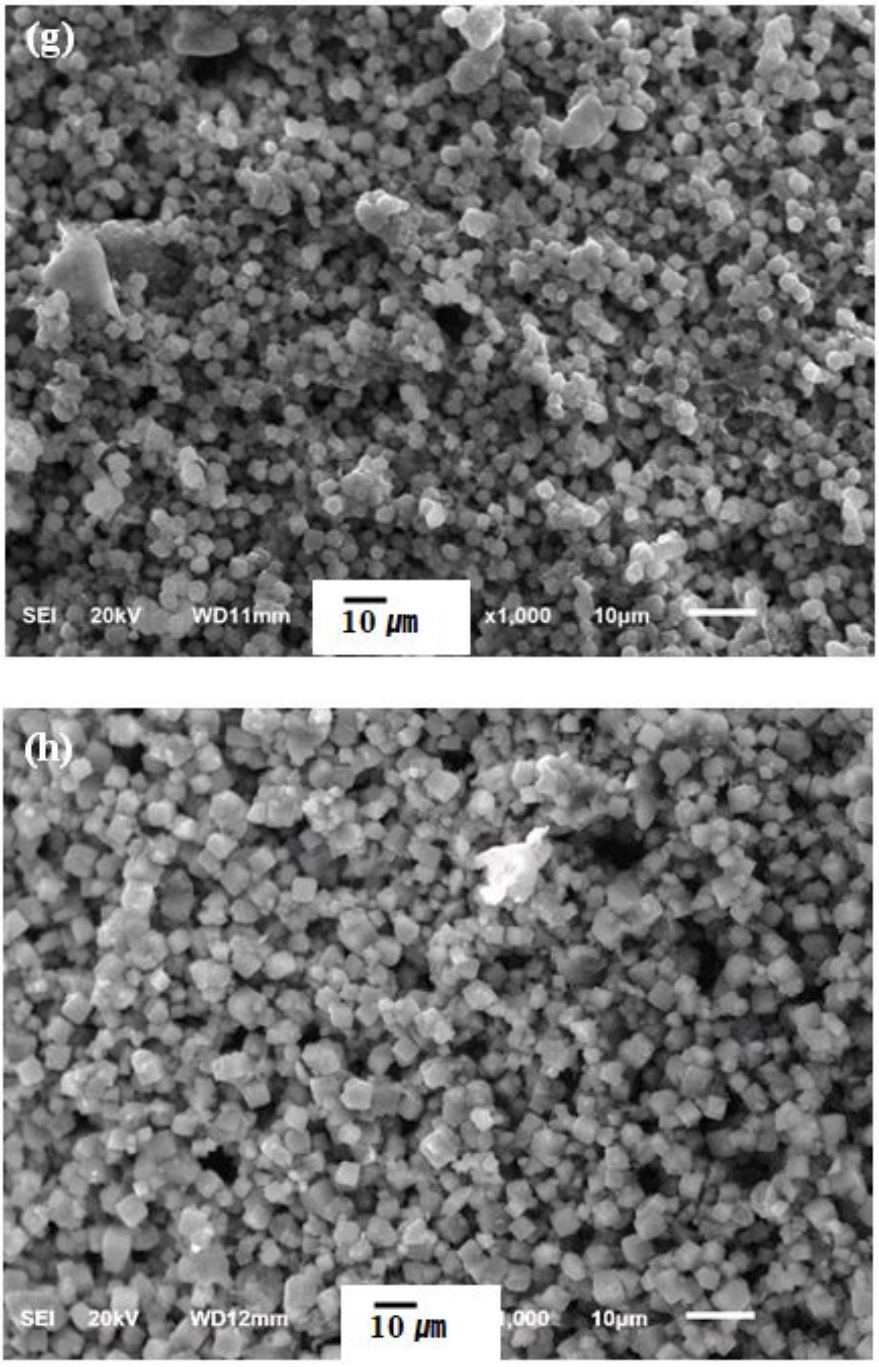

Fig. 2.23.: SEM Images of (g) green state Zeolite 3A and (h) sintered Zeolite 3A 3D - printed monoliths at 10μm magnification

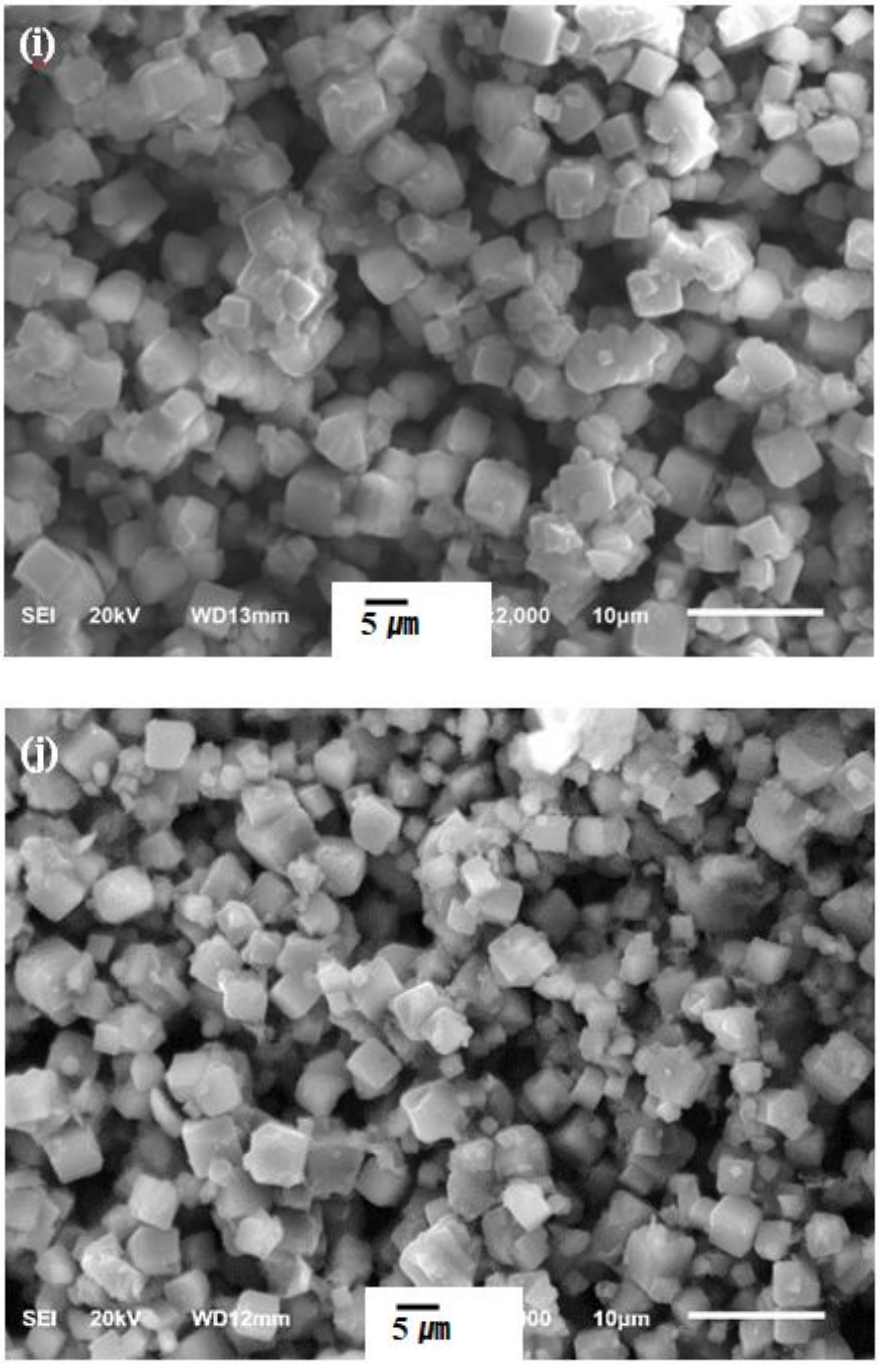

Fig. 2.24.: SEM Images of (i) green state Zeolite 3A and (j) sintered Zeolite 3A 3D - printed monoliths at 5μm magnification

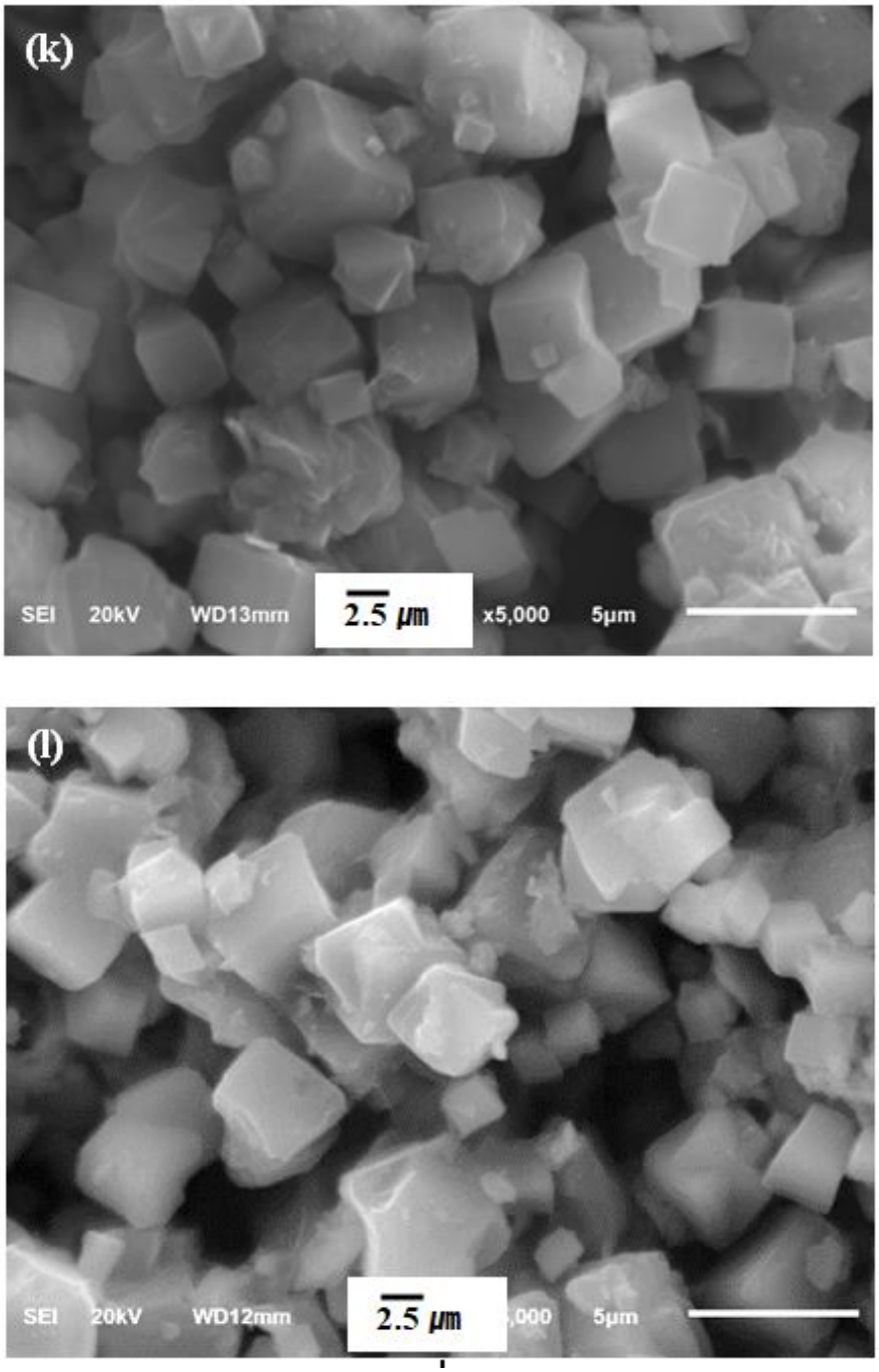

Fig. 2.25.: SEM Images of (k) green state Zeolite 3A and (l) sintered Zeolite 3A 3D - printed monoliths at 2.5μm magnification

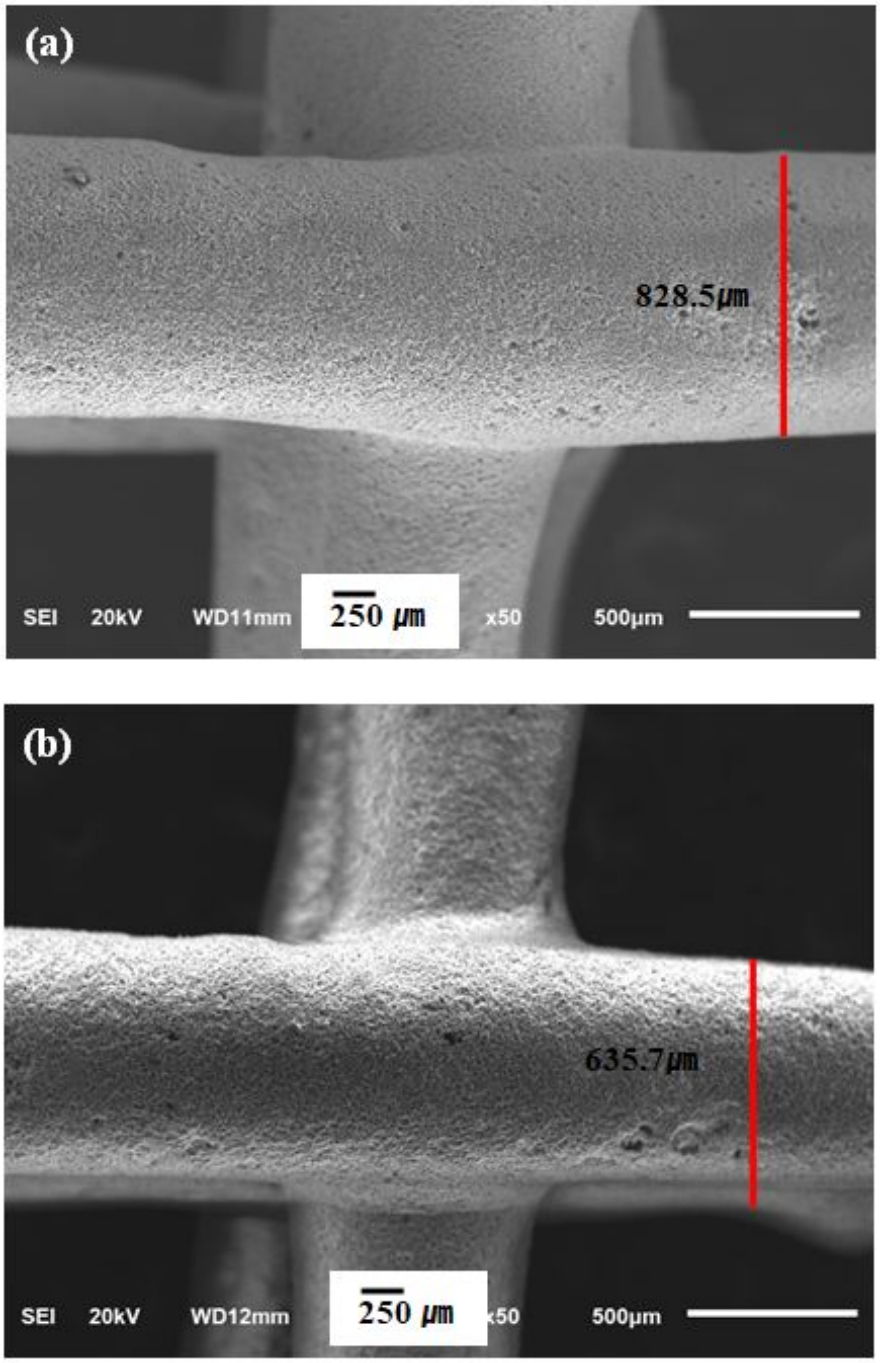

Fig. 2.26.: SEM Images of (a) green state Zeolite 4A and (b) sintered Zeolite 4A 3D - printed monoliths at 250μm magnification

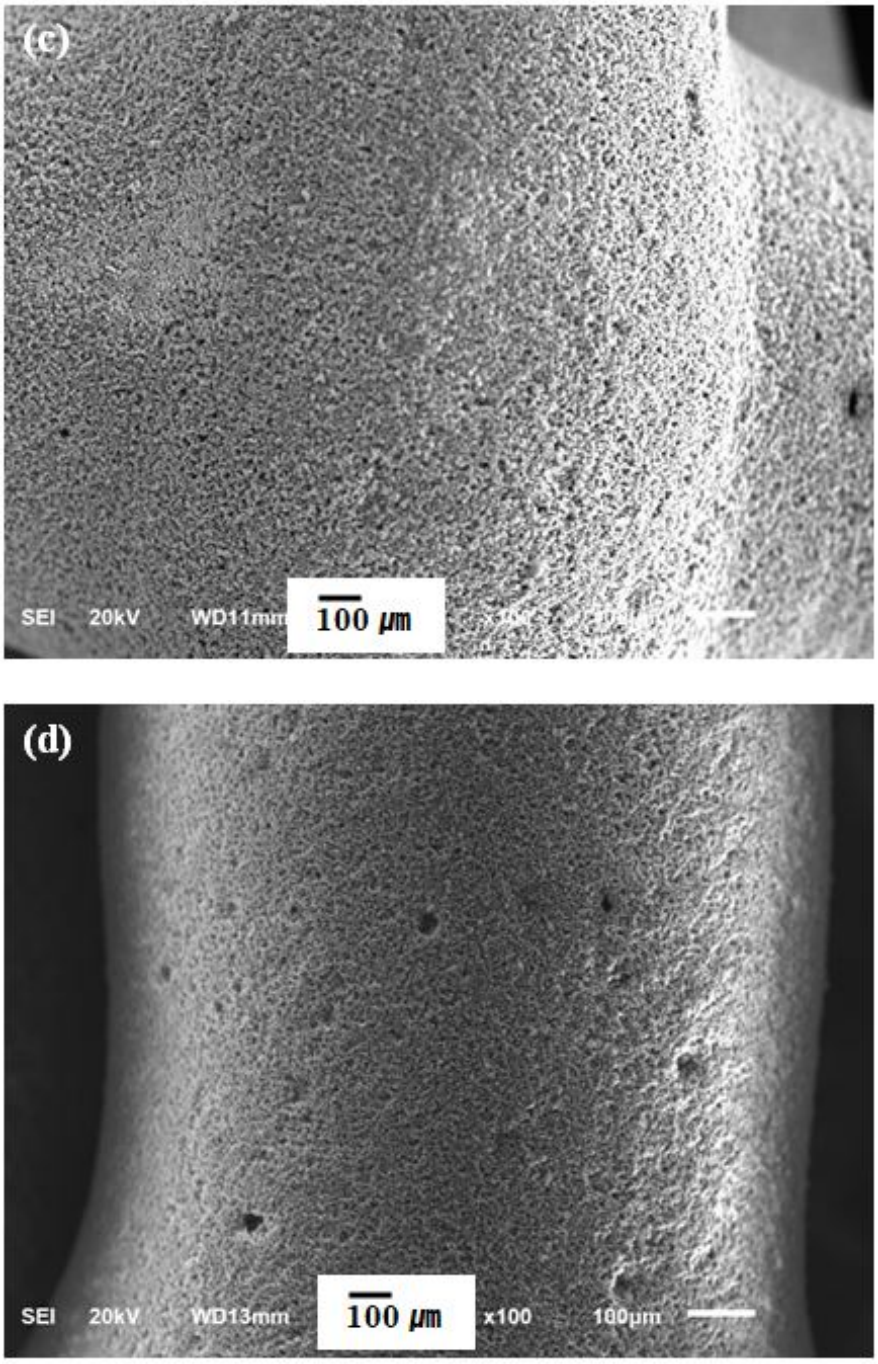

Fig. 2.27.: SEM Images of (c) green state Zeolite 4A and (d) sintered Zeolite 4A 3D - printed monoliths at 100μm magnification

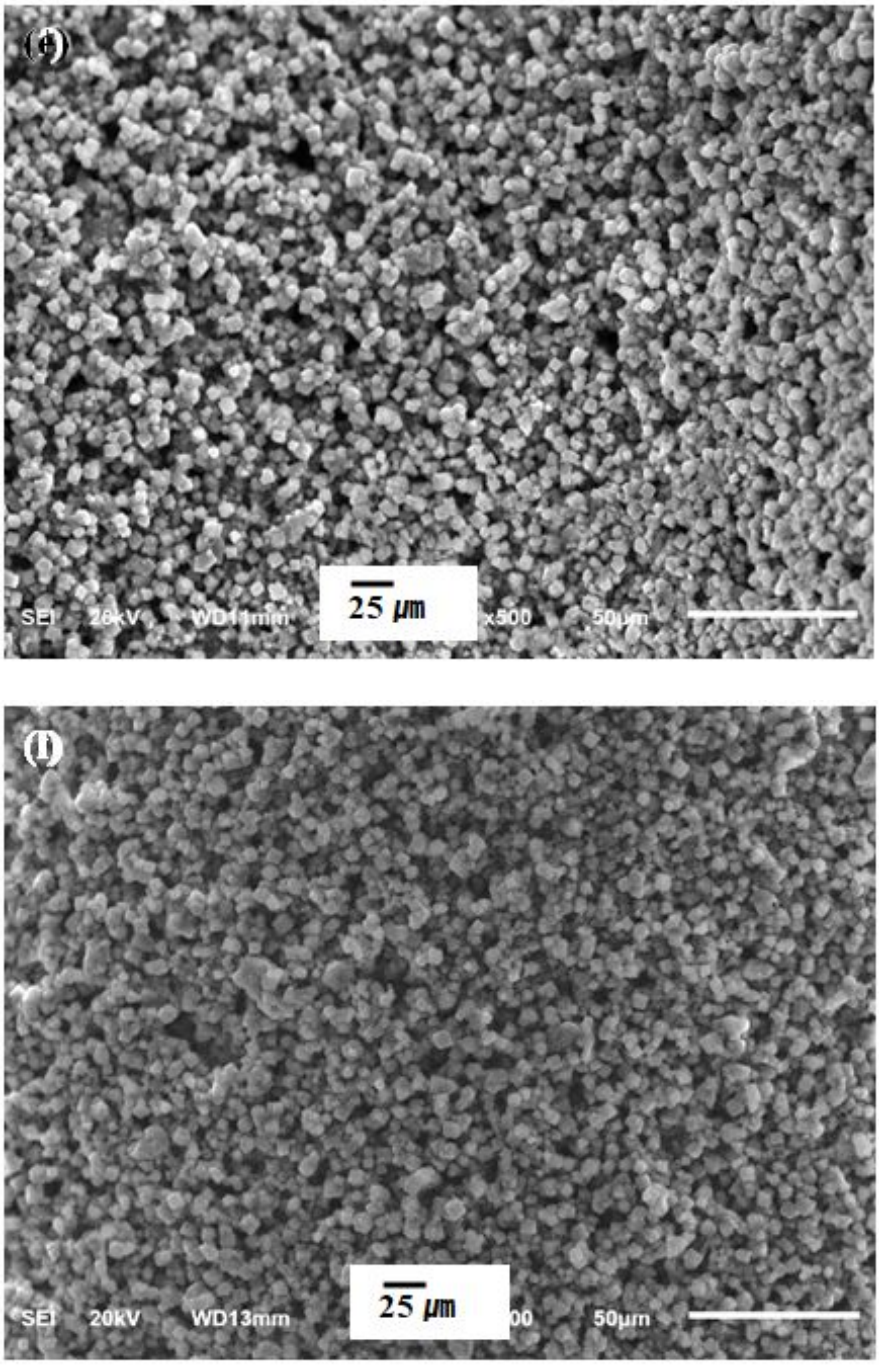

Fig. 2.28.: SEM Images of (e) green state Zeolite 4A and (f) sintered Zeolite 4A 3D - printed monoliths at 25μm magnification

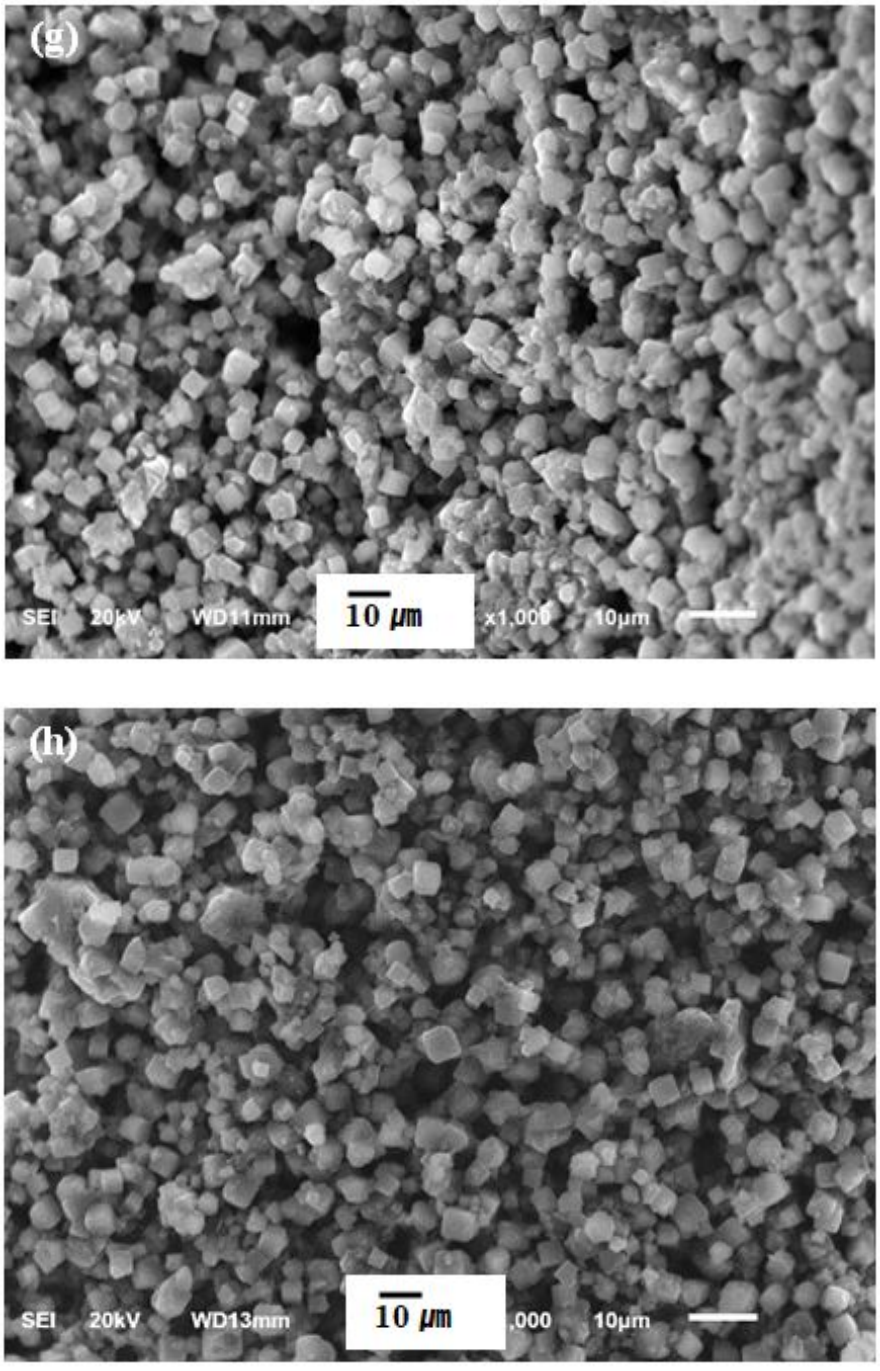

Fig. 2.29.: SEM Images of (g) green state Zeolite 4A and (h) sintered Zeolite 4A 3D - printed monoliths at 10μm magnification

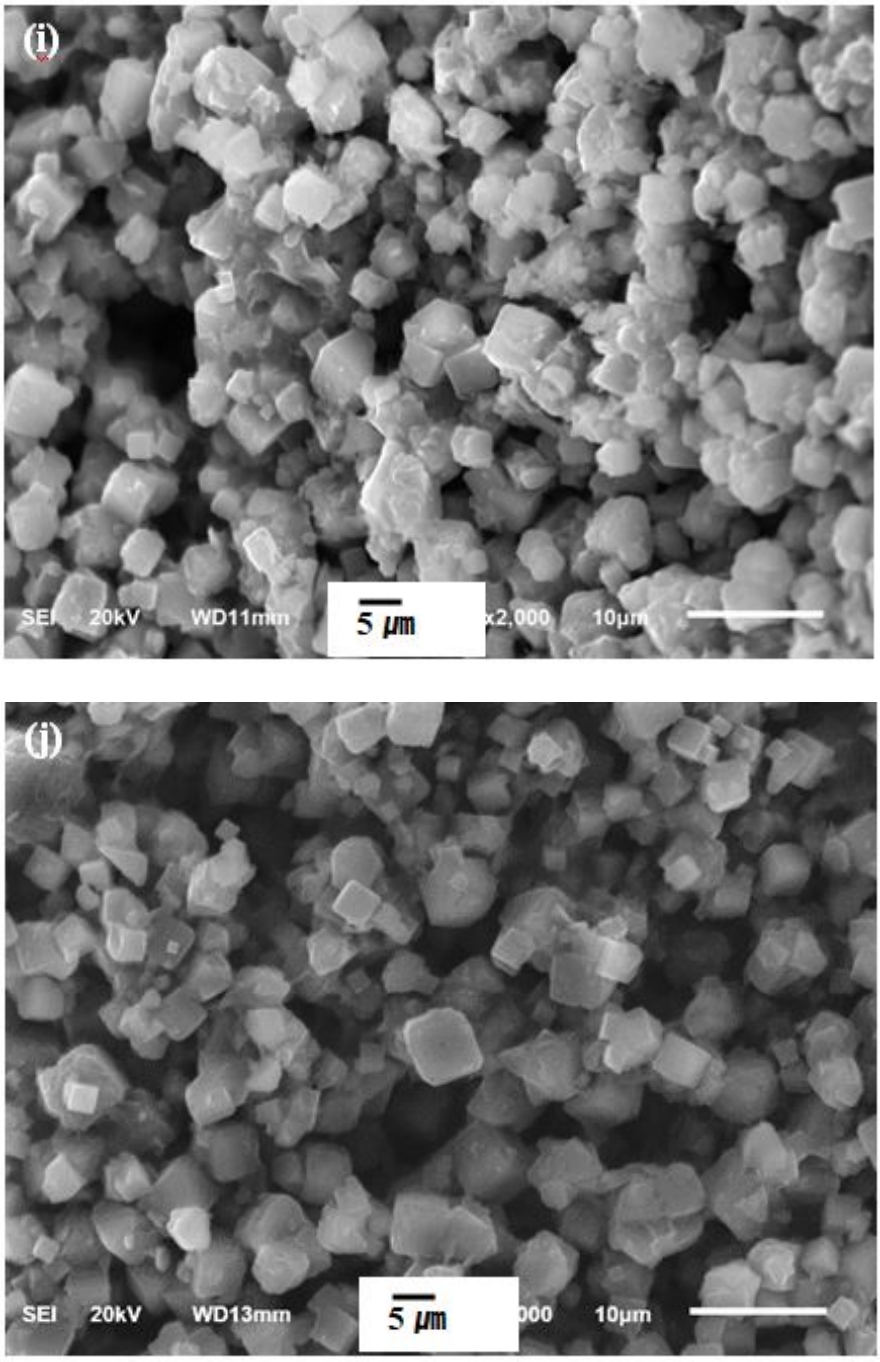

Fig. 2.30.: SEM Images of (i) green state Zeolite 4A and (j) sintered Zeolite 4A 3D - printed monoliths at 5μm magnification

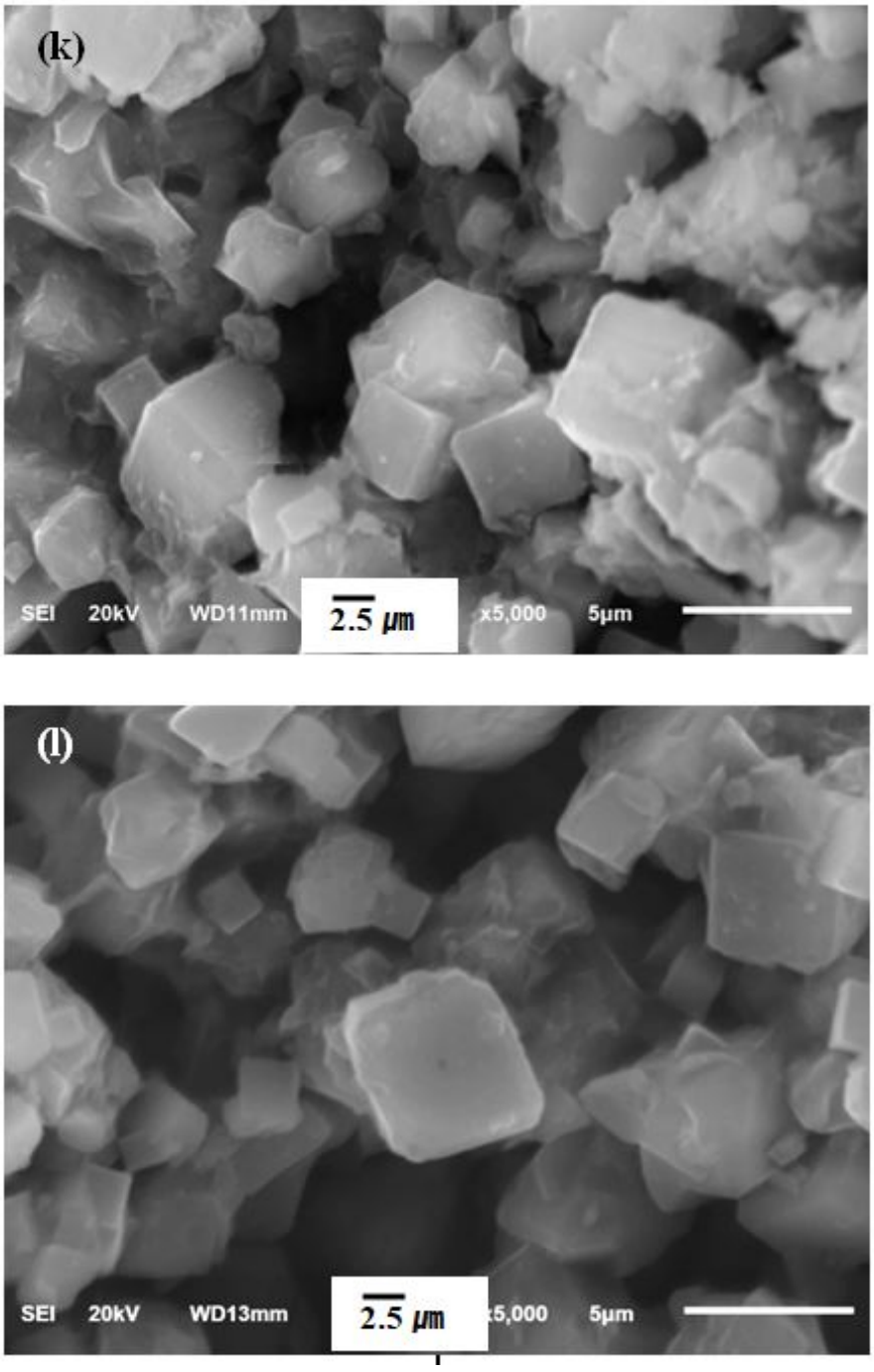

Fig. 2.31.: SEM Images of (k) green state Zeolite 4A and (l) sintered Zeolite 4A 3D - printed monoliths at 2.5μm magnification

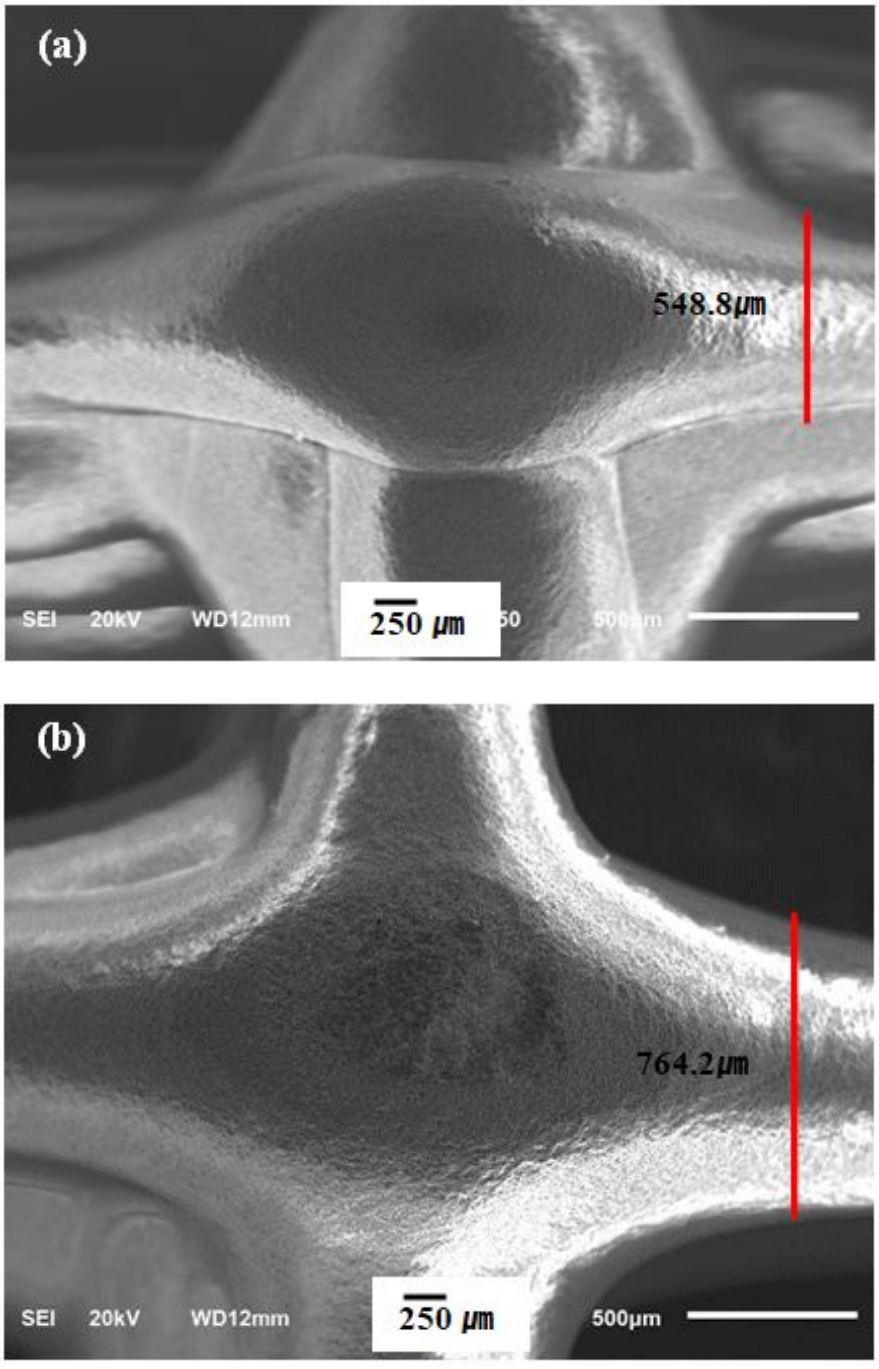

Fig. 2.32.: SEM Images of (a) green state Zeolite 5A and (b) sintered Zeolite 5A 3D - printed monoliths at 250μm magnification

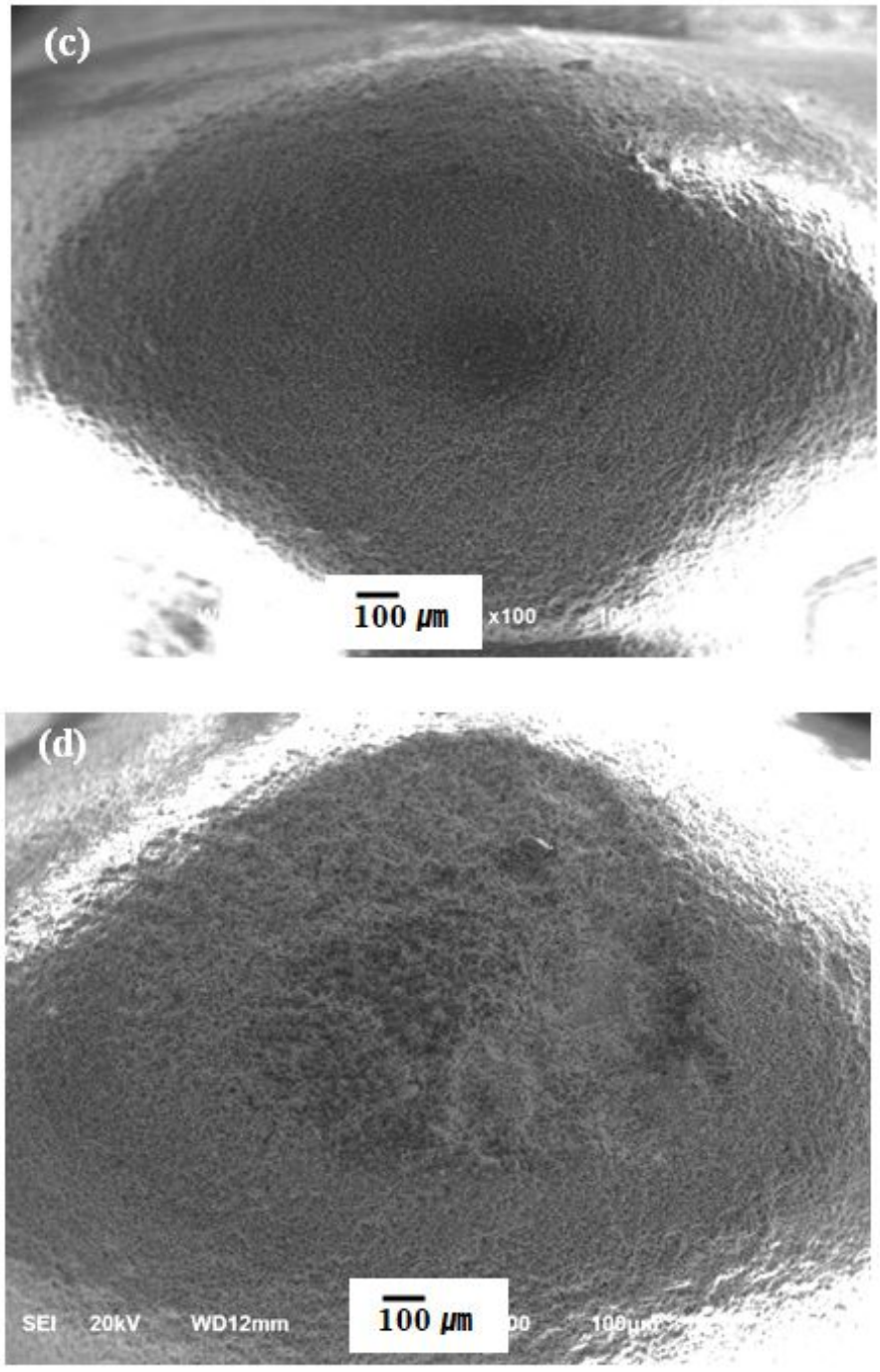

Fig. 2.33.: SEM Images of (c) green state Zeolite 5A and (d) sintered Zeolite 5A 3D - printed monoliths at 100μm magnification

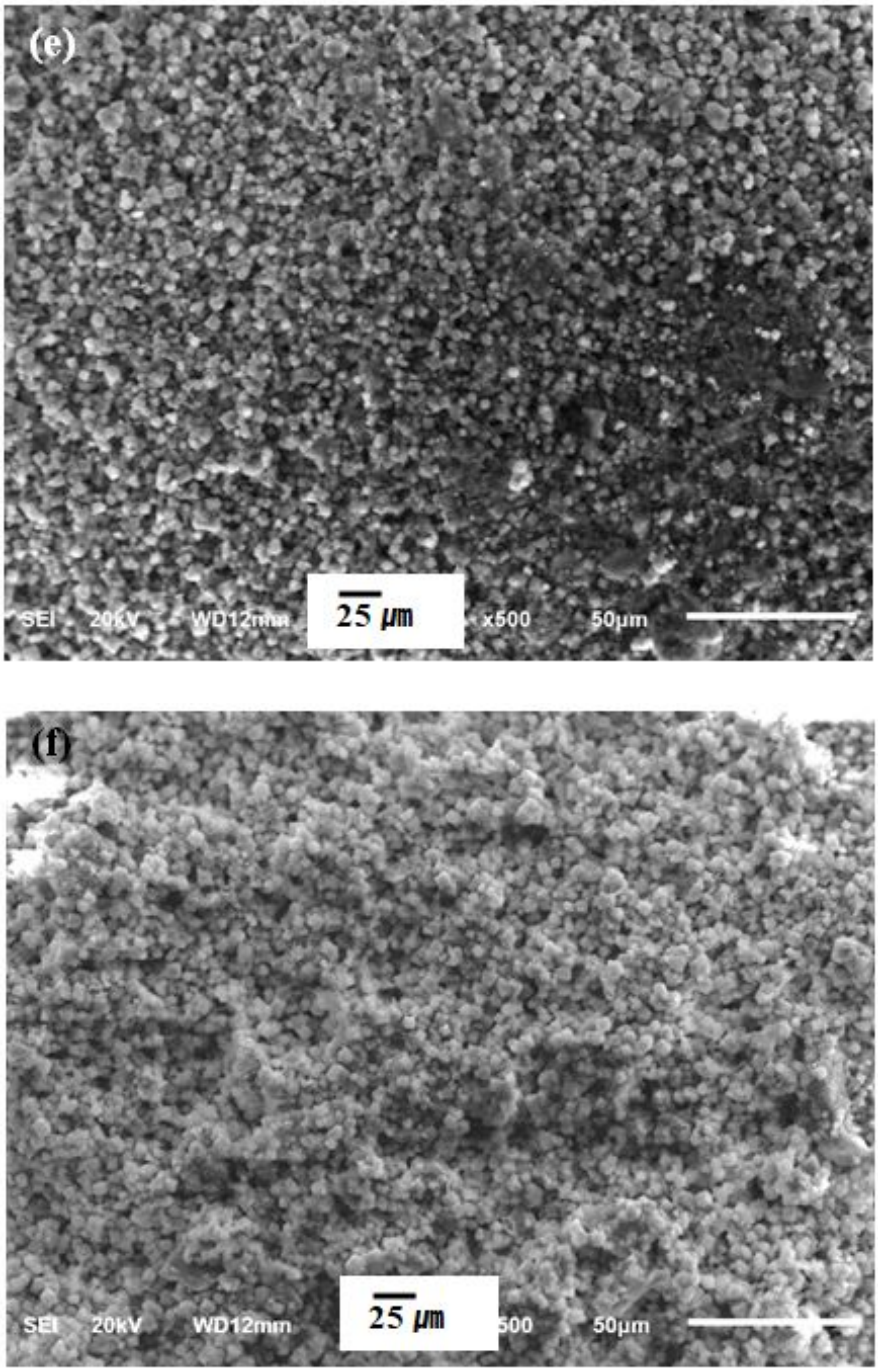

Fig. 2.34.: SEM Images of (e) green state Zeolite 5A and (f) sintered Zeolite 5A 3D - printed monoliths at 25μm magnification

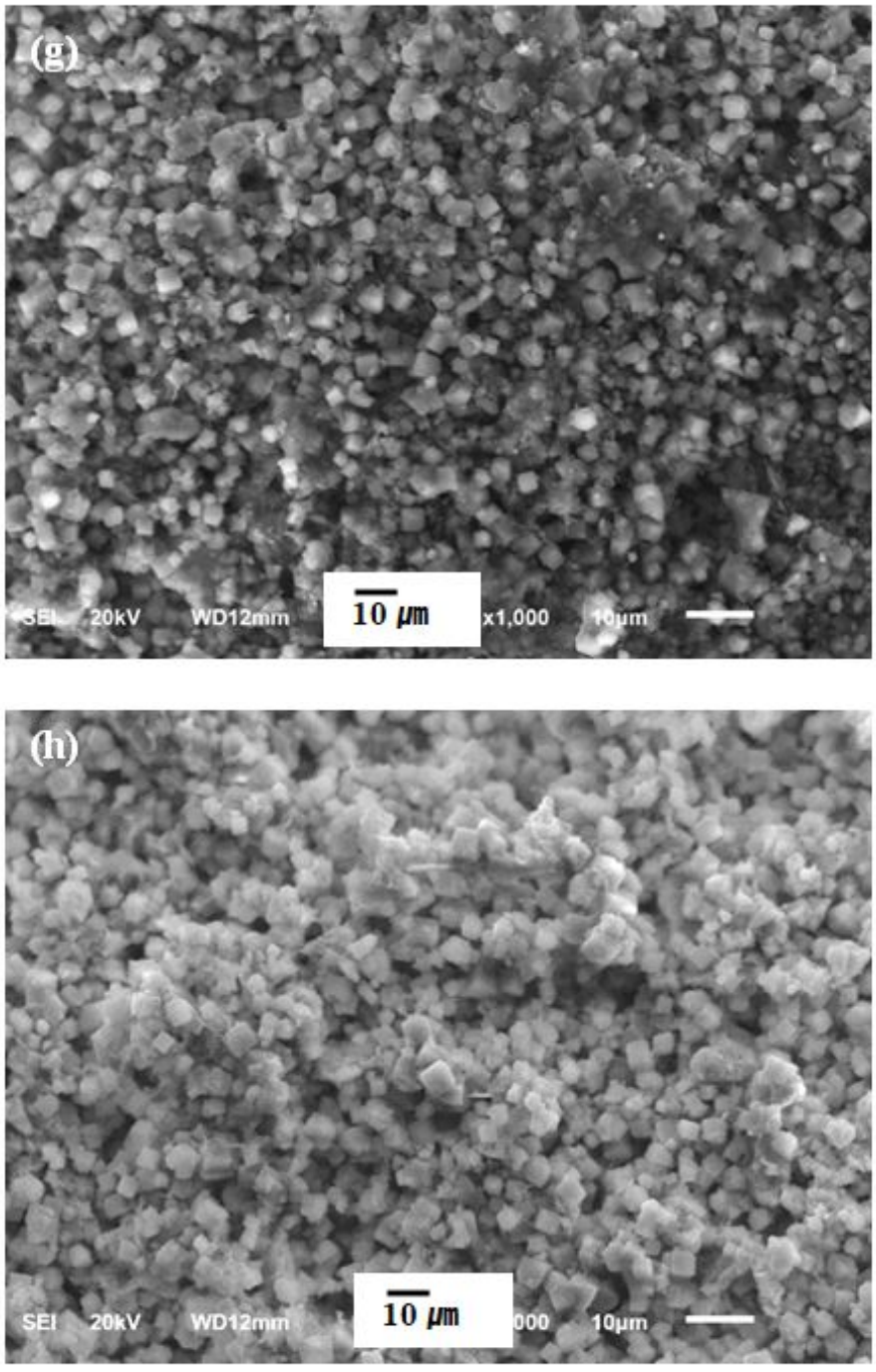

Fig. 2.35.: SEM Images of (g) green state Zeolite 5A and (h) sintered Zeolite 5A 3D - printed monoliths at 10μm magnification

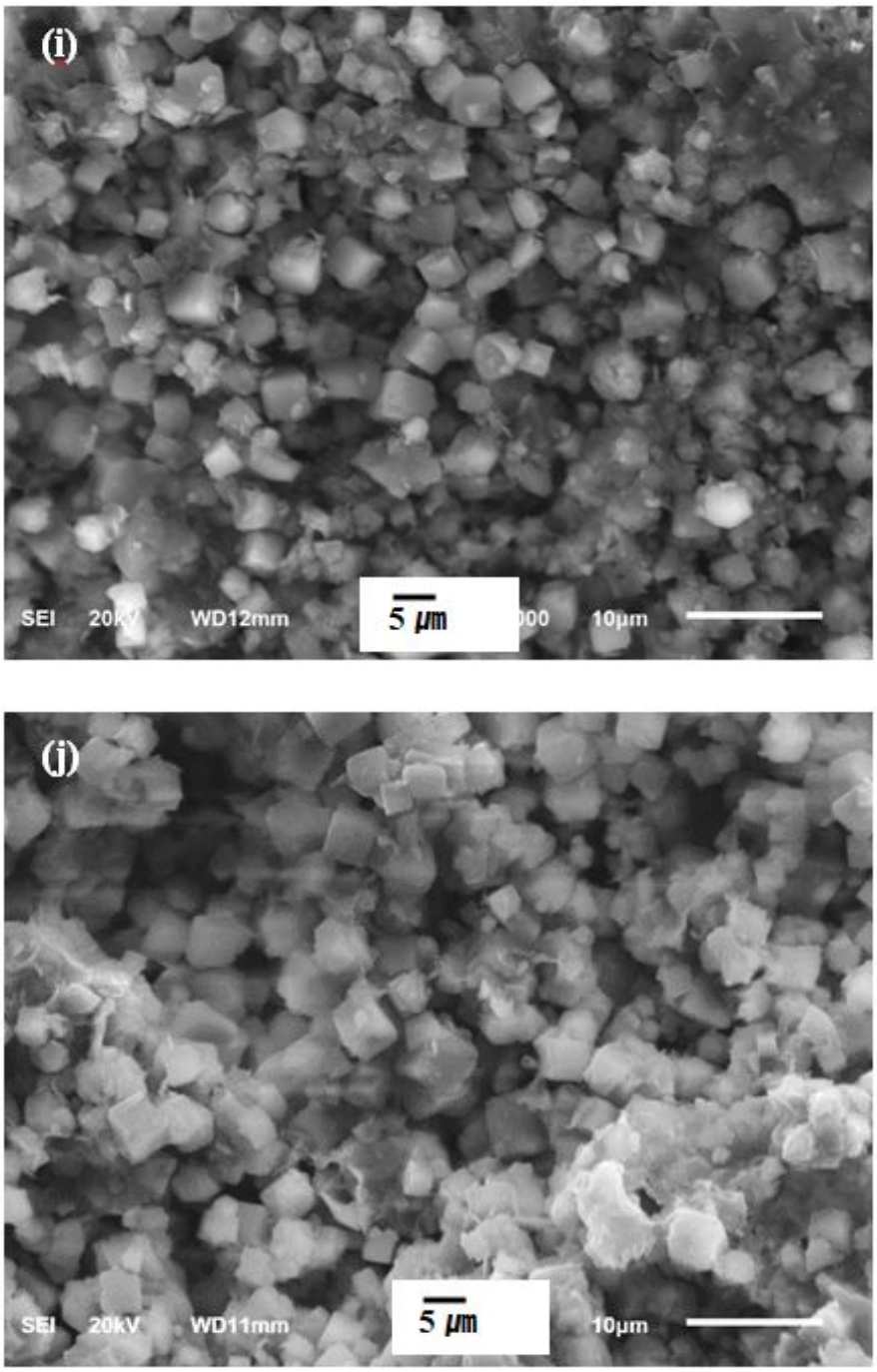

Fig. 2.36.: SEM Images of (i) green state Zeolite 5A and (j) sintered Zeolite 5A 3D - printed monoliths at 5μm magnification

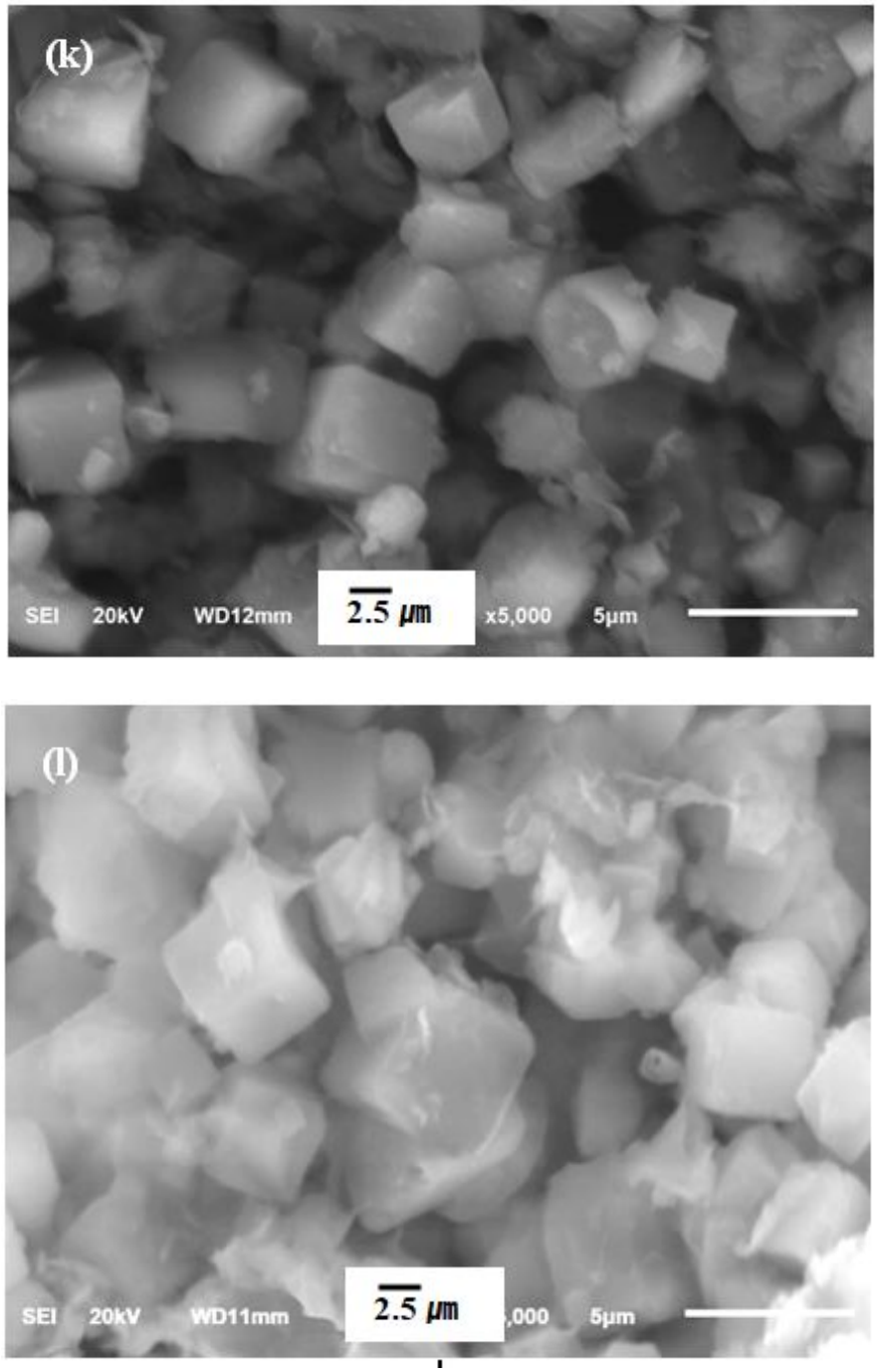

Fig. 2.37.: SEM Images of (k) green state Zeolite 5A and (l) sintered Zeolite 5A 3D - printed monoliths at 2.5μm magnification

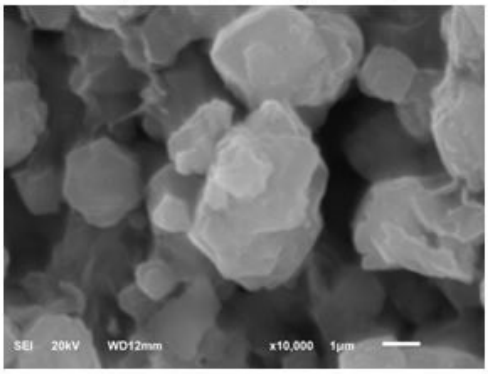

Element	Wt%	Wt% Sigma	Atomic %
C	16.39	0.82	23.95
O	47.35	0.51	51.95
Na	9.64	0.14	7.36
Al	11.26	0.14	7.33
Si	14.08	0.17	8.80
Cl	0.80	0.03	0.40
K	*0.48*	*0.03*	*0.22*
Total:	100.00		100.00

(a)

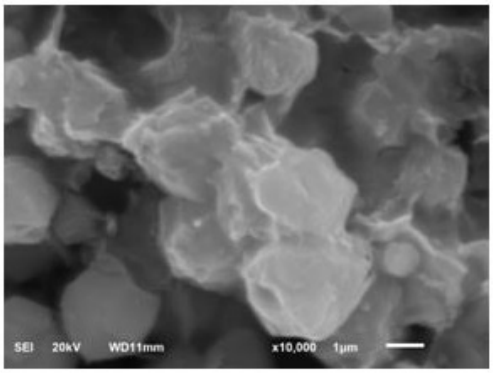

Element	Wt%	Wt% Sigma	Atomic %
C	9.30	0.56	14.22
O	49.84	0.37	57.18
Na	10.74	0.13	8.58
Al	12.94	0.13	8.80
Si	17.18	0.16	11.23
Total:	100.00		100.00

(b)

Fig. 2.38.: EDS analysis of Zeolite 13X : (a) Unsintered (b) Sintered

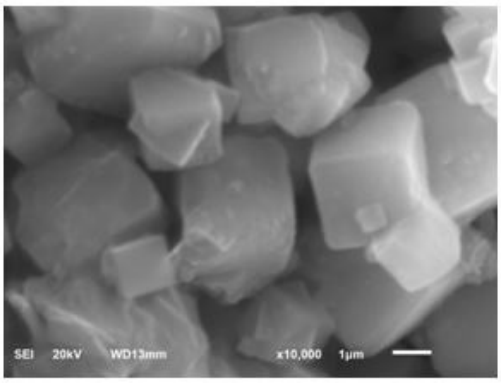

Element	Wt%	Wt% Sigma	Atomic %
C	11.00	0.75	16.79
O	50.10	0.47	57.38
Na	7.57	0.11	6.03
Al	13.02	0.15	8.84
Si	12.88	0.14	8.40
K	5.43	0.08	2.55
Total:	100.00		100.00

(a)

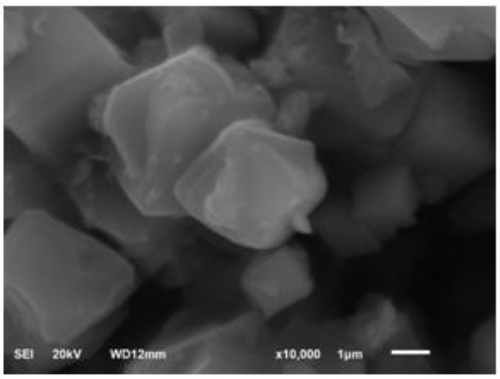

Element	Wt%	Wt% Sigma	Atomic %
C	11.01	0.84	16.48
O	54.32	0.55	61.03
Na	5.67	0.11	4.43
Al	12.24	0.15	8.15
Si	12.13	0.15	7.76
K	4.64	0.08	2.13
Total:	100.00		100.00

(b)

Fig. 2.39.: EDS analysis of Zeolite 3A : (a) Unsintered (b) Sintered

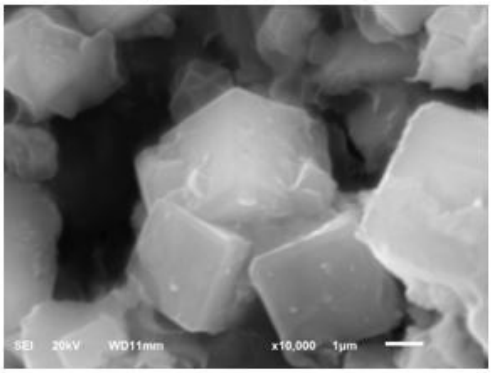

Element	Wt%	Wt% Sigma	Atomic %
O	56.75	0.19	67.98
Na	13.94	0.13	11.62
Al	14.51	0.11	10.31
Si	14.75	0.11	10.07
K	0.04	0.02	0.02
Total:	100.00		100.00

(a)

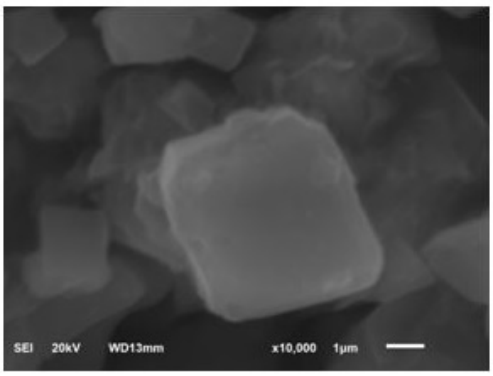

Element	Wt%	Wt% Sigma	Atomic %
C	6.56	0.48	9.92
O	56.99	0.34	64.66
Na	10.56	0.12	8.34
Al	13.19	0.12	8.87
Si	12.70	0.12	8.21
Total:	100.00		100.00

(b)

Fig. 2.40.: EDS analysis of Zeolite 4A : (a) Unsintered (b) Sintered

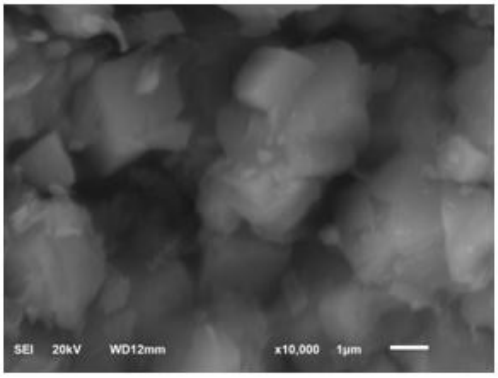

Element	Wt%	Wt% Sigma	Atomic %
C	13.90	0.54	20.53
O	52.30	0.38	58.00
Na	4.31	0.08	3.32
Al	12.08	0.12	7.94
Si	13.24	0.13	8.36
Ca	4.17	0.06	1.85
Total:	100.00		100.00

(a)

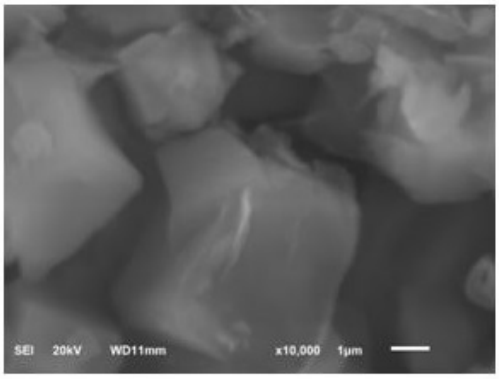

Element	Wt%	Wt% Sigma	Atomic %
C	13.86	0.55	20.67
O	50.65	0.39	56.71
Na	4.38	0.09	3.42
Al	12.67	0.13	8.41
Si	13.35	0.13	8.52
Ca	5.09	0.07	2.27
Total:	100.00		100.00

(b)

Fig. 2.41.: EDS analysis of Zeolite 5A : (a) Unsintered (b) Sintered

The XRD analysis of all the 3D - Printed Zeolite samples before and after sintering, the XRD patterns are shown in **Fig. 2.42 -–Fig. 2.45** The XRD patterns for all Zeolite samples shows that the crystalline nature was maintained except for some peak intensities which showed a slight difference. The addition of binders during slurry preparation may result in these differences in peak intensities. According to International Zeolite Association, every Zeolite has a standard framework. As explained in **Section 2.3.1** Zeolite 13X falls under FAU Type X and Zeolite 3A, 4A, 5A falls under LTA Type A. Looking over these XRD patterns of Zeolite samples it reveals that the standard peak intensities of FAU and LTA frameworks were retained. **Fig 2.24** and **Fig. 2.25** shows standard XRD patterns for FAU and LTA structure. [49]

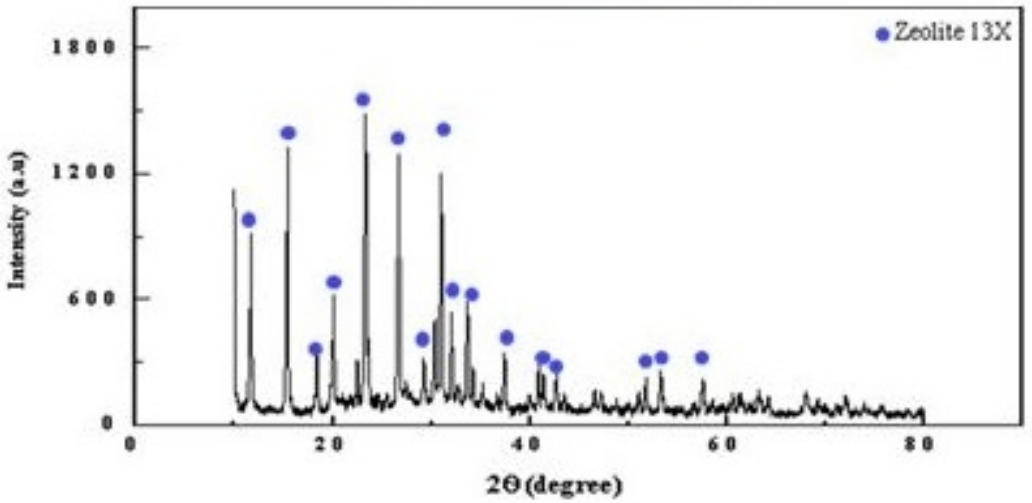

(a)

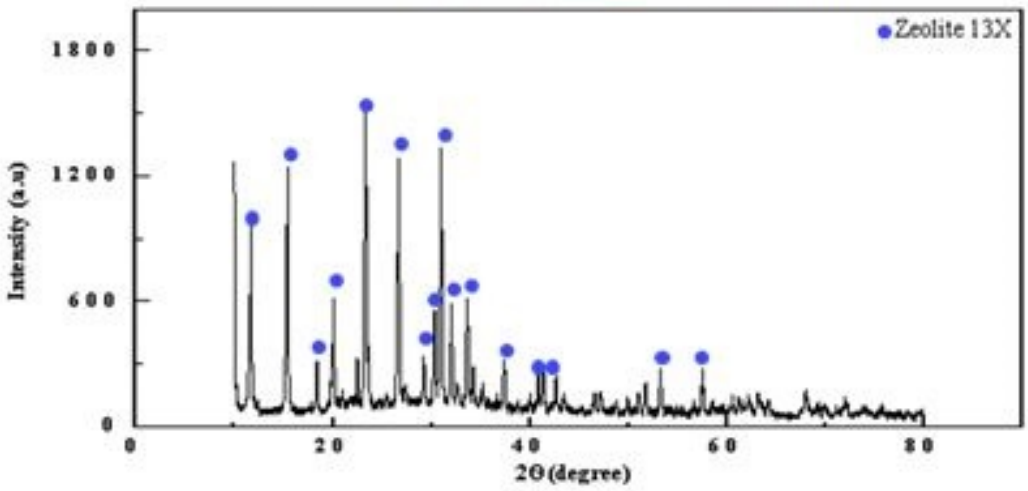

(b)

Fig. 2.42.: Zeolite 13X XRD patterns : (a) Unsintered (b) Sintered

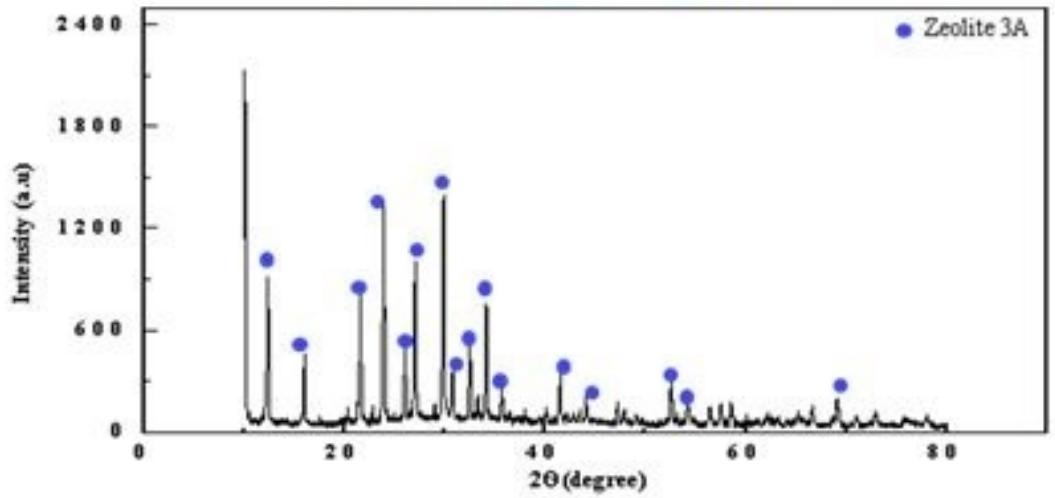

(a)

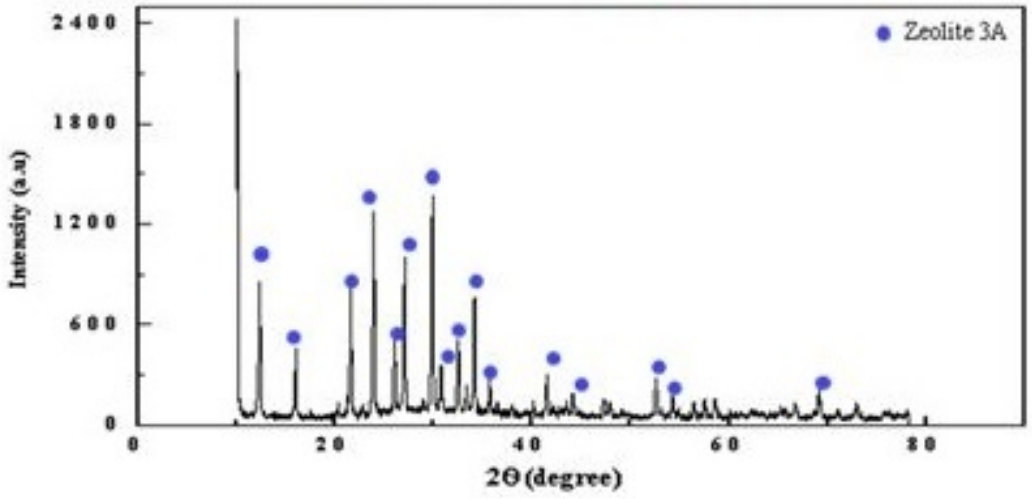

(b)

Fig. 2.43.: Zeolite 3A XRD patterns : (a) Unsintered (b) Sintered

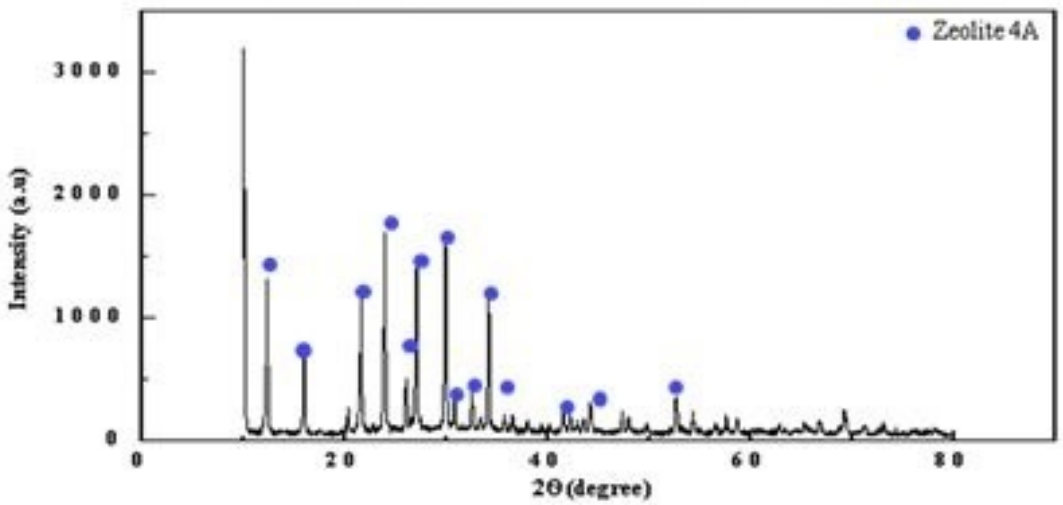

(a)

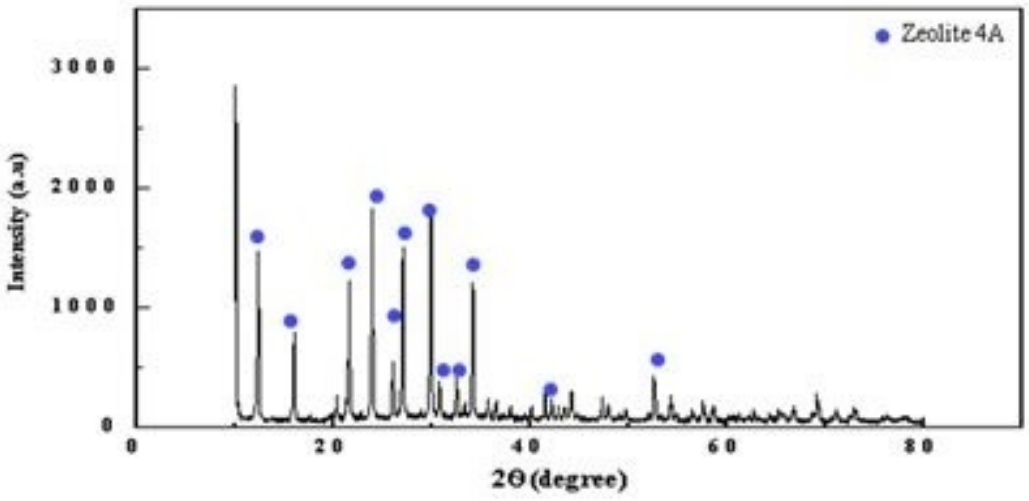

(b)

Fig. 2.44.: Zeolite 4A XRD patterns : (a) Unsintered (b) Sintered

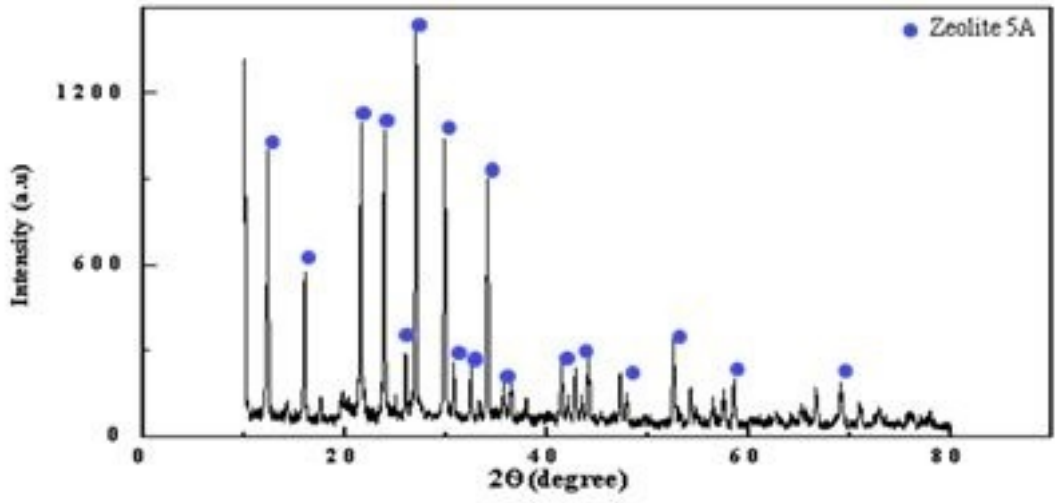

(a)

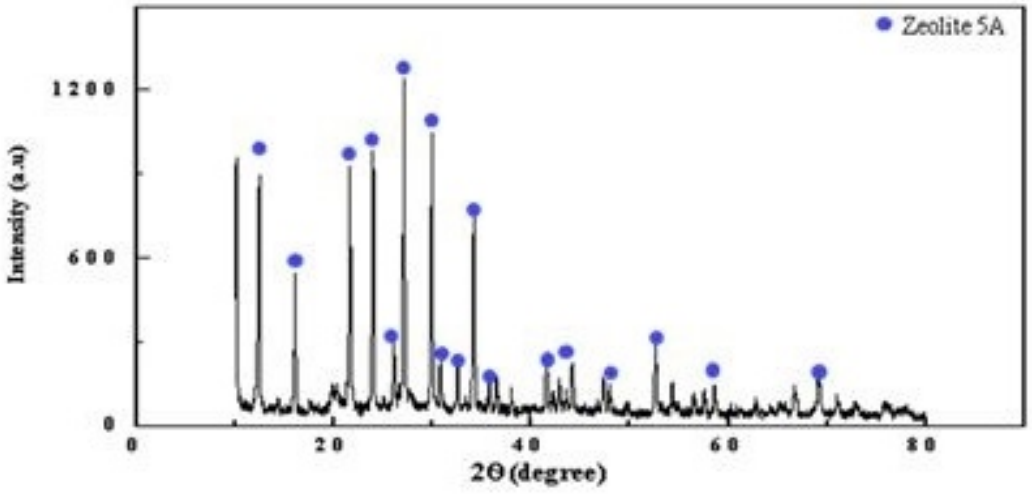

(b)

Fig. 2.45.: Zeolite 5A XRD patterns : (a) Unsintered (b) Sintered

2.3.3 Mechanical Strength of 3D - Printed Zeolite

To determine the standard deviation of the hardness value we conducted five indentations on the mounting specimen. The Vicker hardness values of unsintered and sintered 3D - Printed Zeolite samples are shown in **Table. 2.8.** The standard

Table 2.8.: Vicker hardness values of 3D - printed Zeolite samples

Zeolite 13X		Zeolite 3A		Zeolite 4A		Zeolite 5A	
Unsintere	Sintered	Unsintere	Sintered	Unsintere	Sintered	Unsintere	Sintered
8.33	14.49	3.38	8.92	5.18	7.60	7.49	14.67
9.05	13.21	3.42	8.33	4.35	8.58	6.90	14.31
9.22	12.45	4.68	7.84	6.63	9.56	8.74	13.53
10.61	15.05	4.20	9.04	5.84	6.57	9.90	14.03
8.98	12.6	4.44	8.61	6.72	10.77	8.78	14.21

deviation of microhardness values of both unsintered and sintred Zeolite samples are shown in **Fig. 2.46**. As shown in the chart the hardness of 3D - Printed Zeolite samples increased from 8.3 $\pm$ 2 to 12.5 $\pm$ 3 $HV_{0.05}$ for Zeolite 13X, 3.3 $\pm$ 1 to 7.3 $\pm$ 1 $HV_{0.05}$ for Zeolite 3A, 4.3 $\pm$ 2 to 7.5 $\pm$ 2 $HV_{0.05}$ for Zeolite 4A, 7.4 $\pm$ 1 to 14.0 $\pm$ 0.5 $HV_{0.05}$ for Zeolite 5A respectively. Sintering is most effective process in increasing the strength of 3D - Printed Zeolite samples,as we see from the values from **Table. 2.8** in all the Zeolites samples hardness was increased after sintering process

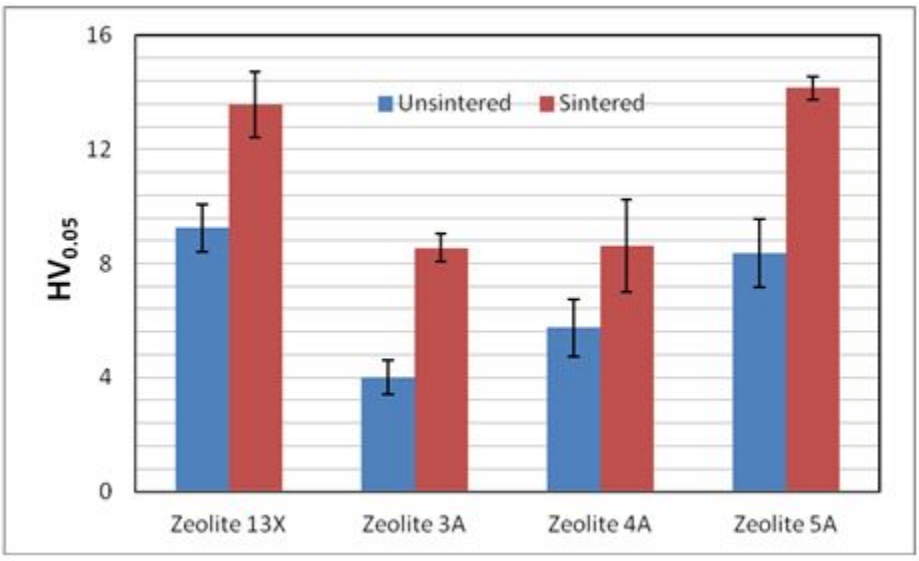

Fig. 2.46.: Vicker hardness values, $HV_{0.05}$, of the 3D - Printed Zeolite samples

2.4 Conclusion

1. The slurries of Zeolite 3A and 4A were successfully synthesized same as Zeolite 13X and 4A.

2. Grated structure of Zeolite 3A and 4A was able to print using customized 3D printer.

3. The BET surface area calculated for 3D printed Zeolite 13X was 767.429m^2/g and comparing it with available literatures BET surface area of 770m^2/g we can conclude that the 3D printed Zeolite 13X has better gas adsorption performance.

4. Based on SEM, EDS and XRD results we can conclude that the microstructure of 3D - Printed Zeolite Type X and Type A was maintained.

5. The microhardness of Zeolite samples before and after sintering was calculated. The hardness values are 8.3 $\pm$ 2 to 12.5 $\pm$ 3 $HV_{0.05}$ for Zeolite 13X, 3.3 $\pm$ 1 to 7.3 $\pm$ 1 $HV_{0.05}$ for Zeolite 3A, 4.3 $\pm$ 2 to 7.5 $\pm$ 2 $HV_{0.05}$ for Zeolite 4A, 7.4 $\pm$

1 to 14.0 ± 0.5 $HV_{0.05}$ for Zeolite 5A respectively.Sintering resulted in increase in hardness value for all the 3D - Printed sample.

6. Increased hardness value after sintering is an indication of the better mechanical strength of 3D printed Zeolite samples. But on the other hand, increased hardness value after sintering made them brittle, it suggests that the sintering temperature need to be optimized along with the printing parameters.

7. Some particle agglomeration was also observed after sintering which is due to binder residual. This binder residual will affect the mechanical strength of the final sample as they will be responsible for the change in micro-structure.

3. METAL - ORGANIC FRAMEWORKS (MOFS)

3.1 Introduction

Metal organic frameworks (MOFs) are a new category of porous materials which is recently being under research for their exceptional properties in the adsorption, separation, gas storage and sensing devises. [26, 29, 50] International Union of Pure and Applied Chemistry (IUPAC) define Metal Organic Framework, abbreviated as MOF, is a coordination network with organic ligands containing potential voids [51]. MOFs come under the category of coordination polymers and according to IUPAC coordinate polymer are defined as a coordinate compound with repeating coordination entities extending in 1, 2, or 3 dimensions. MOFs structure is composed of a metal ion and an organic molecule which forms an organic- inorganic hybrid network of metal ligand bonds [52]. The interactions between a metal ion and organic molecule leads in an empty cavity as a part of a crystallographic unit. These cavities which are formed as a crystallographic unit within the MOFs structure has ability to adsorbs gases [53]. The adsorption property of any adsorbent depends on pore dimension, chemical potential of the surface, and shape of the channels. MOFs have a feature of modifying their structure and functional properties by changing the building blocks used in their construction. This allows an advantage of finely controlling adsorption properties [54].

3.2 MOFs Synthesis

Numerous studies have been done on development of MOFs considering their outstanding properties in the field of gas adsorption for storage of fuel gases like hydrogen and methane [54] and also in the field of gas separation as an adsorbent material [55, 56]. looking over these applications the most important process is synthesis of MOFs, which can be achieved using different techniques. Most of the MOFs are synthesized using liquidphase synthesis method, where a separate metal salt of aluminum, zinc, copper, iron , etc and ligand solutions like Terephthalic acid, 2,5-Dihydroxyterephthalic acid, 1,3,5-Tris(4-carboxyphenyl)benzene, etc are mixed together or solvent is added to a mixture of solid salt and ligand in a reaction vial. **Fig.3.1** illustrates different methods used for synthesis of MOFs [21].

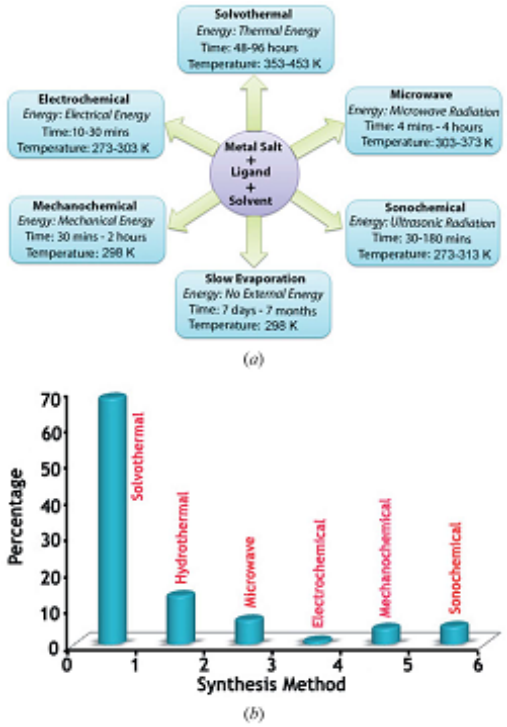

Fig. 3.1.: MOF synthesis review [21]

The slow evaporation method is one of the conventional methods used for preparation of MOFs crystals for few decades. The main advantage of this process is we can perform this synthesis process at room temperature without need of any external energy supply. But compared to other conventional methods this method took more time. Some researchers have been carried out for increasing the evaporation rate by adding low boiling solvents [57–59]. The solvothermal synthesis is one of the largely used MOFs synthesis methods in which the solvothermal reactions are basically carried out in a closed vessel under autogenously control pressure above the boiling point of the solvent. Most of the solvents which are used in this method are high-boiling organic solvents like dimethyl formamide, diethylformamide, acetonitrile, acetone, ethanol, methanol etc [60, 61]. Another commonly used MOFs synthesis method is sonochemical synthesis. In this method an ultrasonic radiations of around 20 kHz10MHz frequencies are used to agitate the particles which results into desired chemical reactions [62, 63]. This is usually done by using ultrasonic bath also known as sonicator. When ultrasonic waves are induced into chemical, instantaneous bubbles are formed and when they collapse creates cavities with high temperature and pressure, results into rapid crystallization [64, 65].

3.2.1 Materials and Methods

Metal organic frameworks (MOFs) can be synthesized using different methods as stated in **Section 3.2.** In this study the MOFs will be synthesized using hydro/solvothermal synthesis method referring to well-established procedure in the literature. Hydro/solvothermal synthesis is the method where a single crystal and different chemical compounds are synthesized and it generally relies upon the solubility of the available elements in water under a pressure higher than 1 atm [61]. The synthesis is generally carried out in stainless steel autoclave, in which the required chemicals are added along with the water. Both the ends of autoclave have different temperature i.e. the upper end has higher temperature and the bottom end is at low

temperature. This temperature gradient causes the reaction in the solute at hotter end and the desired crystals grow at the cooler end.

3.2.2 Experimental Section

In this study we will synthesis the Zinc-MOF-74 (Zn-MOF-74) with the well-established procedure of hydro/solvothermal synthesis [62] and then this Zn-MOF-74 will be mixed with binders and the slurry will be extruded using customized 3D printer. The lists of chemicals which will be used for the synthesis are listed down in **Table. 3.1** and their structural formulas are shown in **Fig. 3.2**.

Table 3.1.: List of chemicals for MOFs synthesis

No.	**Material**	**Molecular Formula**	**Molecular Weight (g/mole)**
1	Zinc Nitrate Hexahyadrate, Reagent Grade, 98%	$Zn(NO_3)_2 \cdot {}_6H_2O$	297.49
2	2,5- Dihydroxyterephthalic Acid, 98%	$(HO_2C_6H_2-1,4-(CO_2H)_2$	198.13
3	N,N-Dimethylformamide, Molecular Biology Reagent	$HCON(CH_3)_2$	73.09
4	Methanol	CH_3OH	32.04

The procedure starts with mixing 4.52 g of Zinc Nitrate Hexahyadrate Zn (NO3)26H2O (Sigma Aldrich) and 1.00 g of 2,5- Dihydroxyterephthalic Acid (DHTA) (Sigma Aldrich). In a 400 mL jar this mixture is dissolved in 100 ml of N,N-Dimethylformamide (DMF) (Sigma Aldrich)and placed into sonication bath. Then 5 mL of water was added to the solution and the sonication was continued till we get a homogenous

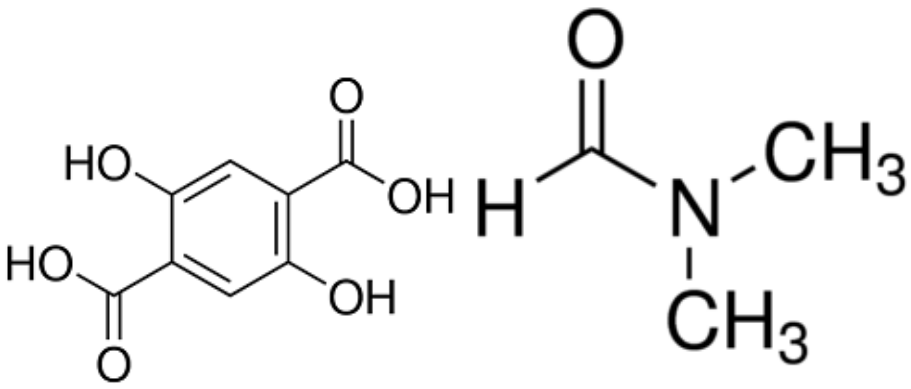

(a) (b)

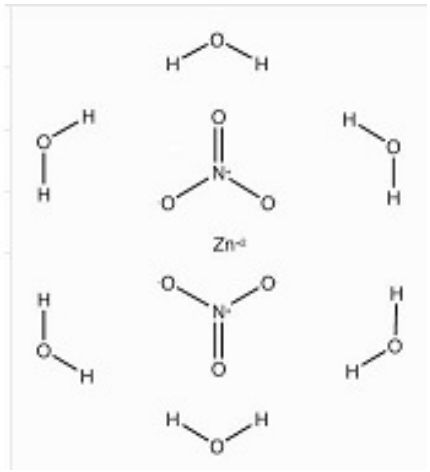

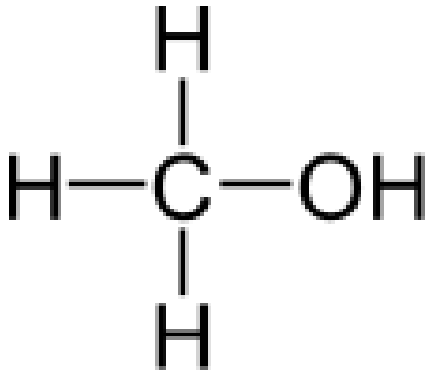

(c) (d)

Fig. 3.2.: Structural formulas : (a) 2 5- Dihydroxyterephthalic Acid (b) N N Dimethylformamide (c) Zinc nitrate hexahydrate (d) Methanol

mixture. **(Fig 3.3)** The stainless steel autoclave shown in **Fig 3.4** will be used for the hydrothermal synthesis.

(a) (b)

Fig. 3.3.: Sonication process : (a) During sonication (b) After sonication

Fig. 3.4.: Stainless steel autoclave

After decanting the products were washed three times with DMF, three times with methanol and then immersed in methanol. Vacuum filter **(Fig. 3.6)** was used to filter the product after every washing cycle. Decanting of methanol solvent was done once per day and followed next three days. **Fig. 3.7** shows the Zn-MOF-74 after three days washing into DMF and methanol.

(a)

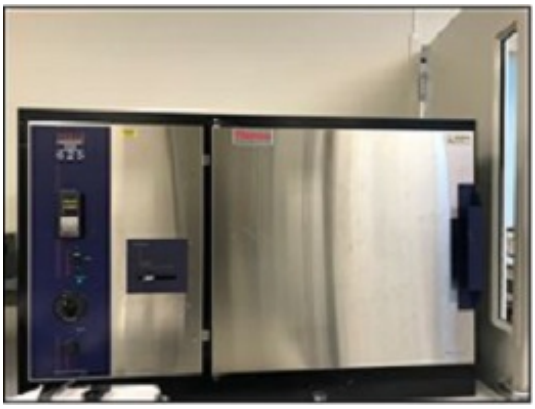

(b)

(c)

Fig. 3.5.: Oven for MOF synthesis : (a) Temperature panel (b) Oven (c) Autoclave placed inside oven

Fig. 3.6.: Washing of Zn-MOF-74 solution

Fig. 3.7.: Zn-MOF-74 after washing

Fig. 3.8.: Zn-MOF -74 powder

The product was then placed into an oven for heating for further drying at 150°C over a period of 1 h under vacuum. The product was kept at 150°C for 10 h and then the heating was increased to 265°C over a period of 1 h and then kept for 10 h at 265°C. **Fig. 3.8** shows the Zn-MOF-74 powder formed at the end of synthesis.After 10 h the product was cooled at room temperature and stored into a nitrogen environment before taking the BET test for surface area and X- ray diffraction analysis.

3.3 Conclusion

1. Zn-MOF-74 was successfully synthesized using well-established synthesis process.

2. As it was the first batch, further optimization of process parameters and equipment needed.

3. The final amount of MOF powder was around 0.45 g, which was not sufficient amount to perform 3D printing. But still, we managed to print a small part.

4. EXTRUSION BASED 3D PRINTING OF MOFS

4.1 Introduction

Slurry preparation of synthezied Zn-MOF-74 was carried out in a similar way as of Zeolite slurry. Considering physical nature of synthezied Zn-MOF-74 some modifications in slurry preparation were done. The synthesized MOF was added with the binders and using a syringe with a nozzle 3D structure was hand printed.

4.2 Experimental Section

4.2.1 Slurry Preparation

Zn-MOF-74 was synthesized using the solvothermal synthesis as explained in **Section 3.2.1** will be mixed with the binders and samples will be extruded. Referring to the literature on well-established slurry preparation procedure for Ni-MOF-74 we will prepare the Zn-MOF-74 slurry for extrusion based 3D printing. [7] In case of Zeolite slurry the chemicals are directly added in the appropriate proportion as per the **Table. 6** and then distilled water was added considering the required viscosity of slurry. But in case of Zn-MOF-74 slurry, we prepared two separate solutions consisting of Zn-MOF-74 powder, bentonite clay (Sigma Aldrich) as a binder and ethanol (Sigma Aldrich) in one solution and in second solution Poly vinyl alcohol (PVA) (ACROS Organics) as a plasticizer is dissolved in ethanol and deionized water (D.I) mixture. The compositional percent of all chemicals for slurry is shown in **Table. 8** The first solution was stirred for 2 h till we get a homogeneous solution and second solution was stirred for 30mins followed by the sonication for 30mins at room temperature. Then both the solutions were combined and mixed using magnetic stirrer (Fisher Scientific) at 250 rpm for 3 h until an extrudable slurry was formed.

Table 4.1.: Vicker hardness values of 3D - printed Zeolite samples

Monoliths	Zn-MOF-74 (Wt%)	Bentonite clay(Wt%)	PVA (wt%)	D.I water:ethanol concentration ratio(Vol%)
1	80	15	5	5:95

4.2.2 3D Printing of MOFs

After achieving the desired viscosity, the slurry was loaded into a 3ml syringe with 1.75 mm nozzle. A square shape was printed as shown in Fig. 4.1After printing the specimen was left to dry at room temperature and then kept into an oven at 100°C to remove remaining amount of binder content.

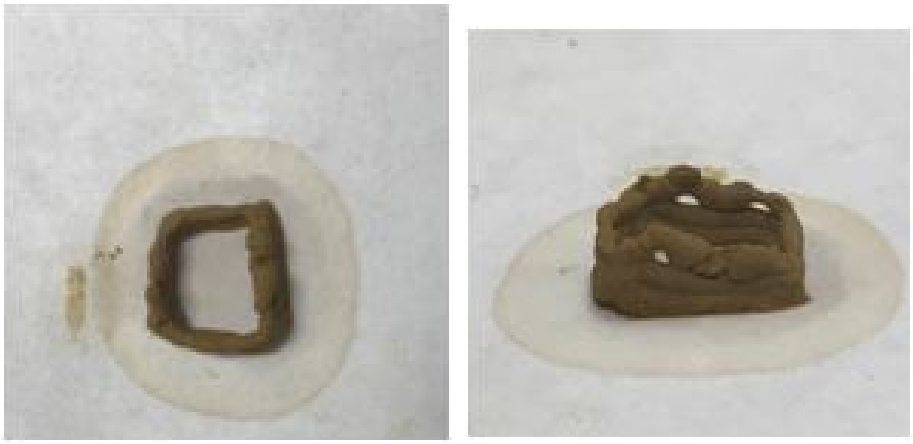

(a) Top View (b) Front view

Fig. 4.1.: 3D Printed Zn-MOF-74

As we see in **Fig. 4.1** the top seems more uneven compared to bellow layers. The amount of D.I. water and ethanol mixture wasnt able to extrude the slurry i.e. the flowability was reduced. This is because the Zn-MOF-74 was not well dispersed into the binders.

4.3 Conclusion

1. As this was our first batch of developing MOFs, we can expect variations in results comparing with available literature.

2. Optimization of binder contents needed as the slurry was getting dry while printing.

3. The layer formation collapsed after getting dry, this suggest the sintering was improper and need to perform at different temperature and controlled atmosphere.

5. CONCLUSION AND FUTURE WORK

5.1 Conclusion

1. The extrusion based 3D printing done for Zeolite 13X, 3A, 4A and 5A was successfully carried out. For extrusion based 3D printing the mechanical and structural properties mostly depend on the slurry formation and binder system used for preparing a slurry. Along with this printing parameter also correlated with final part.

2. The extrusion was performed using a customized 3D printer with some modifications. We used compressed air for our previous ceramic printing to extrude the slurry; we modified it and installed a feeder motor to extrude Zeolite slurry. The flowability of the slurry was maintained while using feeder motor instead of compressed air.

3. The most important factor to be considered while printing was feed rate at which the slurry was extruded. Controlled feed rate helped in achieving good integrity of layers.

4. The slurry for Zeolite 3A and 4A was prepared to refer the prior work done on Zeolite 13X and 5A, and we successfully prepared the slurry using same binders with different compositions and mixing procedure.

5. We prepared 20 g slurry for all the Zeolite samples, which can be mixed using a magnetic stirrer at 200-250 rpm. But for making up the slurry in large amount it is preferable to use the high performance dispersing instrument because for large amount of slurry related amount of binders i.e. bentonite clay and PVA increases which makes slurry more gluey and sticky.

6. The pore diameter for Zeolite 3A and 4A is less than Zeolite 13X and 5A, we were required to optimize the amount of binders percentage used while preparing the slurry as excess amount of binder may affect the microstructure.

7. Comparing the samples before and after sintering we noticed some amount of cracking over the surface of 3D - printed Zeolite samples. This suggests that the sintering temperature was not optimal for all the Zeolite samples as we did sintering at same temperature for all the 3D - printed samples. It also suggests that we will need more controlled post-sintering to be performed.

8. The SEM, EDS and XRD analysis was performed for all the Zeolite samples before and after sintering. The analysis results showed that the microstructure, phase and structure were not changed after sintering as we know in case of Zeolite the structure plays a vital role in adsorption property.

9. Using 3D printing technique for Zeolite we can tune the physical and structural properties along with mechanical strength. This will be definitely a helpful approach while considering applications where Zeolite will be used for adsorption.

10. Both the materials that are used in this research work has similar synthesis procedure and has similar applications i.e., gas adsorption, gas separation, and gas storage, but considering cost factor Zeolite is cheaper than MOFs and can be easily available.

11. Metal Organic Frameworks (MOFs) synthesis was carried out successfully referring to the well-established solvothermal synthesis process.

12. 3D printing of our first batch of Zn-MOF-74 mixed with binders was performed, but final results were not considered good. Optimization of chemical content and binder to MOF ratio is required.

5.2 Future Work

1. Zeolite is used in the application of gas adsorption, for which surface area plays a vital role. Knowing surface area of Zeolite will give us the amount of gas that will be adsorbed into it.

2. BET test for surface area calculation can be done for evaluating gas adsorption capacity of Zeolite.

3. Zeolite 13X and 5A have shown good results in CO_2 adsorption based on our literature survey, we can try for Zeolite 3A and 4A to check their adsorptive performance for CO_2.

4. Composite materials made up of Zeolite and ABS using solvent casting can be developed with higher strength.

5. The mixing procedure for making slurry still can be optimized for better results considering structural morphology.

6. Sintering at different temperature for each type of Zeolite can be done to check changes in structural morphology of Zeolite.

7. Printing parameters like feed and speed can be optimized to achieve better layer thickness and this will help in building parts with larger vertical height.

REFERENCES

REFERENCES

[1] I. Gibson, D. W. Rosen, and B. Stucker, "Sheet lamination processes," in *Additive Manufacturing Technologies*. Springer, 2010, pp. 223–252. 1

[2] F. Doreau, C. Chaput, and T. Chartier, "Stereolithography for manufacturing ceramic parts," *Advanced Engineering Materials*, vol. 2, no. 8, pp. 493–496, 2000. 1

[3] O. Cheung, "Narrow-pore zeolites and zeolite-like adsorbents for co2 separation," Ph.D. dissertation, Department of Materials and Environmental Chemistry (MMK), Stockholm University, 2014. 1

[4] P. M. Vitousek, "Beyond global warming: ecology and global change," *Ecology*, vol. 75, no. 7, pp. 1861–1876, 1994. 1

[5] D. M. D'Alessandro, B. Smit, and J. R. Long, "Carbon dioxide capture: prospects for new materials," *Angewandte Chemie International Edition*, vol. 49, no. 35, pp. 6058–6082, 2010. 1

[6] H. Thakkar, S. Eastman, A. Hajari, A. A. Rownaghi, J. C. Knox, and F. Rezaei, "3d-printed zeolite monoliths for co2 removal from enclosed environments," *ACS applied materials & interfaces*, vol. 8, no. 41, pp. 27 753–27 761, 2016. 1, 13

[7] H. Thakkar, S. Eastman, Q. Al-Naddaf, A. A. Rownaghi, and F. Rezaei, "3d-printed metal–organic framework monoliths for gas adsorption processes," *ACS applied materials & interfaces*, vol. 9, no. 41, pp. 35 908–35 916, 2017. 1, 74

[8] M. E. Boot-Handford, J. C. Abanades, E. J. Anthony, M. J. Blunt, S. Brandani, N. Mac Dowell, J. R. Fernández, M.-C. Ferrari, R. Gross, J. P. Hallett *et al.*, "Carbon capture and storage update," *Energy & Environmental Science*, vol. 7, no. 1, pp. 130–189, 2014. 1

[9] H. M. Magee and M. Sullivan, "Nitrogen gas adsorption in zeolites 13x and 5a," *Walla Walla University*, 2010. 1

[10] J. Vermesse, D. Vidal, and P. Malbrunot, "Gas adsorption on zeolites at high pressure," *Langmuir*, vol. 12, no. 17, pp. 4190–4196, 1996. 1

[11] M. C. Kreider, M. Sefa, J. A. Fedchak, J. Scherschligt, M. Bible, B. Natarajan, N. N. Klimov, A. E. Miller, Z. Ahmed, and M. R. Hartings, "Toward 3d printed hydrogen storage materials made with abs-mof composites," *Polymers for Advanced Technologies*, vol. 29, no. 2, pp. 867–873, 2018. 1, 7

[12] M. E. Davis, "Ordered porous materials for emerging applications," *Nature*, vol. 417, no. 6891, p. 813, 2002. 2

[13] S. Inagaki, S. Guan, Y. Fukushima, T. Ohsuna, and O. Terasaki, "Novel mesoporous materials with a uniform distribution of organic groups and inorganic oxide in their frameworks," *Journal of the American Chemical Society*, vol. 121, no. 41, pp. 9611–9614, 1999. 2

[14] A. Imhof and D. Pine, "Ordered macroporous materials by emulsion templating," *Nature*, vol. 389, no. 6654, p. 948, 1997. 2

[15] C. Baerlocher, L. B. McCusker, and D. H. Olson, *Atlas of zeolite framework types*. Elsevier, 2007. 2, 3

[16] I. Z. Association *et al.*, "Database of zeolite structures," *Library and Museum in Yorba Linda, California. The mission of the Festival is to educate students about water-related and conservation issues that correspond to California Science Standards. This years Festival will reach about*, vol. 6, 2008. viii, 3, 4

[17] P. Jacobs, E. M. Flanigen, J. Jansen, and H. van Bekkum, *Introduction to zeolite science and practice*. Elsevier, 2001, vol. 137. 3

[18] A. D. McNaught and A. D. McNaught, *Compendium of chemical terminology*. Blackwell Science Oxford, 1997, vol. 1669. 3

[19] S. Brunauer, P. H. Emmett, and E. Teller, "Adsorption of gases in multimolecular layers," *Journal of the American chemical society*, vol. 60, no. 2, pp. 309–319, 1938. 5

[20] S. R. Batten, N. R. Champness, X.-M. Chen, J. Garcia-Martinez, S. Kitagawa, L. Öhrström, M. OKeeffe, M. P. Suh, and J. Reedijk, "Terminology of metal–organic frameworks and coordination polymers (iupac recommendations 2013)," *Pure and Applied Chemistry*, vol. 85, no. 8, pp. 1715–1724, 2013. 5

[21] C. Dey, T. Kundu, B. P. Biswal, A. Mallick, and R. Banerjee, "Crystalline metal-organic frameworks (mofs): synthesis, structure and function," *Acta Crystallographica Section B: Structural Science, Crystal Engineering and Materials*, vol. 70, no. 1, pp. 3–10, 2014. viii, x, 5, 7, 66

[22] J. G. Vitillo, B. Smit, and L. Gagliardi, "Introduction: Carbon capture and separation," 2017. 5

[23] L. Pan, B. Parker, X. Huang, D. H. Olson, J. Lee, and J. Li, "Zn (tbip)(h2tbip= 5-tert-butyl isophthalic acid): a highly stable guest-free microporous metal organic framework with unique gas separation capability," *Journal of the American Chemical Society*, vol. 128, no. 13, pp. 4180–4181, 2006. 5

[24] L. Pan, D. H. Olson, L. R. Ciemnolonski, R. Heddy, and J. Li, "Separation of hydrocarbons with a microporous metal–organic framework," *Angewandte Chemie*, vol. 118, no. 4, pp. 632–635, 2006. 5

[25] A. U. Czaja, N. Trukhan, and U. Müller, "Industrial applications of metal–organic frameworks," *Chemical Society Reviews*, vol. 38, no. 5, pp. 1284–1293, 2009. 5, 8

[26] U. Mueller, M. Schubert, F. Teich, H. Puetter, K. Schierle-Arndt, and J. Pastre, "Metal–organic frameworksprospective industrial applications," *Journal of Materials Chemistry*, vol. 16, no. 7, pp. 626–636, 2006. 6, 8, 65

[27] F. Rezaei and P. Webley, "Structured adsorbents in gas separation processes," *Separation and Purification Technology*, vol. 70, no. 3, pp. 243–256, 2010. 6

[28] C. Liu, F. Li, L.-P. Ma, and H.-M. Cheng, "Advanced materials for energy storage," *Advanced materials*, vol. 22, no. 8, 2010. 6

[29] J. L. Rowsell and O. M. Yaghi, "Strategies for hydrogen storage in metal–organic frameworks," *Angewandte Chemie International Edition*, vol. 44, no. 30, pp. 4670–4679, 2005. 6, 65

[30] P. Silva, S. M. Vilela, J. P. Tomé, and F. A. A. Paz, "Multifunctional metal–organic frameworks: from academia to industrial applications," *Chemical Society Reviews*, vol. 44, no. 19, pp. 6774–6803, 2015. 7

[31] T. Sakakura, J.-C. Choi, and H. Yasuda, "Transformation of carbon dioxide," *Chemical Reviews*, vol. 107, no. 6, pp. 2365–2387, 2007. 7

[32] H. Furukawa, N. Ko, Y. B. Go, N. Aratani, S. B. Choi, E. Choi, A. Ö. Yazaydin, R. Q. Snurr, M. OKeeffe, J. Kim *et al.*, "Ultrahigh porosity in metal-organic frameworks," *Science*, vol. 329, no. 5990, pp. 424–428, 2010. 7

[33] G. Haselden, "Gas separation fundamentals," *Gas Separation & Purification*, vol. 3, no. 4, pp. 209–215, 1989. 7

[34] S. S. Han, J. L. Mendoza-Cortés, and W. A. Goddard Iii, "Recent advances on simulation and theory of hydrogen storage in metal–organic frameworks and covalent organic frameworks," *Chemical Society Reviews*, vol. 38, no. 5, pp. 1460–1476, 2009. 7

[35] J. L. Rowsell and O. M. Yaghi, "Metal–organic frameworks: a new class of porous materials," *Microporous and Mesoporous Materials*, vol. 73, no. 1-2, pp. 3–14, 2004. 7

[36] Y. Cui, H. Xu, Y. Yue, Z. Guo, J. Yu, Z. Chen, J. Gao, Y. Yang, G. Qian, and B. Chen, "A luminescent mixed-lanthanide metal–organic framework thermometer," *Journal of the American Chemical Society*, vol. 134, no. 9, pp. 3979–3982, 2012. 8

[37] X. Kong, E. Scott, W. Ding, J. A. Mason, J. R. Long, and J. A. Reimer, "Co2 dynamics in a metal–organic framework with open metal sites," *Journal of the American Chemical Society*, vol. 134, no. 35, pp. 14 341–14 344, 2012. 8

[38] A. M. Shultz, O. K. Farha, J. T. Hupp, and S. T. Nguyen, "A catalytically active, permanently microporous mof with metalloporphyrin struts," *Journal of the American Chemical Society*, vol. 131, no. 12, pp. 4204–4205, 2009. 8

[39] V. Stavila, R. K. Bhakta, T. M. Alam, E. H. Majzoub, and M. D. Allendorf, "Reversible hydrogen storage by naalh4 confined within a titanium-functionalized mof-74 (mg) nanoreactor," *ACS nano*, vol. 6, no. 11, pp. 9807–9817, 2012. 8

[40] Y. Lin, C. Kong, Q. Zhang, and L. Chen, "Metal-organic frameworks for carbon dioxide capture and methane storage," *Advanced Energy Materials*, vol. 7, no. 4, 2017. 8

[41] Z. Bao, S. Alnemrat, L. Yu, I. Vasiliev, Q. Ren, X. Lu, and S. Deng, "Kinetic separation of carbon dioxide and methane on a copper metal–organic framework," *Journal of colloid and interface science*, vol. 357, no. 2, pp. 504–509, 2011. 8

[42] M. Palomino, A. Corma, F. Rey, and S. Valencia, "New insights on co2- methane separation using lta zeolites with different si/al ratios and a first comparison with mofs," *Langmuir*, vol. 26, no. 3, pp. 1910–1917, 2009. 8

[43] B. L. Karger, L. R. Snyder, C. Horvath *et al.*, "Introduction to separation science," 1973. 8

[44] D. Shekhawat, T. H. Gardner, and D. A. Berry, "Natural gas odorants desulfurization," in *AIChE Annual National Meeting, Austin, TX*, 2004. 8

[45] P. Horcajada, T. Chalati, C. Serre, B. Gillet, C. Sebrie, T. Baati, J. F. Eubank, D. Heurtaux, P. Clayette, C. Kreuz *et al.*, "Porous metal–organic-framework nanoscale carriers as a potential platform for drug delivery and imaging," *Nature materials*, vol. 9, no. 2, p. 172, 2010. 8, 9

[46] T. J. Drozda, *Tool and manufacturing engineers handbook: machining*. Society of Manufacturing Engineers, 1983, vol. 1. 10

[47] D. Owen, J. Hickey, A. Cusson, O. I. Ayeni, J. Rhoades, Y. Deng, Y. Zhang, L. Wu, H.-Y. Park, N. Hawaldar *et al.*, "3d printing of ceramic components using a customized 3d ceramic printer," *Progress in Additive Manufacturing*, pp. 1–7, 2018. 10

[48] F. Akhtar and L. Bergström, "Colloidal processing and thermal treatment of binderless hierarchically porous zeolite 13x monoliths for co2 capture," *Journal of the American Ceramic Society*, vol. 94, no. 1, pp. 92–98, 2011. 26

[49] M. M. Treacy, J. B. Higgins, and R. von Ballmoos, "Collection of simulated xrd powder patterns for zeolites," *Zeolites*, vol. 5, no. 16, pp. 330–802, 1996. 57

[50] R. Q. Snurr, J. T. Hupp, and S. T. Nguyen, "Prospects for nanoporous metal-organic materials in advanced separations processes," *AIChE Journal*, vol. 50, no. 6, pp. 1090–1095, 2004. 65

[51] N. G. Connelly, *Nomenclature of inorganic chemistry: IUPAC recommendations 2005*. Royal Society of Chemistry, 2005. 65

[52] S. Choi, J. H. Drese, and C. W. Jones, "Adsorbent materials for carbon dioxide capture from large anthropogenic point sources," *ChemSusChem*, vol. 2, no. 9, pp. 796–854, 2009. 65

[53] D. Alezi, Y. Belmabkhout, M. Suyetin, P. M. Bhatt, Ł. J. Weselinski, V. Solovyeva, K. Adil, I. Spanopoulos, P. N. Trikalitis, A.-H. Emwas *et al.*, "Mof crystal chemistry paving the way to gas storage needs: aluminum-based soc-mof for ch4, o2, and co2 storage," *Journal of the American Chemical Society*, vol. 137, no. 41, pp. 13 308–13 318, 2015. 65

[54] P. D. Dietzel, V. Besikiotis, and R. Blom, "Application of metal–organic frameworks with coordinatively unsaturated metal sites in storage and separation of methane and carbon dioxide," *Journal of Materials Chemistry*, vol. 19, no. 39, pp. 7362–7370, 2009. 65, 66

[55] T. Düren, L. Sarkisov, O. M. Yaghi, and R. Q. Snurr, "Design of new materials for methane storage," *Langmuir*, vol. 20, no. 7, pp. 2683–2689, 2004. 66

[56] D. M. Ruthven, *Principles of adsorption and adsorption processes*. John Wiley & Sons, 1984. 66

[57] M. Du, C.-P. Li, and X.-J. Zhao, "Metal-controlled assembly of coordination polymers with the flexible building block 4-pyridylacetic acid (hpya)," *Crystal growth & design*, vol. 6, no. 1, pp. 335–341, 2006. 67

[58] S. R. Halper, L. Do, J. R. Stork, and S. M. Cohen, "Topological control in heterometallic metal- organic frameworks by anion templating and metalloligand design," *Journal of the American Chemical Society*, vol. 128, no. 47, pp. 15 255–15 268, 2006. 67

[59] Y. Yoo, V. Varela-Guerrero, and H.-K. Jeong, "Isoreticular metal- organic frameworks and their membranes with enhanced crack resistance and moisture stability by surfactant-assisted drying," *Langmuir*, vol. 27, no. 6, pp. 2652–2657, 2011. 67

[60] S. Bhattacharjee, J.-S. Choi, S.-T. Yang, S. B. Choi, J. Kim, and W.-S. Ahn, "Solvothermal synthesis of fe-mof-74 and its catalytic properties in phenol hydroxylation," *Journal of nanoscience and nanotechnology*, vol. 10, no. 1, pp. 135–141, 2010. 67

[61] C.-C. Wang and J. Y. Ying, "Sol- gel synthesis and hydrothermal processing of anatase and rutile titania nanocrystals," *Chemistry of materials*, vol. 11, no. 11, pp. 3113–3120, 1999. 67

[62] T. G. Glover, G. W. Peterson, B. J. Schindler, D. Britt, and O. Yaghi, "Mof-74 building unit has a direct impact on toxic gas adsorption," *Chemical Engineering Science*, vol. 66, no. 2, pp. 163–170, 2011. 67, 68

[63] C. A. Grande, V. I. Águeda, A. Spjelkavik, and R. Blom, "An efficient recipe for formulation of metal-organic frameworks," *Chemical Engineering Science*, vol. 124, pp. 154–158, 2015. 67

[64] C. G. Carson, A. J. Brown, D. S. Sholl, and S. Nair, "Sonochemical synthesis and characterization of submicrometer crystals of the metal–organic framework cu [(hfipbb)(h2hfipbb) 0.5]," *Crystal Growth & Design*, vol. 11, no. 10, pp. 4505–4510, 2011. 67

[65] S. Dharmarathna, C. K. Kingondu, W. Pedrick, L. Pahalagedara, and S. L. Suib, "Direct sonochemical synthesis of manganese octahedral molecular sieve (oms-2) nanomaterials using cosolvent systems, their characterization, and catalytic applications," *Chemistry of Materials*, vol. 24, no. 4, pp. 705–712, 2012. 67

VITA

VITA

Nishant Hemant Hawaldar

SUMMARY

Mechanical Engineer with 2+ years of hand on experience and technical knowledge in production and additive manufacturing. Have worked on different additive manufacturing technologies like binder jetting, fused deposition modeling and extrusion based 3D printing and manufacturing processes like sand casting, CNC machining. I am passionate about advance technologies in manufacturing world.

SKILLS

- 3D Printing
- FDM
- FANUC
- Creo Parametric
- Autocad
- Extrusion
- Ansys
- Microsoft Office

EDUCATION

M.S. Mechanical Engineering GPA : 3.23/4.0 August 2016 - May 2018
Indiana University - Purdue University Indianapolis, Indianapolis, Indiana

B.E. Mechanical Engineering GPA : 3.6/4.0 July 2010 - June 2013
Shivaji University, Kolhapur, India

Diploma in Mechanical Engineering GPA : 3.75/4.0 June 2008 - June 2010
Sou. Venutai Chawan Polytechnic, Pune, India

RESEARCH EXPIRENCE

Graduate Research Assistant

School of Engineering and Technology,IUPUI, Indianapolis

Jan 2017-May 2018

- Develop an extrusion based 3D printer using freeform fabrication technique for printing Zeolite 3A and 4A and Zinc Metal Organic Frameworks (Zn-MOF-74) for evaluation of their performance in gas adsorption.
- Structural morphology of 3D - printed Zeolite 3A and 4A will be studied by performing SEM/XRD Analysis.
- Brunauer-Emmett-Teller (BET) test of 3D printed samples will be performed to check the specific surface area.
- Extrusion based 3D printing of water atomized 17-4PH stainless steel powder using customized FDM Printer.

PROFESSIONAL EXPERIENCE

Assistant Manager (Production)

M/s. Girija industries, Palus, India

Dec 2014 - Jan 2016

- Monitored and controlled the scope, cost and time for new projects.
- Developed production plan and designed new tooling for fabricating heavy column pipes.
- Supervised manufacturing activities at shop floor level and was handling 20 workers.

Graduate Apprentice Trainee (GAT)

Kirloskar Brothers Limited, Kirloskarwadi, India

Dec 2013 - Dec 2014

- Assisted senior in designing manufacturing process plan for R&D project on Canned Motor Pump.
- Prepared and updated SAP- Material Management module.
- Conducted material delivery, inspection, assembly of split case pumps.

ACADEMIC PROJECTS

Aerodynamics of Phoenix RC plane with design for Additive Manufafacturing

Aug 2017 - Dec 2017

- In this project we manufactured a Phoenix RC plane using Additive Manufacturing for which we designed patterned wing on the basis of Microbial Structures of Cell. For that we did Aerodynamics calculations of RC plane wing.
- We designed all the parts of RC plane in Creo Parametric and assembled in Creo Parametric itself. Then the assembled plane was converted into .stl format and inputted it to 3D printer for printing.
- Considering the design of RC plane we printed the RC plane on LULZABOT, MAKERBOT and AFINIBOT FDM printers. Further we performed DOE to check the Aerodynamic parameters and compare it with standard values.

Fatigue Analysis of Shaft for Centrifugal Oil Filter

Jan 2017 - Apr 2017

- Simulation of shaft was done in ANSYS Workbench under specified working parameters.
- The fatigue life and safety factor was calculated using ANSYS Fatigue tool and the results were compared with hand calculations.

Offshore Blowout Prevention Access Platform in Composite Materials
Jan 2017 - Apr 2017

- Existing steel platform faced the major problem of corrosion which increased maintenance cost.
- Micromechanics of composite with E- glass as a fiber and Vinyl Ester as matrix was performed.
- The simulation of the model was performed in ANSYS Workbench for Tsai Wu failure criteria.

Rapid Prototyping Technology - Innovation in Casting sponsored by Kirloskar Brothers Limited, Kirloskarwadi
Aug 2012 - Mar 2013

- In this project we had a case study on Conventional Casting Process, Investment Casting Process and Casting using 3D Printing Technology.
- We designed three small models of Vertical Turbine Bowl using all three processes. We compared the three Bowls on the basis of process requirements, weight of the component, build time and total cost.
- After comparing the three processes we came to the conclusion that casting using 3D Printing is much better in comparison. This project helped company to introduce this new technology of 3D printing for casting, which resulted in increased cost-time effectiveness.

PUBLICATIONS AND PRESENTATIONS

- Nishant Hawaldar, Jing Zhang, A Comparative Study of Fabrication of Sand Casting Mold Using Additive Manufacturing and Conventional Process. International Journal of Advanced Manufacturing Technology, (http://dx.doi.org/10.1007/s00170-018-2020-z)

- Nishant, H., Jing, Zhang., et al., 3D printing of ceramic components using a customized 3D ceramic printer. Progress in Additive Manufacturing, 2018. (https://doi.org/10.1007/s40964-018-0037-3)
- Nishant Hawaldar, Jing Zhang, Comparing Conventional and 3D Printing Processes for Sand Casting, Additive Manufacturing Magazine, 2018. (https://www.additivemanufacturing.media)
- Nishant Hawaldar, Jing Zhang, Extrusion based 3D printing of Molecular Sieve Zeolite for gas adsorption applications, MS&T18 Conference, Additive Manufacturing of Composites and Complex Materials III Symposium,2018
- Nishant Hawaldar, Jing Zhang, Extrusion based 3D printing of water atomized 17-4 PH stainless steel powder, AMPM2018 conference, San Antonio, TX, 2018
- Nishant Hawaldar, Jing Zhang, 3D printing of Zeolite 13X, 3A, 4A, and 5A Monoliths for Gas Adsorption Applications, IUPUI Student Research Day, 2018
- Nishant Hawaldar, Jing Zhang, Additive Manufacturing of Mold and Core for Sand Casting, POWDERMET2017 conference, Las Vegas, NV, 2017
- Nishant Hawaldar, Jing Zhang, Additive Manufacturing for Foundry, IUPUI Student Research Day, 2017

AWARDS

- National Science Foundation (NSF) Travel Grant for POWDERMET2017 Conference, Las Vegas, NV
- National Science Foundation (NSF) Travel Grant for POWDERMET2018 Conference, San Antonio, TX
- Best Poster Award at IUPUI Research Day, 2017.

ACTIVITIES

- Assessment based course on Introduction to Additive Manufacturing under ASME. Sept 2017
- Active member of ASME, ASTM and APMI International.